Požarna analiza armirano betonskih stupova: utjecaj različitih parametara na konačni proračun otpornosti na požar

Rogulj, Marko

Master's thesis / Diplomski rad

2022

Degree Grantor / Ustanova koja je dodijelila akademski / stručni stupanj:
University of Split, Faculty of Civil Engineering, Architecture and Geodesy / Sveučilište u Splitu, Fakultet građevinarstva, arhitekture i geodezije

Permanent link / Trajna poveznica: https://urn.nsk.hr/urn:nbn:hr:123:543986

Rights / Prava: In copyright/Zaštićeno autorskim pravom.

Download date / Datum preuzimanja: **2024-04-27**

SVEUČILIŠTE U SPLITU

FAKULTET GRAĐEVINARSTVA, ARHITEKTURE I GEODEZIJE

DIPLOMSKI RAD

Marko Rogulj

Split, 2022.

SVEUČILIŠTE U SPLITU

FAKULTET GRAĐEVINARSTVA, ARHITEKTURE I GEODEZIJE

Marko Rogulj

Požarna analiza armirano betonskih stupova: utjecaj različitih parametara na konačni proračun otpornosti na požar

Diplomski rad

Split, 2022.

Požarna analiza armirano betonskih stupova: utjecaj različitih parametara na konačni proračun otpornosti na požar

Sažetak:

Prema zahtjevima EN 1992-1-2, analize požara armiranobetonskih (RC) stupova danas se mogu izvoditi na različite načine s različitim razinama točnosti ovisno o tome koje i koliko pretpostavki (pojednostavljenja) podrazumijevaju. Danas je poznato da bi inženjeri u svakodnevnoj inženjerskoj praksi trebali težiti što većem izostavljanju ovih pojednostavljenja. Naime, zbog svoje konzervativnosti, jednostavnije metode su često više na tzv. „sigurnoj strani" i stoga mogu dovesti do skupljih inženjerskih rješenja (npr. propisivanje pretjerane konstrukcijske protupožarne zaštite). Nažalost, do danas još nije dovoljno razjašnjeno koju bi od pretpostavki bilo najsmislenije eliminirati među prvima. Ovaj diplomski rad pokušava dati odgovor na ovo pitanje

Ključne riječi: Požarna analiza, analiza nosivosti, armirani beton, ABAQUS, FDS, parametri požara, metoda analize članova

Fire analyses of RC columns: effect of different parameters on final calculation of fire resistance

Abstract:

According to requirements of EN 1992-1-2, fire analyses of reinforced concrete (RC) columns today can be performed in different ways with different levels of accuracy depending on which and how many assumptions (simplifications) they entail. It is known today that engineers in their daily engineering practice should strive for omittance of these simplifications as much as possible. Namely, because of their conservatism, the more simple methods are often more on the so-called "safe side" and thus can lead toward more expensive engineering solutions (e.g. prescribing excessive structural fire protection). Unfortunately, to date it is not yet clarified sufficiently which of the assumptions would make the most sense to be eliminated among the first. This master's thesis tries to contribute to answering this question.

Keywords: Fire analysis, load bearing analysis, reinforced concrete, ABAQUS, FDS, fire parameters, member-analysis method

STUDIJ: **DIPLOMSKI SVEUČILIŠNI STUDIJ GRAĐEVINARSTVA**

SMJER: **KONSTRUKCIJE**

KANDIDAT: **Marko Rogulj**

JMBAG: **00832214684**

KATEDRA: **Katedra za Betonske konstrukcije i mostove**

PREDMET: **Betonske konstrukcije**

ZADATAK ZA DIPLOMSKI RAD

Tema: **Požarna analiza armirano betonskih stupova: utjecaj različitih parametara na konačni proračun otpornosti na požar**

Opis zadatka: Zadatak diplomskog rada je analiza požarnih krivulja na armirano betonski stup uz pomoć programa ABAQUS. Požarne krivulje je potrebno dobiti pomoću simulacija putem FDS programa. Na temelju dobivenih požarnih krivulja je potrebno je analizirati armirano betonski stup te zaključiti kako pojedini parametri utječu na konačnu otpornost stupa. Rezultate dobivenih analiza potrebno međusobno usporediti.

U Splitu, ožujak, 2022.

Voditelj diplomskog rada:

Prof.dr.sc. Alen Harapin

Komentori diplomskog rada:

Doc.dr.sc. Jerneja Češarek Kolšek

Doc.dr.sc. Peter Češarek

Predsjednik Povjerenstva za završne i diplomske ispite:

Izv.prof.dr.sc. Ivo Andrić

Ovaj diplomski rad je izrađen na na Fakultetu Građevinarstva i Geodezije, Sveučilišta u Ljubljani, Slovenija.

University of Ljubljana
Faculty of Civil and Geodetic Engineering

Jamova 2,
1000 Ljubljana, Slovenia
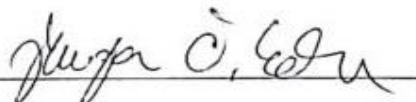telephone +386 1 47 68 500
fgg@fgg.uni-lj.si

Letter of Confirmation

This is to confirm that student **Marko Rogulj** from the **University of Split** spent **5** months at the **University of Ljubljana, Faculty of Civil and Geodetic Engineering, Department of Civil Engineering**, within the framework of the Erasmus + Programme and for the purpose of research and preparation of his **Master thesis** titled:

Fire analyses of RC columns: effect of different parameters on final calculation of fire resistance.

Name and surname: Jerneja Češarek Kolšek

Title and function: Assistant Professor, Mentor

Signature: _____

Date: 30. 6. 2022

Stamp of the Institution:

Contents

1. INTRODUCTION

According to requirements of EN 1992-1-2 [1], fire analyses of reinforced concrete (RC) columns today can be performed in several different ways, which can have different levels of accuracy. The simplest way is *member-analysis methods.* The latter usually refer to methods where instead of the structure as a whole (or at least a larger part of it) we only consider its individual (isolated) structural element (i.e. RC column). Of course, this is only possible if two essential assumptions are made:

(i)   internal forces in the element will not change during fire and

(ii) there will be no changes in kinematic boundary conditions at the ends of the element.

In addition, the following simplifications are also normally included in a member-analysis method of a RC column:

(iii) The temperature of the column's surroundings in the analysis is described by a so-called *fire curve* which depends on time and corresponds to the simplified analytical form of a selected specific *nominal fire curv*e from EN 1991-1-2 [2], Section 3.2. This means that, beside on time, this curve also depends on the general 'type' of the fire (standard, external, or hydrocarbon fire), however, it does not also depend on the specifics of the analysed building compartment (floor area, volume, openings such as doors and windows, amount and distribution of burning objects and materials etc.). More accurate computer simulations of actual possible building fires accoutning also for all of these parameters, which could be used to calculate a more precise alternative *natural fire curve,* are not normally exploited.

(iv) The temperature of the column's surroundings at a specific time of the fire is assumed to be the same along with its entire height and around the column.

(v) Convection and radiative heat fluxes generated at the contact of the column and its surroundings during a fire are calculated using the selected fire curve and recommendations on convection and radiation coefficients as given in EN 1992-1-2 [1] and EN 1991-1-2 [2].

(vi) It is assumed that during fire there will be no concrete spalling.

(vii) Mathematical description of the mechanical response of a column is more or less simplified, for example described by equations according to the *second-order theory* instead of according to the most accurate *third-order* theory. The temperature dependence of mechanical characteristics of concrete is more or less precisely taken into consideration.

In general, fire analysis of a RC column can be upgraded from the simplest 'member analysis' form to a more advanced form by omitting one or more of the above assumptions (i) - (vii). It is already well known today that engineers in their daily engineering practice should strive for such an upgrade as much as possible. Namely, because of their conservatism, the member-analysis methods are often more on the so-called "safe side" and thus can lead toward more expensive engineering solutions (e.g. prescribing excessive structural fire protection). Unfortunately, however, to date it is not yet clarified sufficiently which of the above assumptions (i) - (vii) would make the most sense to be eliminated first (i.e. which are the ones that most influence the conservatism of the member-analysis results). Thus, this master's thesis will try to contribute to answering this question. This will be done by analysing a selected case of a RC building and a selected fire. To limit the scope of the task, we will focus in particular on assessing the conservatism of assumptions (iv) - (vii). However, we will not specifically investigate the potential conservatism of assumptions (i)-(ii), as some information on this can be found in other available literature (e.g. [5], [6], [7], [13]). We will also not assess the level of conservatism of assumption (iii) in this master's thesis as this has been studied several times in literature before and already recognized previously as potentially very high for some cases.

2. THEORETICAL BACKGROUND

2.1. Fire analyses of RC structures according to EN 1992-1-2

In section 2.1 of the thesis we will take a look at the theoretical foundations of fire analysis of reinforced concrete (RC) structures following provisions of EN 1992-1-2 [1]. The text of this section will be summarised mostly from sources [3] and [8]

Standard EN 1992-1-2 [1] generally requires that the design resistance of a fire-exposed RC structure is greater than the impact of the fire on it:

$$R_{fi,d,t} \geq E_{fi,d,t} \tag{1}$$

Symbol $R_{fi,d,t}$ here refers to design resistance of the structure at a specific time t of the assumed fire and at the prescribed load combination for *fire design situation*. Symbol $E_{fi,d,t}$ is the design value of internal forces in the structure at this load combination and at time t. Note that according to EN 1990 [9], Section 6.4.3.3, the fire design situation is a part of the group of the so called *ultimate limit state* (ULS) situations, more precisely of the group of *accidental design situations*. The general form of the corresponding load combination is as follows:

$$\sum_{j\geq1} G_{k,j} + A_d + (\psi_{1,1} \ or \ \psi_{2,1}) * Q_{k,1} + \sum_{i\geq1} \psi_{2,i} + Q_{k,i,} \tag{2}$$

where $G_{k,j}$ denotes a permanent action on the structure, $Q_{k,1}$ is the predominant variable action, and $Q_{k,i}$ are other variable actions. Moreover, A_d are accidental actions, i.e. in this thesis representing the effects of elevated temperatures due to the fire. These can be of a *direct* or *indirect* nature. Direct actions A_d are influences of high temperature on essential material properties (reduction of strength of concrete and reinforcng steel, thermal expansion *etc*.). However, indirect actions A_d are influences of high temperatures that not only depend on the material but also on characteristics of the structure. A good example of an indirect action A_d is an increase in the axial force of a RC column in the initial stages of the fire due to its tendency for fire-induced thermal elongations which are being hindered by the rest of the structure (e.g. by an RC plate on top of the column). Moreover, $\psi_{1,1}$ and $\psi_{2,1}$ are load combination factors where application of one or the other is normally prescribed by a national annex to EN 1991-1-2 [2] depending on the type of the accident.

The values on both sides of inequality (1) as written above generally change over time, so it is necessary to define the *ultimate time t* by which this condition should still be met in the assumed fire. Normally, the ultimate time will be prescribed in the scope of a some kind of a document presenting results of a study

of the building's fire safety. This will be prepared by the fire engineer responsible for the specific building and will be a mandatory part of the construction permit project documentation. In the study, these data will be given in a form of symbol 'R' (referring to the term 'resistance') and a following number, e.g. R30, R60 or R120 *etc.*, where the number will apply to the above mentioned ultimate time in minutes. In addition, definition of the fire curve, i.e. fire scenario, to which this ultimate time should apply, will be given in the study as well.

2.1.1. Fire scenario

A fire scenario in its most general form means a time- and space-dependent function of temperatures of the surroundings of the fire-exposed structure (i.e. temperature of surrounding gas being important for convective transfer of heat to and from the analysed structure and temperature of the surrounding walls and other obstructions exchanging heat with the structure through radiation). During a fully developed fire which usually interests us the most from the point of view of the load-bearing capacity of the building's structure, this function can usually be simplified to a simpler (time-dependent only) function, i.e. so called *fire curve* (Figure *1*). With application of a fire curve along a specific structure (or along a part of it) we accept the assumption that at a certain time *t* the temperature of the surroundings of the structure will be the same along and around the entire structure.

When searching for a sutiable fire curve, a fire engineer may choose between the so called *nominal curves*, which normally only describe the heating but not also the cooling fire phase, or *parametric curves* (also: *natural fire curves*). The former are defined by simple analytical expressions, e.g. from EN 1991-1-2 [2], and the latter are most often determined with the help of more or less advanced numerical procedures (for example in computer programs such as Ozone [10], FDS [11]..).

When a nominal fire curve of EN 1991-1-2 [2] is applied, this is chosen exclusively on the general type of the fire (i.e. cellulosic fire, external fire, or hydrocarbon fire) considering no other building's specifics. The so called *standard fire curve*, for example, represents the time evolution of temperatures within the affected fire compartment in typical cellulosic fires. These are common in typical office and/or residential buildings. Furthermore, the *external fire curve* is used for fire analyses of structural elements installed on the external side of buildings (e.g. beams of canopies *etc.*) which are normally exposed to flames from façade fires. Because in such a fire heat from the flame is constantly reduced by the cool external air, somewhat lower gas temperatures are normally applied with this curve compared to a curve of an inside building fire. Moreover, the *hydrocarbon curve* is used when analysing structural elements exposed to a hydrocarbon fire (e.g. to fire of an oil tank truck in a road tunnel, a fire in an industrial facility *etc.*).

In addition to nominal fire curves, parametric fire curves may be also applied to take into account several other building and fire parameters (e.g. the size of fire compartments, the amount and distribution of flammable materials, the size of openings of the building's envelope such aswindows and doors, which provide access to oxygen during a fire and increase burning rate, *etc*). This gives the parametric curves an important advantage over the nominal ones while substantially enhancing their accuracy.
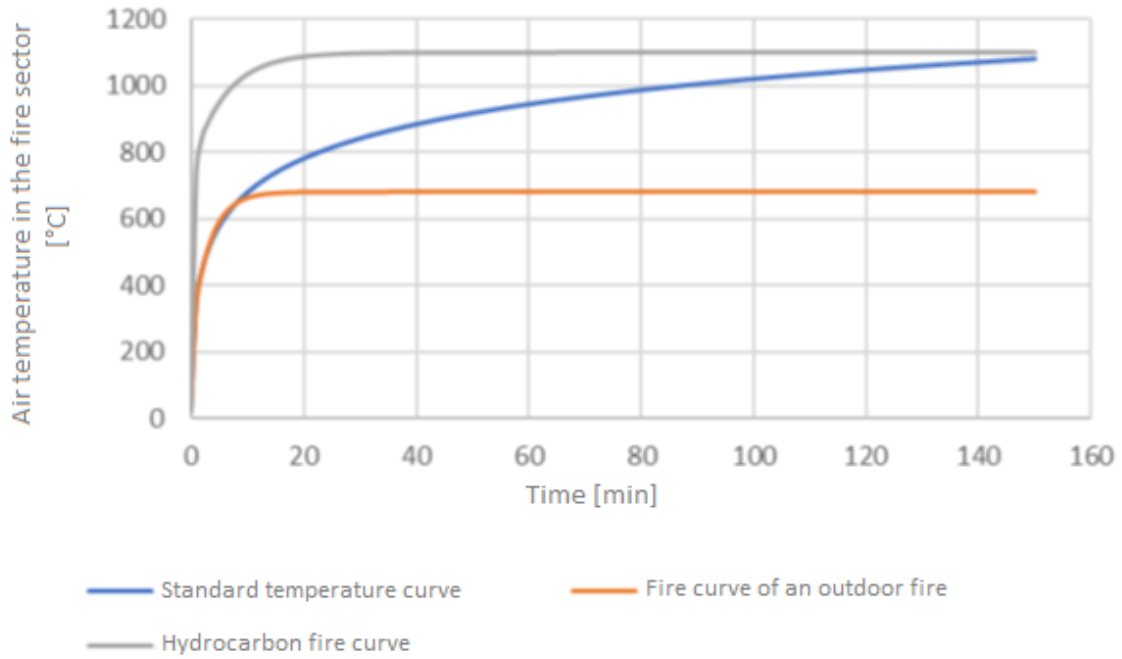

Figure 1: Graph of nominal fire curves according to EN 1991-1-2 [2]. The figure is taken from [3]

2.1.2. Direct impact Ad

Under the term direct impact of fire, we usually first think of a change in the mechanical properties of the material (strength, deformation at the achieved strength, deformation at the point of failure...) due to high temperature. According to EN 1992-1-2[1], new design values of mechanical properties can be calculated using the following equation:

$$X_{d,fi,\theta} = k_\theta \frac{X_k}{\gamma_{M,fi}}.$$ (3)

$X_{d,fi,\theta}$ is the structural mechanical property in case of fire or elevated temperature, k_θ is the temperature-dependent reduction factor,X_k is the characteristic value of mechanical property at a room temperature of 20°C and $\gamma_{M,fi}$ is a safety factor of material, which according to Eurocode instructions is equal to 1.

For concrete, coefficient k_θ depends on the type of concrete or aggregate (silicieous or calcelareous aggregate), and in the case of reinforcing steel, whether it is cold-formed or hot-rolled steel. Following EN 1992-1-2 [1] coefficients k_θ for concrete and reinforcing steel can be determined using the tables below.

Concrete temp. θ	Siliceous aggregates			Calcareous aggregates		
	$f_{c,\theta}/f_{ck}$	$\varepsilon_{c1,\theta}$	$\varepsilon_{cu1,\theta}$	$f_{c,\theta}/f_{ck}$	$\varepsilon_{c1,\theta}$	$\varepsilon_{cu1,\theta}$
[°C]	[-]	[-]	[-]	[-]	[-]	[-]
1	2	3	4	5	6	7
20	1,00	0,0025	0,0200	1,00	0,0025	0,0200
100	1,00	0,0040	0,0225	1,00	0,0040	0,0225
200	0,95	0,0055	0,0250	0,97	0,0055	0,0250
300	0,85	0,0070	0,0275	0,91	0,0070	0,0275
400	0,75	0,0100	0,0300	0,85	0,0100	0,0300
500	0,60	0,0150	0,0325	0,74	0,0150	0,0325
600	0,45	0,0250	0,0350	0,60	0,0250	0,0350
700	0,30	0,0250	0,0375	0,43	0,0250	0,0375
800	0,15	0,0250	0,0400	0,27	0,0250	0,0400
900	0,08	0,0250	0,0425	0,15	0,0250	0,0425
1000	0,04	0,0250	0,0450	0,06	0,0250	0,0450
1100	0,01	0,0250	0,0475	0,02	0,0250	0,0475
1200	0,00	-	-	0,00	-	-

Table 1: Mechanical characteristics of concrete with siliceous and calcareous aggregates at high temperatures (i.e. compressive strength compared to its initial value at ambient temperature, strain at peak stress, and ultimate strain at failure). Table is taken from EN 1992-1-2 [1].

| Steel Temperature | $f_{sy,\theta}/f_{yk}$ | | $f_{sp,\theta}/f_{yk}$ | | $E_{s,\theta}/E_s$ | |
$\theta\,[°C]$	hot rolled	cold worked	hot rolled	cold worked	hot rolled	cold worked
1	2	3	4	5	6	7
20	1,00	1,00	1,00	1,00	1,00	1,00
100	1,00	1,00	1,00	0,96	1,00	1,00
200	1,00	1,00	0,81	0,92	0,90	0,87
300	1,00	1,00	0,61	0,81	0,80	0,72
400	1,00	0,94	0,42	0,63	0,70	0,56
500	0,78	0,67	0,36	0,44	0,60	0,40
600	0,47	0,40	0,18	0,26	0,31	0,24
700	0,23	0,12	0,07	0,08	0,13	0,08
800	0,11	0,11	0,05	0,06	0,09	0,06
900	0,06	0,08	0,04	0,05	0,07	0,05
1000	0,04	0,05	0,02	0,03	0,04	0,03
1100	0,02	0,03	0,01	0,02	0,02	0,02
1200	0,00	0,00	0,00	0,00	0,00	0,00

Table 2: Mechanical characteristics of reinforcing steel at high temperatures compared to their initial values at ambient temperature, i.e. maximum stress level (strength of steel), proportional limit, and elastic modulus. Table is taken from EN 1992-1-2 [1].

The Term direct effects usually also refer to the thermal expansion to which the material tends due to the influence of high temperatures. The relative coefficient of expansion for concrete, which EN 1992-1-2 [1] designates as $\Delta l/l$, is defined here, for example, as:

Siliceous aggregates:

$$\varepsilon_c(\theta) = -1{,}8{\cdot}10^{-4} + 9{\cdot}10^{-6}\theta + 2{,}3\cdot10^{-11}\,\theta^3 \quad \text{for } 20°C \leq \theta \leq 700°C$$

$$\varepsilon_c(\theta) = 14\cdot\ 10^{-3} \quad \text{for } 700°C < \theta \leq 1200°C \tag{4}$$

Calcareous aggregates:

$$\varepsilon_c(\theta) = -\ 1{,}2\cdot10^{-4} + 6{\cdot}10^{-6}\theta + 1{,}4\cdot10^{-11}\,\theta^3 \quad \text{for } 20°C \leq \theta \leq 805°C$$

$$\varepsilon_c(\theta) = 12\cdot\ 10^{-3} \quad \text{for } 805°C < \theta \leq 1200°C \tag{5}$$

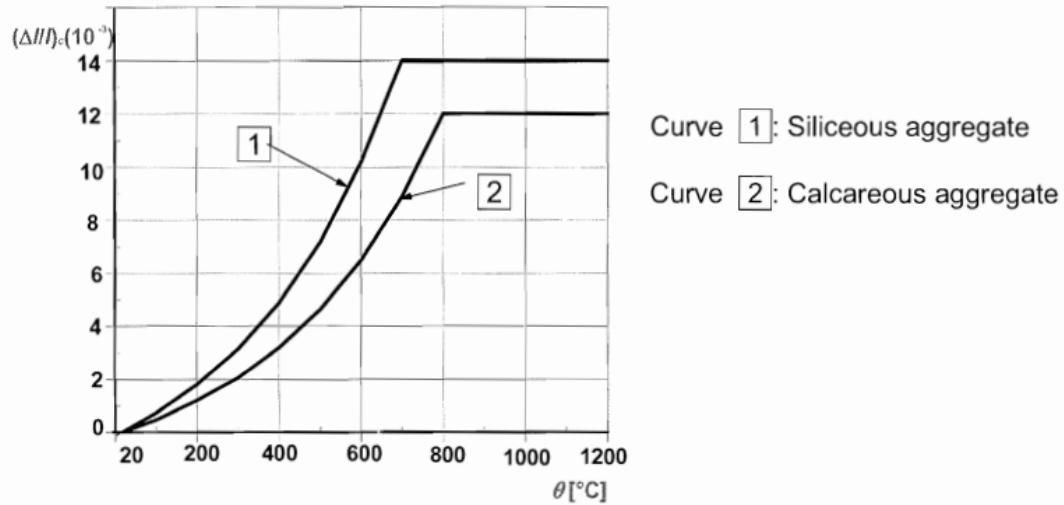Where θ is the concrete temperature (°C).

Figure 2: Total thermal elongation of concrete. Graph is taken from EN 1992-1-2 [1].

The relative coefficient of expansion for reinforcing steel is as:

$$\varepsilon_s(\theta) = -2{,}416{\cdot}10^{-4} + 1{,}2{\cdot}10^{-5}\theta + 0{,}4 \cdot 10^{-8}\,\theta^2 \quad \text{for } 20°C \leq \theta \leq 750°C$$

$$\varepsilon_s(\theta) = 11 \cdot 10^{-3} \quad \text{for } 750°C < \theta \leq 860°C$$

$$\varepsilon_s(\theta) = -6{,}2 \cdot 10^{-3} + 2 \cdot 10^{-5}\theta \quad \text{for } 860°C < \theta \leq 1200°C \tag{6}$$
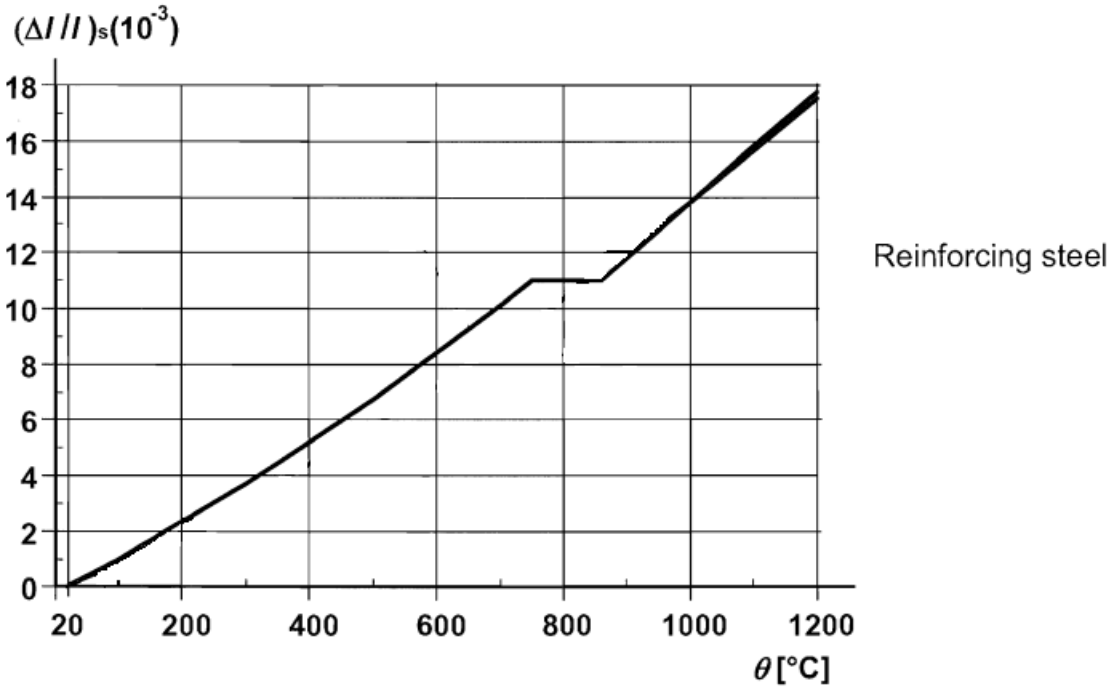
Figure 3: Total thermal elongation of reinforcing steel. Graph is taken from EN 1992-1-2 [1].

2.1.3. Indirect impact Ad

Indirect impacts are creep of concrete and reinforcement, restrained thermal deformations and spalling of concrete. They depend on the material and construction characteristics.

Creep is a phenomenon of an increase in deformations at constant stress within the cross-section. Tension is affected by mechanical and fire loads. The phenomenon is always more pronounced at higher temperatures. According to EN 1992-1-2 [1] we can assume, that the influence of high-temperature creep in the computational analysis is already indirectly included in the values of the reduction coefficients k_θ, shown in the above chapter 2.1.2, only if the heating rate of the material is between 2K/min - 50K/min. Otherwise, the Eurocode calculation procedures must be upgraded accordingly.

Within the overall structural system, thermal elongations of individual structural elements are often hindered in one way or another, which causes additional stress. This phenomenon is called *hindered (or restrained) temperature deformations*.

In what follows, another indirect fire action on a concrete structure will be discussed, i.e. *concrete spalling*. The text is taken from the work [5]. "Concrete is a composite of aggregate, cement stone and gel pores that are filled with chemically bound water. The remaining part is represented by capillary pores in which there is free water and air. When temperature of the material rises, water vaporizes first in concrete causing increase in internal pressure- and moisture concentration gradients, which evokes flow of free water, water vapor and dry air through the pores. In this way, heat passes through the interior of the concrete not only by conduction but also by convection. In addition, at around 200°C, dehydration (release of chemically bound water) occurs, which causes an accelerated deterioration of the material mechanical properties.

When flowing through the pores of the element, free water and gases travel partly towards the heated edge of the structural element and partly towards the colder interior of the element, where water vapor condenses. Especially in concretes with low permeability or high humidity (concrete structures of underground garages, tunnels, etc.), the condensation may lead toward a formation of a clogged zone. The result is an increase in pore pressures in front of the zone and an increase in the degree of damage to the material in this region (opening and propagation of concrete cracks). Over time, this can lead to phenomenon of a sudden detachment of the outer layers of the concrete element, which is called explosive spalling. The latter can result in a significantly increased exposure of the reinforcement to high

temperatures and, thus, in a reduction in fire resistance of the structural element. In extreme cases, the result of explosive spalling can even be a complete break in the contact between concrete and its steel reinforcement and an abrupt collapse of the element."
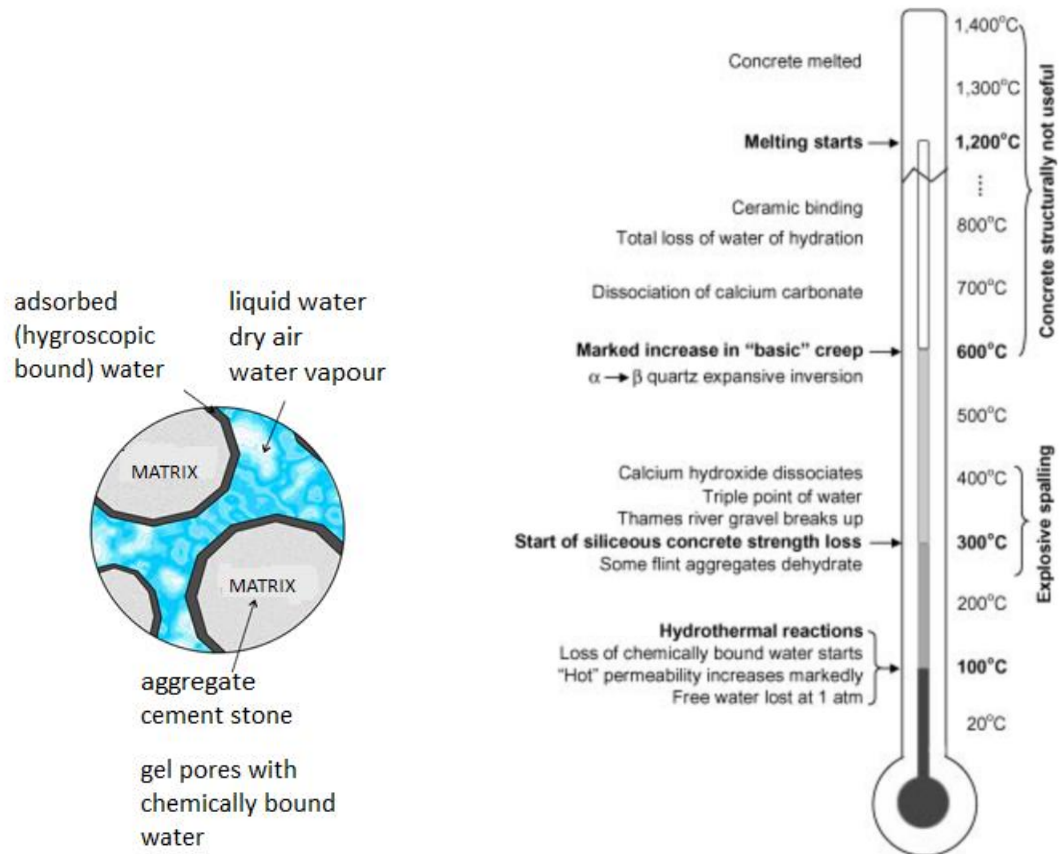

Figure 4: Left: scheme of microstructure of concrete (the image is taken from the source [13]), right: scheme of physicochemical processes in concrete during a fire (the image is taken from the source [14]).
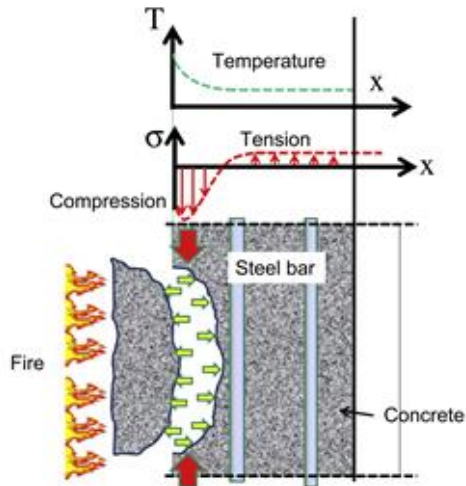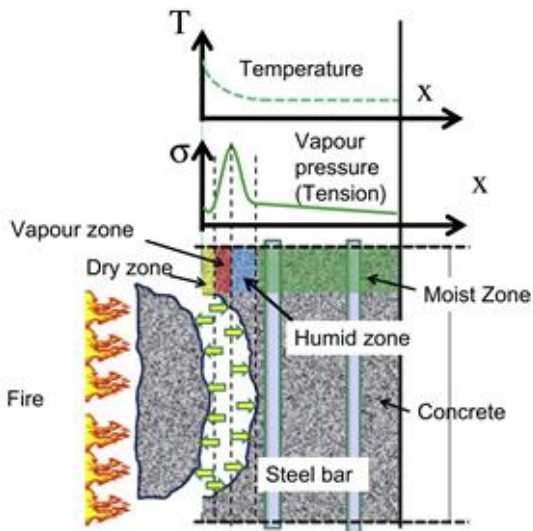
Fig. 1. Spalling mechanism: thermal dilation.

Fig. 2. Spalling mechanism: vapour pressure.

Figure 5: RC column loaded with fire. Left (above and below) scheme of the mechanisms of explosive cracking of the concrete (the image is taken from the source [27], right: photo of the damage to the post after the fire test (the image is taken from the source [15]).

Figure 6: Consequences of explosive cracking of concrete after a fire. (a) Tunnel under the canal after the fire in August 2008. (b) Mont Blanc tunnel after the fire in March 1999 (the image is taken from the source [16]).

2.2.   Meeting the criterion $R_{\text{fi,d,t}} \geq E_{\text{fi,d,t}}$ in cases of RC columns

The process of proving the criteria $R_{fi,d,t} \geq E_{fi,d,t}$ generally comprises three essential phases:

- determination of fire scenario (determination of temperature of the column's surrounding)
- thermal analysis of the structure
- mechanical analysis of the structure

2.2.1. Analysis of temperature of the column's surroundings

As we announced already in chapter 1 (Introduction), in this thesis we will focus only on the more accurate of the two general possibilities of determination of fire scenario, i.e. computer simulations of natural fires. More precisely, we will focus on the simulations that can be prepared with the widely known FDS (Fire Dynamics Simulator) software environment.

The following text of this chapter is summarised from sources [17],[18], and [4].

Computer simulation of a building fire in FDS

In [18], a description of a computer simulation of a building fire (referring explicitily to simulations put together in FDS [11] and softwares of similar modeling capabilities) is described as follows:

»Computer simulation of a fire means (i) simulation of the progressive ignition of combustible objects located within the fire compartment and the release of heat and gaseous products during their combustion; and (ii) simulation of the transport of released heat and smoke across the compartment and the rest of the building. The basis for the latter analyses (i.e. the analysis of the transport of heat and gases) are transport equations, also better known as numerical *models of fluid dynamics* (CFD models - "Computational Fluid Dynamics") *and thermal radiation*. Because these are the models also widely used in other scientific disciplines, such as in mechanical engineering and physics, historically they have received much scientific attention and are at date available for immediate use also in many of fire engineering softwares, e.g. FDS (Fire Dynamics Simulator). A complete contrast, however, are the models of ignition of combustible objects and the corresponding release of heat (*pyrolysis models*) and gases (*combustion models*). These models are still under an intense development and are at a date in a larger part still a responsibility of each fire safety designer.«

A general scheme of such a simulation with numerical models that it combines is shown in the figure below.
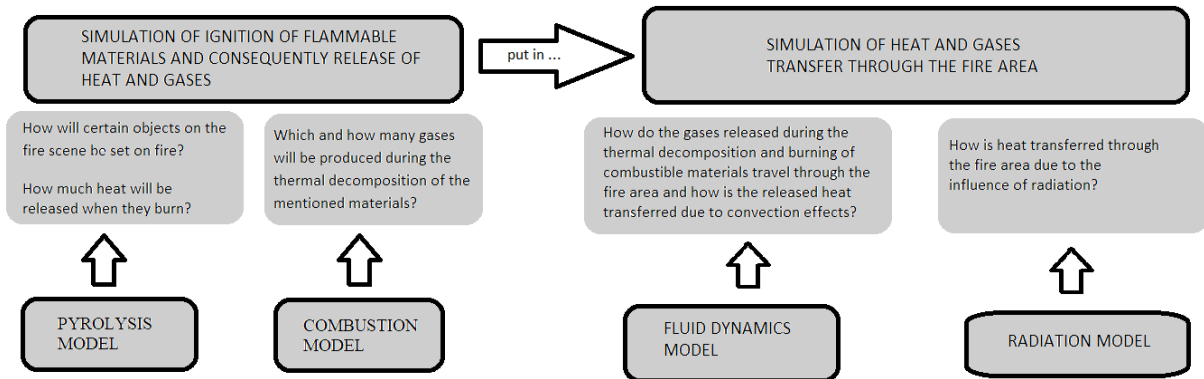
Figure 7: A general scheme of computer simulation of a building fire in FDS with numerical models that it combines.

Basic terms and definitions

Heating of a material that eventually leads toward its burning has basically three stages. In [4] definitions are given for each of them as follows below:

- **Thermal degradation** is defined as a chemical reaction that happens during heating of a material when a chemical substance falls apart into at least two chemical substances. The reaction is usually endothermic because heat is consumed to break chemical bonds in the material. Thermal degradation can produce volatile gases which diffuse into the surrounding air.

 Sticking to its precise definition, technically, thermal degradation is called *pyrolysis* if it happens in the absence of oxygen. Otherwise (re-gardless of the oxygen concentration) the process is called *thermolysis*. Nevertheless, throughout much of the relevant available literature (as also in this master's thesis), the term *pyrolysis* is used to describe thermal degradation at elevated temperatures both in inert ambient and in the presence of oxygen.

 The rate of pyrolysis is usually slower for charring materials, such as wood. Char creates an insulating surface layer that reduces penetration of heat into the core of the material. An example of a group of materials that, in contrast, do not char is the group of so called *thermoplastics*. These materials only soften and melt under high temperatures but no char is formed. After ignition, they burn similar to a liquid pool fire.

14

Two commonly used small-scale laboratory experiments for studying thermal degradation of a material are *TGA* (Thermogravimetric Analysis) experiment and *cone calorimeter* test.

TGA measures loss of mass during material heating in a small heating chamber (furnace). A very small sample of a material is typically used for this test to eliminate dependency of material heating to its material thermal properties, such as thermal conductivity (at every time of the experiment, temperature of the sample will, thus, be equal to temperature of the furnace). The change in mass that happens in this apparatus typically corresponds to loss of mass described via the well-known Arrhenius equation (see below for descriptions of this equation).

In a cone calorimeter (Figure *8*) a larger sample of the material is normally heated (i.e. sample of a floor size 10 cm × 10 cm and of a selected thickness). Usually, not all the volume of the sample is heated to a same temperature at the same time (unlike in a TGA experiment, namely, because of its larger size, penetration of heat into the sample will also depend on material thermal characteristics such as thermal conductivity). The sample is heated by a cone radiator (Figure *8*) and ignited with spark. The combustion gases are collected with hood and routed to gas analyzers. Beside combustion gases, which show on the nature of the combustion, the most important output of the equipment are also rate of heat release (HRR) and mass loss rate (MLR)..
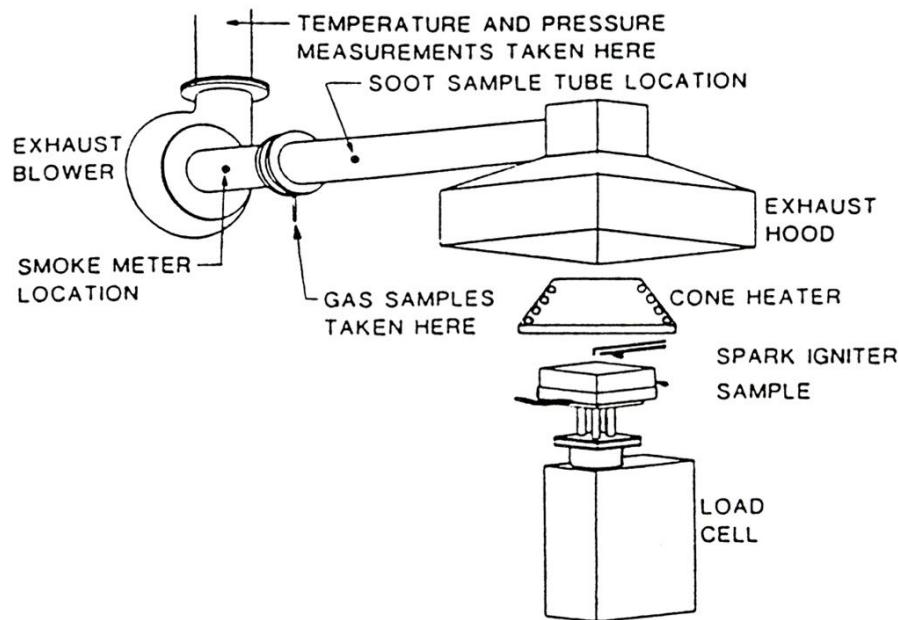

Figure 8: Standard cone calorimeter (figure taken from source [4]).

- **Combustion.** After the volatile gases being a result of thermal degradation are mixed with air and heated to the ignition temperature, combustion begins. This exothermic reaction happens in the gas phase. The heat from the reaction re-radiates to the original material and therefore propagates the thermal degradation reaction on the solid surface. The phenomenon is called *flaming combustion* if enough heat is accumulated to emit radiation in the visible spectrum.

- **Oxidation.** Oxidation usually happens at the end of flaming combustion and after it. This exothermic surface reaction, that cannot progress without oxygen, is only known for some materials (e.g. wood). Oxidation decreases the insulating char layer and (due to heat produced in the reaction) accelerates thermal degradation of the initial material.

Pyrolysis (thermal degradation) model

The pyrolysis rate of a solid material depends strongly on temperature and is in FDS typically represented by two important governing equations. The first one is the so called Arrhenius equation of the following general form:

$$\frac{dY}{dt} = -\sum_{j=1}^{N_j} A_j Y^{N_j} e^{-\frac{E_j}{RT}} Y_{O_2}^{N_{O_2}}. \tag{7}$$

The equation assumes that for each material there are several types of chemical bonds between molecules that break down at different temperatures, so the loss of material mass during pyrolysis is a combination of N_j different reactions. The following symbols are used in the equation:

- Y is the current mass of the material to its initial mas,
- Y_{O2} is the concentration of oxygen and N_{O2} is its corresponding coefficient,
- R is the universal gas constant (8.31431 J/K·mol),
- T is material temperature, and
- A_j, E_j and N_j are the *kinetic parameters* of the jth reaction:
    - A_j is called pre-exponential factor (unit s^{-1}),
    - E_j is activation energy (unit kJ/k·mol),
    - N_j is scalar reaction order.

Note that, typically, kinetic parameters A_j, E_j and N_j of the material are not determined in a physical manner (i.e. by some specific laboratory test or similar) but they are established by numerical fitting of the Arrhenius equation to results of TGA experiments. Often, the so called *genetic algorithms* are used here as a fitting tool. In order to capture different heating rates, that the material can be exposed to during a real fire, with one fixed value per each individual parameter, results of TGA experiments at different

heating rates should be used in the numerical fit. The results of the fit should be within tolerable limits for all of the gathered TGA data.

Furthermore, the second equation governing the pyrolysis model in FDS is the classic Fourier equation of heat conduction:

$$\rho c_p \frac{dT}{dt} = \frac{\partial}{\partial x} k \frac{\partial T}{\partial x} + \dot{q}_s''' \ . \tag{8}$$

Here x is the direction of heat transfer through the substance and $\dot{q}_s'''$ is the internal heat source representing heat of reaction of the above mentioned N_j internal reactions. ρ, c_p, k are *thermal parameters* (density of the solid, its specific heat, and its thermal conductivity). These are determined via a numerical fit of the pyrolysis model to results of cone calorimeter experiments. Because in an FDS fire simulation different possible circumstances of material burning will need to be captured with only one fixed set of parameters' values, cone calorimeter experiments should be carried out at different heat fluxes of the cone radiator (and possibly also for different oxygen concentration) and the numerical fit should be within tolerable limits for all of the gathered experimental data.
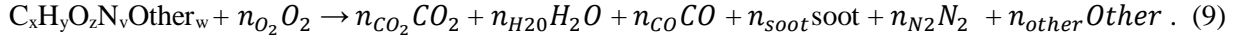
For more information on derivation of kinetic and thermal parameters of a material ($\rho, c_p, k, A_j, E_j, N_j$, where $j = 1, \ldots, N_j$) for FDS, see, e.g., [4].

Note: As already pointed out above, material kinetic and thermal parameters for FDS are not normally measured in a physical manner (i.e. by some laboratory tests) but they are defined through a numerical fit of the FDS pyrolysis model (governed by Arrhenius and the classic Fourier equation) first to results of TGA experiments and later to results of cone calorimeter tests. In other words, during the fitting, the applied fitting tool (e.g. genetic algorithm) will call FDS for creating TGA and cone calorimeter tests simulations. Although at least for fitting the TGA data, it would be easier to simply solve the Arrhenius equation without the simulator, using it makes sure that the solution is applicable to FDS for later use. On the same time, this also means, that the values of the determined kinetic and thermal parameters might be FDS-version specific. It is a responsibility of the FDS user to check this prior to implementing the selected parameters within an FDS simulation if this was prepared with a different FDS version than the one which was used for fitting the parameters. Namely, it should be kept in our minds, that the general form of FDS equations invoked by a TGA and/or a cone calorimeter simulation can reform over the FDS versions.

Combustion model

Combustion model defines the equation of chemical reaction in the gaseous phase, i.e. the reaction of fuel vapor and oxygen (*stoichiometric equation*). Two possible ways of such definition are available in FDS,

i.e. simpler *mixture fraction model* and the more complex *finite rate combustion model*. For purposes of this thesis the former will be used. As stated in the FDS User's guide [11], using the mixture fraction model, the reaction is assumed to be of the form:

$$C_xH_yO_zN_vOther_w + n_{O_2}O_2 \rightarrow n_{CO_2}CO_2 + n_{H20}H_2O + n_{CO}CO + n_{soot}\text{soot} + n_{N2}N_2 + n_{other}Other . \quad (9)$$

The FDS user only needs to specify the chemical formula of the fuel along with the yields of CO, soot, and H_2, and the amount of hydrogen in the soot. For completeness the N_2 content of the fuel and the presence of other species can be defined as well. FDS will use that information internally to calculate the amount of combustion products that are formed.

2.2.2. Thermal analysis of the column

This analysis calculates the column temperature change with the selected fire curve or selected fire scenario. We have to take into account the geometric properties of the column and the thermal properties of the concrete material (thermal conductivity, density, specific heat of concrete). The result of the analysis is the temperature field of the column T(x,y,z,t) depending on time and location, which is often simplified in the form T(y,z,t) (coordinate axes y and z are considered axes in the plane of the cross-section of the column). In such a simplification, we assume that the temperature around the column at a certain moment of fire is the same in height and around the column and therefore the temperature of the column itself changes only according to its cross-section. A common alternative is to divide the area around the column by height into two typical areas (thermal zones), first a hotter upper zone and a second cooler lower zone, with a different fire curve prescribed for each of them. Here we take into account the fact that in real fires inside buildings, the air temperatures below the ceiling are higher than those at the ground (warmer air rises due to buoyancy, and cooler air descends). Less often, we decide to consider more than two areas (thermal zones) per column height.

Normally, thermal analysis of an RC column is based on recognized principles, assumptions and equations of the theory of non-stationary transfer of heat through solid bodies, bearing in mind that such transfer can take place by *conduction, radiation* and/or *convection*. The governing equation of the theory is the classic Fourier partial differential equation:

$$V: \quad \frac{\partial}{\partial x_i}\left(\lambda_{ij}\frac{\partial T}{\partial x_j}\right) + Q - \rho c\frac{\partial T}{\partial t} = 0 ; (i,j = 1,2,3) . \quad (10)$$

The symbols used in the above equation represent the following:

- T represents temperature of an individual point of the column [°C],
- λ_{ij} is a component of the thermal conductivity tensor of concrete [W/mK],
- Q is specific volume heat flux [W/m³],
- ρ is density of concrete [kg/m^3],
- c is specific heat of concrete [J/kgK],

Thermal conductivity of concrete varies with material temperature (*Figure 9*). In EN 1992-1-2 [1], the following equations are given to describe this change for temperatures between 20°C and 1200°C:

- upper limit:

$$\lambda_c = 2 - 0{,}2451 \left(\frac{T}{100}\right) + 0{,}0107 (\frac{T}{100})^2 \quad \text{[W/mK]} \tag{11}$$

- lower limit:

$$\lambda_c = 1{,}36 - 0{,}136 \left(\frac{T}{100}\right) + 0{,}0057 (\frac{T}{100})^2 \quad \text{[W/mK]} \tag{12}$$

Specific heat of concrete also varies with temperature as well with the content of moisture in the material. Accordingly, EN 1992-1-2 [1] provides the following equation (*Figure 10*):

- content of moisture is 0% by weight of concrete:

$$c_p = 900 \text{ [J/kgK]; 20°C} \leq \text{T} \leq 100\text{°C} \tag{13}$$

$$c_p = 900 + (T - 100); \text{ [J/kgK]; 100°C} < \text{T} \leq 2\,00\text{°C} \tag{14}$$

$$c_p = 1000 + \frac{T-200}{2}; \text{ [J/kgK]; 200°C} < \text{T} \leq 400\text{°C} \tag{15}$$

$$c_p = 1100; \text{ [J/kgK]; 400°C} < \text{T} \leq 1200\text{°C} \tag{16}$$

- content of moisture is 1.5% by weight of concrete:
  Generally the same equations apply as for 0% moisture content with one essential difference. I.e. at 100 ° C the specific heat suddenly rises to 1470 (J/kgK), after that it is remaining constant (i.e. at the value of 1470 J/kgK) on the interval [100°C, 115°C], finally it is decreasing linearly to 1000 (J/kgK) on the interval [115°C, 200°C].

- content of moisture is 3.5% by weight of concrete:

The same holds true as in the case of 1.5% content of moisture. The only difference here is that the specific heat at 100°C increases to 2020 (J/kgK).
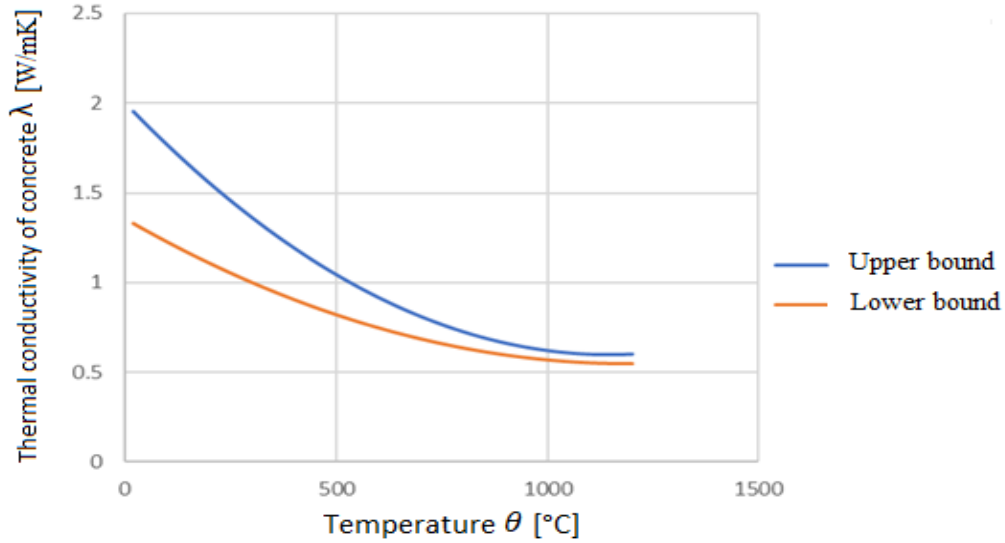

Figure 9: Thermal conductivity of concrete λ_c [W/mK] as a function of temperature as defined in EN 1992-1-2 [1]. The figure is taken from [3].
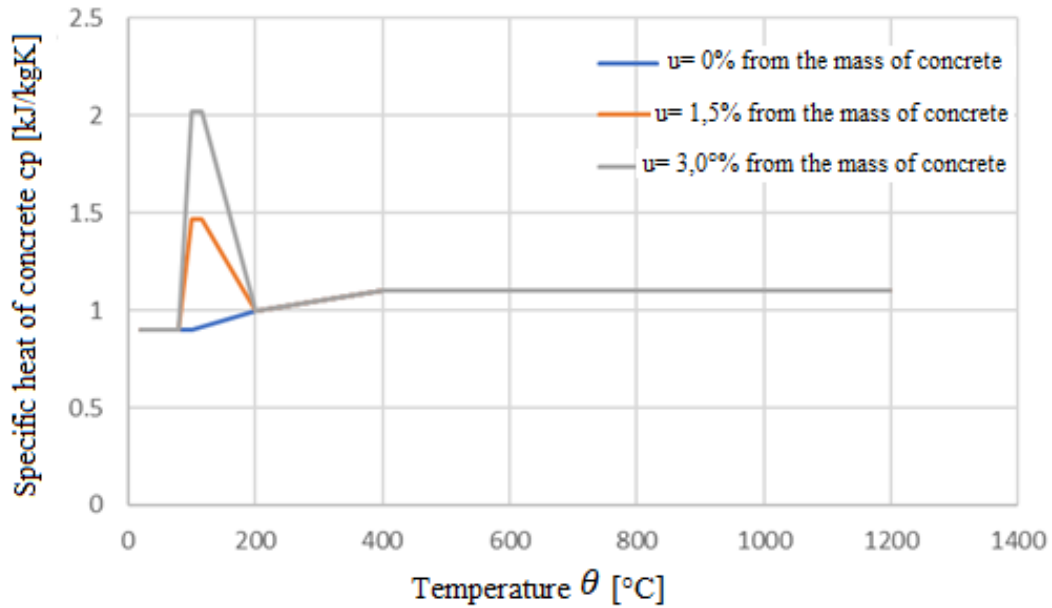

Figure 10: Specific heat c_p [kJ/kgK] as a function of temperature as defined in EN 1992-1-2 [1]. The figure is taken from [3].

20

Similar to thermal conductivity and specific heat, density of concrete also changes with temperature, although these changes are much less pronounced and usually do not significantly affect results of the calculation. In this thesis a constant value of 2500 kg/m³ will be assumed for density of concrete.

Furthermore, for solving the classic Fourier equation as written at the beginning of this section, it is important to define appropriate boundary conditions determining the flow of heat at the solid boundary (i.e. at the surface of the solid):

$$S_d: \lambda_{ij} \frac{\partial T}{\partial xi} n_i = q_s \tag{17}$$

The following symbols are used in the above equation:

- S_d is surface of the solid throughout the heat is penetrated by convection or radiation,
- n_i is the ith component of the unit vector of the normal to the surface,
- q_s is specific surface heat flux [W/m²] where this is defined as the sum of two fluxes, i.e. convective and radiative:

$$q_s = q_{s,c} + q_{s,r} \text{ , with:}$$

$$q_{s,c} = \alpha_c (T_g + T_m)$$

$$q_{s,r} = \varepsilon_m \sigma [(T_g + 274)^4 - (T_m + 274)^4]. \tag{18}$$

The variables and coefficients of the last two equations are as follows:

- α_c is convective heat transfer coefficient [W/m²K]; for natural fires this equals 35 W/m²K (fire–exposed side of the structure) or 9 W/m²K (unexposed side) according to EN 1991-1-2 [2]
- T_g is temperature of the surroundings of the structure that the structure is exposed to during the fire [°C],
- T_m is surface temperature of the structure [°C],
- ε_m is surface emissivity of the structure [–]; this can be taken as 0.7 for concrete structures according to instructions of EN 1992-1-2 [1]
- σ is the Stefan–Boltzmann constant.

In addition to suitable boundary conditions, initial conditions (initial temperatures of the structure) need to be prescribed as well for solving the governing Fourier equation. Usually this is given in the following general form:

$$V: T(t = 0) = \theta_0 \tag{19}$$

where:

- V is volume of the solid and
- θ_0 is its initial temperature [°C].

In general, the Fourier equation of non-stationary heat transfer as discussed above cannot be solved analytically. Thus, numerical methods are applied (FEM, differential method, *etc.*) exploiting capabilities of relevant softwares, such as ABAQUS [19], ANSYS [20], SAFIR [21] and others.

2.2.3. Structural analysis of the column

In a fire, a RC column will essentially collapse because of one of two possible reasons: (i) loss of the cross-sectional load–bearing capacity (collapse due to excessive stress in the cross-section exceeding material strength at a specific material temperature) or (ii) buckling of the column and consequential loss of its stability. Which one of the two mentioned ways of collapse will be trigerred first, however, will be affected by the column's slenderness. The latter will change over time as an indirect result of high concrete temperatures causing, for example, gradual reduction of material strength in the outer (hotter) layers of the column, detachment of these layers on account of concrete spalling *etc*.

In what follows, three selected possible calculation procedures will be presented for assessment of fire resistance of RC columns – all of them accounting for both possible mechanisms of structural collapse (cross–sectional collapse or buckling). The first two procedures are simplified procedures where the so called second order theory is used to account for the column's deformations and the temperatures of the cross–section and the corresponding strengths of materials are accounted for in a more (*simplified procedure 2*) or less (*simplified procedure 1*) exact manner. The third procedure is a more *advanced procedure* which is not only based on a detailed consideration of material temperatures but also on description of column's deformations according to the most advanced third-order theory.

The following text is taken mainly from source [3].

Simplified procedure 1

This procedure is a representative of the so-called *reduced cross-section procedures* where the reduced area of the concrete part of the column's cross-section is to be determined first for the observed time of the fire under our consideration. This is done by the so called 500°C isotherm method. The 500°C isotherm method assumes that the strength and elastic modulus of concrete are fully preserved up to

concrete temperature of 500°C (they remain the same as at the concrete initial temperature, i.e. as at around 20°C). But at temperatures above 500°C the load capacity of concrete is lost entirely. After the reduced concrete cross-section (i.e. concrete area enclosed by the 500°C isotherm) is known, the load-bearing capacity of the column is checked by generally the same procedures that are known well from basic design of slender RC columns in permanent design situations. Only the reduced part of concrete is considered here and this is assumed to preserve its initial temperature. Reinforcement bars, however, are considered with actual steel temperature (thus, mechanical characteristics of rebars are properly reduced).

The details of the procedure that follows after determination of cross-sectional temperatures and the corresponding reduced concrete area is presented step by step below.

- *Step 1:* determination of axial internal force $N_{Ed,0}$ and bending moment $M_{Ed,0}$ in the column for load combination for fire design situation according to the first-order theory (accounting for equilibrium of forces on undeformed structure)

- *Step 2:* determination of the first-order bending moment capacity of the column M_{Rd0} using the predefined M- κ relationship

Despite the fact that RC columns are normally predominantly affected by an axial force, a certain bending moment usually also evolves in these structural elements. The latter is true also if only vertical external loads are applied on the building (e.g. permanent, snow load…). In such cases in the undeformed state of the structure, the initial bending moment in the column may evolve due to: (i) eccentricity of the axial loads acting on the column[1] and/or (ii) initial geometric imperfections of the column. In the deformed position of the column, the bending moment may increase further because of the increase of curvature of the column and the corresponding increase in eccentricity of the axial load acting on the column (Figure *11*).

---

[1] Position of the resultant of surface loads distributed across the neighbouring upper (floor or roof) slab which transfers to the observed column, often does not match exactly with the center of the column's cross-section.

(a)   (b)
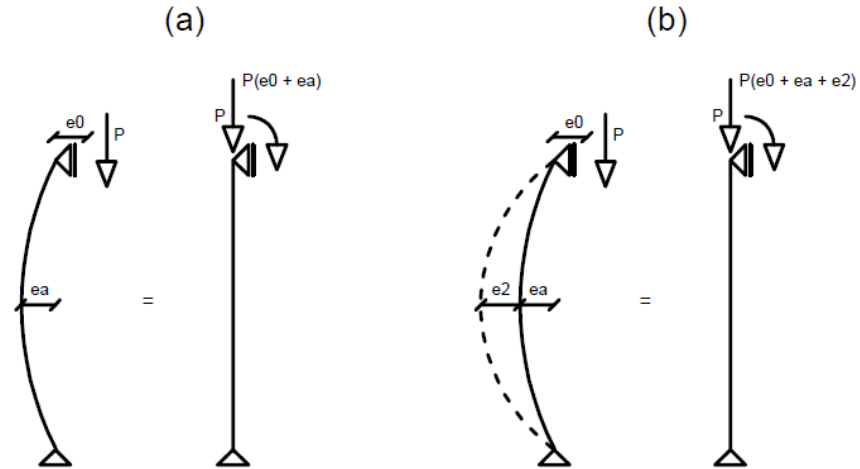
e0 - the eccentricity of the external force P in relation to the center of gravity of the cross section of the column
ea - the initial geometric imperfection of the column
e2 - the horizontal movement of the column at the middle of its height, which occurs during deformation due to
the bending load of the column due to the force P on the leg other than zero

Figure 11: (a) Left: Eccentric compressive axial force P acting on an imperfect column in the initial (undeformed) position. Right: corresponding calculation model (i.e. the column is modeled as a perfectly straight element exposed to a centric axial force P and, additionally, to a suitable bending moment). (b) Force P acting on the column in the deformed position and the corresponding calculation model.

Together with the increase of the column's internal bending moment M, the curvature of the column κ increases simultaneously following a typical M- κ curve as shown in the figure below.
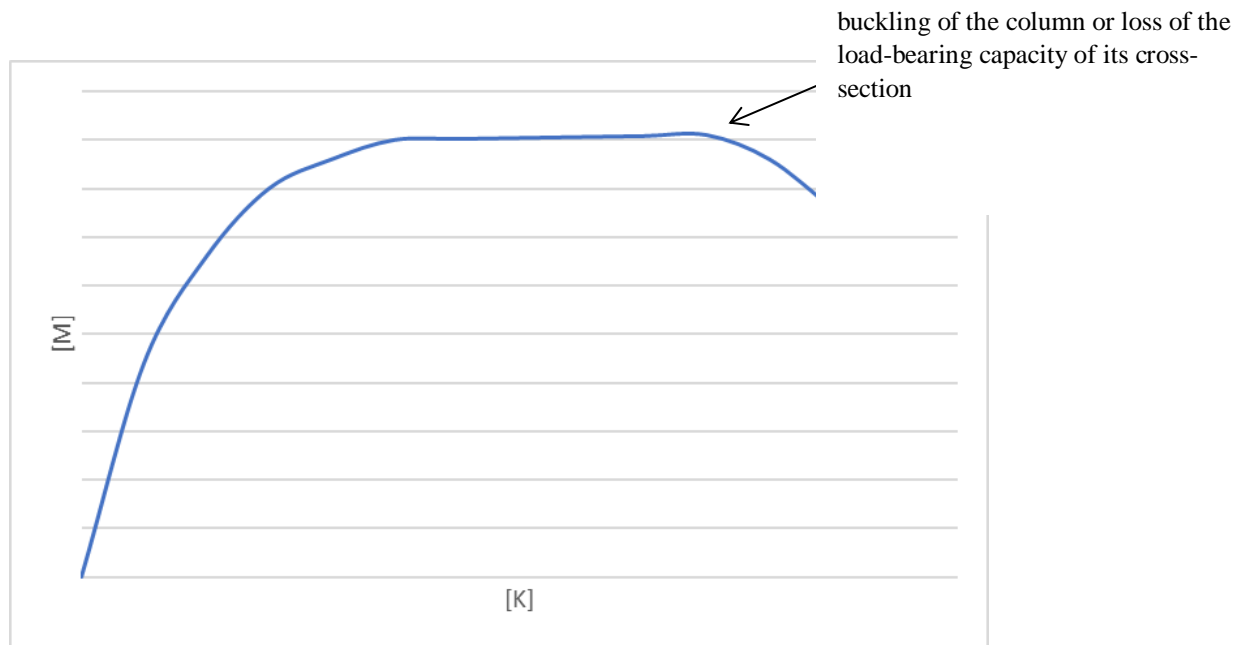
Figure 12: Typical M- κ curve for a RC column deformed by fixed axial and variable bending loads. Figure is taken from [3].

The *M-* κ curve is very useful in the process of design of the column because it defines the column's flexural (bending moment) capacity at a specific value of its axial force. The capacity should, obviously, be read from the point of the curve where the latter is passing into its descending part. This is the point of collapse of the column which comes due to buckling of the column or due to exceeded cross-sectional capacity.

-   *Step 2a:* determination of *M-* κ relationship

    The *M-* κ curve is determined iteratively by a gradual calculation of its individual points. A point of the curve is calculated by first selecting the value of κ in this point (e.g., for the first point, κ will be set to 0, for the next ones κ will be gradually increased) and then calculating the corresponding value of moment *M*. If *M* is representing internal bending moment about y-axis, its calculation is done by the following procedure (if it is representing internal moment about z-axis, the procedure is analogous):

    ➢ Firstly, the longitudinal strain of the column in a generic point of its cross-section is given in terms of the *Bernoulli's hypothesis*. The latter states that at any given time cross-sections of any beam-like structural element remain undeformed and perpendicular to the longitudinal axis of the element, thus:

25

$$\varepsilon\ (y,\ z) = \varepsilon_o + z \cdot \kappa \tag{20}$$

In the equation above, κ and z are known quantities, but the value of ε_0, which represents the longitudinal strain of the column at the centroid of its cross-section, is unknown. Furthermore, $\varepsilon\ (y,\ z)$ is longitudinal strain in point (x,z) which refers to concrete or a reinforcing bar. We assume that at the position of a reinforcement bar (y_s, z_s), concrete strain equals to rebar strain, thus: $\varepsilon_C\ (y_s, z_s) = \varepsilon_S\ (y_s, z_s)$.

Additionally, we also consider that at elevated temperatures longitudinal strain $\varepsilon\ (y,\ z)$ equals to a sum of two parts, i.e. mechanical strains and thermal strains with the latter being a consequence of thermal expansions of the material, thus:

$$\varepsilon\ (y,\ z) = \varepsilon_o + z \cdot \kappa = \varepsilon_m\ (y,z) + \varepsilon_{th}\ (y,z)\ . \tag{21}$$

According to EN 1992-1-2 [1] temperature strains $\varepsilon_{th}\ (y,z)$ can be calculated as $\varepsilon_{th}\ (y,z) = \alpha_T\ \Delta T\ (y,z)$, where α_T is relative thermal expansion coefficient, marked as $\Delta l/l$ in Eurocode, as has been already presented previously in the thesis (see Section 2.1.2).

➢ Secondly, stress−mechanical strain relationships for concrete and reinforcing steel at elevated temperatures $\sigma_c(\varepsilon_{m,c})$ and $\sigma_s(\varepsilon_{m,s})$ are collected from EN 1992-1-2 [1] (see the two figures below and Section 3.2 of the standard).
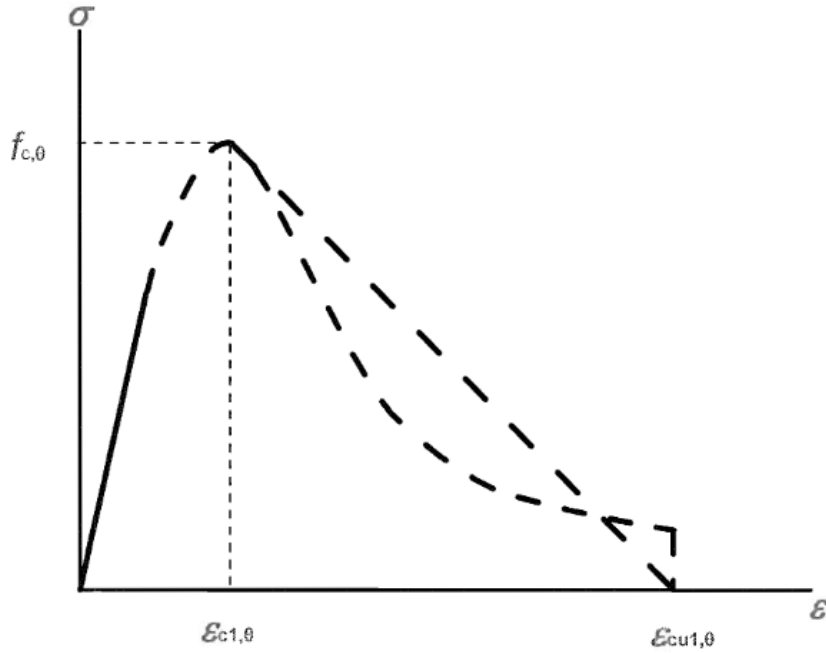
Range	Stress $\sigma(\theta)$
$\varepsilon \leq \varepsilon_{c1,\theta}$	$$\dfrac{3\varepsilon\, f_{c,\theta}}{\varepsilon_{c1,\theta}\left(2+\left(\dfrac{\varepsilon}{\varepsilon_{c1,\theta}}\right)^{3}\right)}$$
$\varepsilon_{c1(\theta)} < \varepsilon \leq \varepsilon_{cu1,\theta}$	For numerical purposes a descending branch should be adopted. Linear or non-linear models are permitted.

Figure 13: Stress-strain relationships of concrete under compression at elevated temperatures according to EN 1992-1-2 […]. Figure is taken from EN 1992-1-2 [1]. Note: symbol ε corresponds to symbol ε_m as used in this thesis.
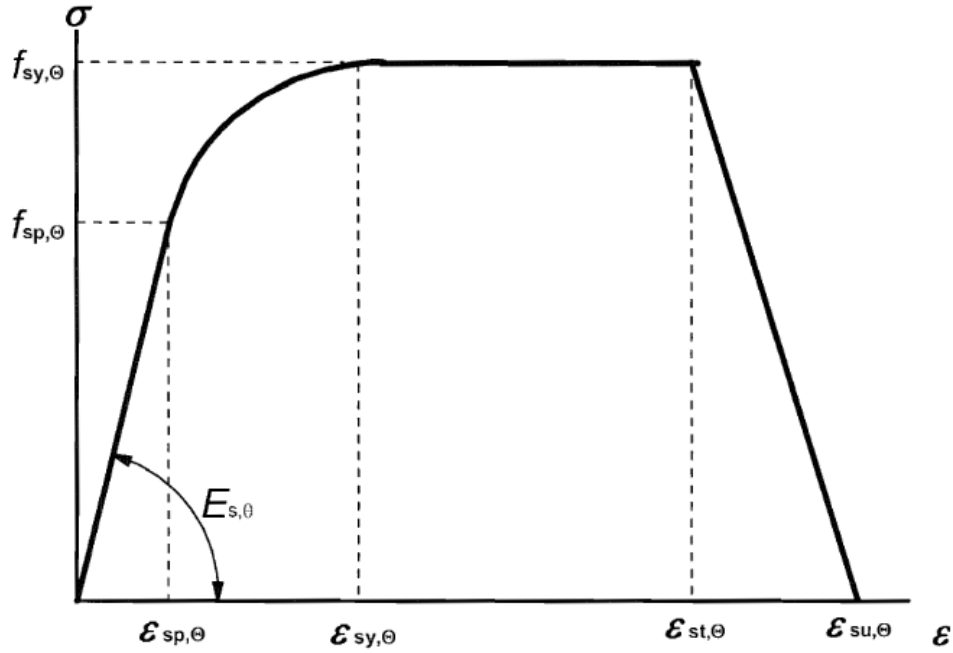
Range	Stress $\sigma(\theta)$	Tangent modulus
$\varepsilon_{sp,\theta}$	$\varepsilon\, E_{s,\theta}$	$E_{s,\theta}$
$\varepsilon_{sp,\theta} \leq \varepsilon \leq \varepsilon_{sy,\theta}$	$f_{sp,\theta} - c + (b/a)[a^2 -(\varepsilon_{sy,\theta}- \varepsilon)^2]^{0,5}$	$\dfrac{b(\varepsilon_{sy,\theta} - \varepsilon)}{a\left[a^2 -\left(\varepsilon - \varepsilon_{sy,\theta}\right)^2 \right]^{0,5}}$
$\varepsilon_{sy,\theta} \leq \varepsilon \leq \varepsilon_{st,\theta}$	$f_{sy,\theta}$	0
$\varepsilon_{st,\theta} \leq \varepsilon \leq \varepsilon_{su,\theta}$	$f_{sy,\theta}\,[1-(\varepsilon - \varepsilon_{st,\theta})/(\varepsilon_{su,\theta} - \varepsilon_{st,\theta})]$	-
$\varepsilon = \varepsilon_{su,\theta}$	$0,00$	-
Parameter *)	$\varepsilon_{sp,\theta} = f_{sp,\theta}\,/\,E_{s,\theta} \qquad \varepsilon_{sy,\theta} = 0,02 \qquad \varepsilon_{st,\theta} = 0,15 \qquad \varepsilon_{su,\theta} = 0,20$ Class A reinforcement: $\qquad \varepsilon_{st,\theta} = 0,05 \qquad \varepsilon_{su,\theta} = 0,10$	
Functions	$a^2 = (\varepsilon_{sy,\theta} - \varepsilon_{sp,\theta})(\varepsilon_{sy,\theta} - \varepsilon_{sp,\theta} +c/E_{s,\theta})$ $b^2 = c\,(\varepsilon_{sy,\theta} - \varepsilon_{sp,\theta})\,E_{s,\theta} + c^2$ $c = \dfrac{\left(f_{sy,\theta}-f_{sp,\theta}\right)^2}{\left(\varepsilon_{sy,\theta} - \varepsilon_{sp,\theta}\right)E_{s,\theta} - 2\left(f_{sy,\theta} -f_{sp,\theta}\right)}$	

Figure 14: Stress-strain relationships of reinforcing steel at elevated temperatures according to EN 1992-1-2 [1]. Figure is taken from EN 1992-1-2 [1]. Note: symbol ε_s corresponds to symbol ε_m as used in this thesis.

➤ Thirdly, the relationships $\sigma_c(\varepsilon_{m,c})$ and $\sigma_s(\varepsilon_{m,s})$ are implemented into the known constitutional equation of beam-like structural elements defining that the axial force in the cross-section of the element is equal to the cross-sectional integral of longitudinal normal stresses σ [22]:

$$N = \int_A \sigma\,(y,z)dA = \int_{Ac} \sigma_c\,(y,z)\,dA_c + \int_{As} \sigma_s\,(y,z)\,dA_s \,. \tag{22}$$

Here we account for the fact that the column's cross-section consists of two parts: the concrete part (section A_c) and the part occupied by the steel reinforcement (section A_s).

Since the applied stress-strain relationship for concrete $\sigma_c(\varepsilon_{m,c})$ is a rather complex mathematical function, its integration according to A_c is usually solved in a simplified manner by dividing the concrete part of the cross-section into smaller parts, e.g., to smaller rectangles (*Figure 14*). An assumption of stress being in each point of a specific rectangle area equal to stress in the centroid of this area is made for each of them, what simplifies our last equation to the following form:

$$N = \int_A \sigma\,(y,z)dA = \sum_{A_{c,i}} \sigma_{c,i} A_{c,i} + \sum_{A_{s,j}} \sigma_{s,j} A_{s,j} \,. \tag{23}$$

Here $\sigma_{c,i}$ is stress at the centroid of each rectangle part of the concrete section, $A_{c,i}$ is the surface of this part, $\sigma_{s,j}$ is stress in the j-th longitudinal reinforcing bar of the column, and $A_{s,j}$ is the corresponding cross-sectional area of this rebar.

➤ Furthermore, the actual value of the axial force in the column is inserted in the above equation as calculated in step 1 of the procedure ($N = N_{Ed,0}$). Then, for calculation of the only remaining unknown ε_0, expression is derived from this modified equation.

➤ After the value of ε_0 is known, we can finally determine the moment M corresponding to the initially selected value of κ:

$$N = \int_A \sigma(y,z) \cdot z \, dA = \sum_{A_{c,i}} \sigma_{c,i} \, z_{c,i} \, A_{c,i} + \sum_{A_{s,j}} \sigma_{s,j} \, z_{s,j} \, A_{s,j} \qquad (24)$$

Here $z_{c,i}$ and $z_{s,j}$ are coordinates of centroid of individual rectangle part of the concrete cross-section and of individual reinforcing bar.
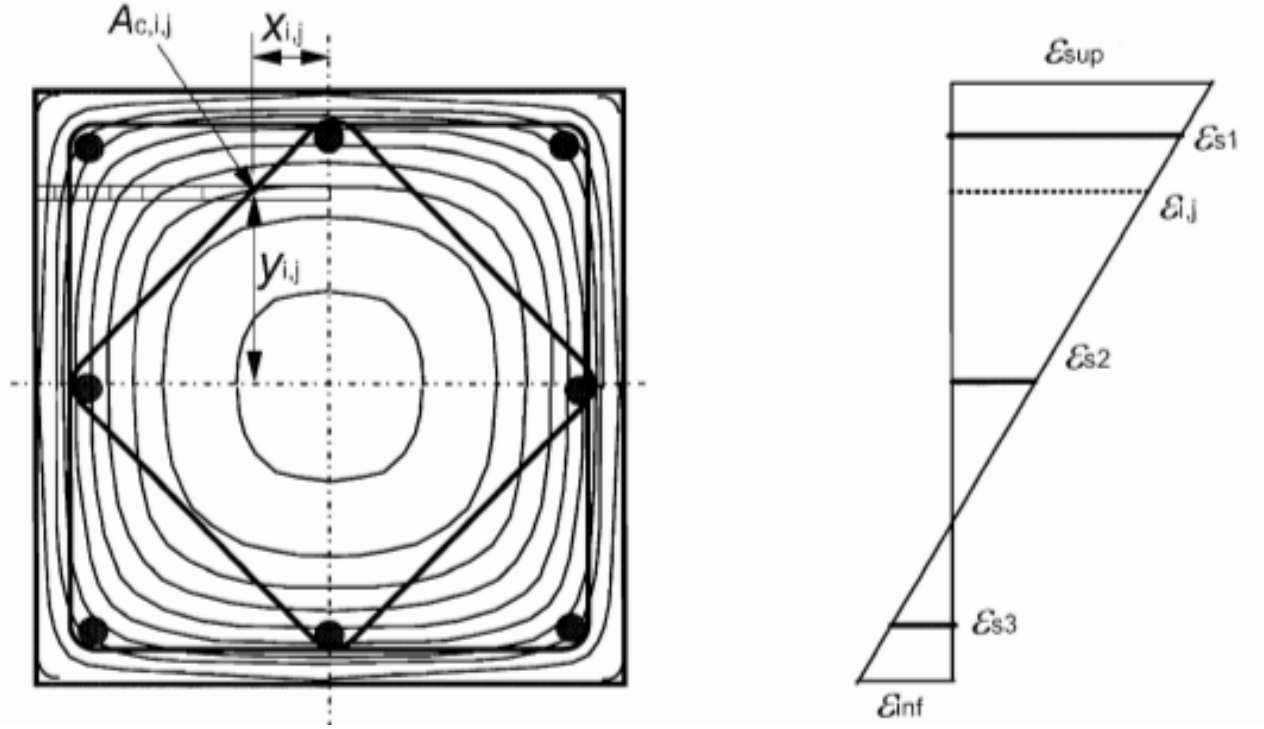

Figure 15: Division of concrete cross-section into subzones (figure taken from EN 1992-1-2 [1]).

➤ The equations for *N* and *M* derived previously are not analytically solvable but we can solve them numerically, e.g., using the tool *FindMKappa* [23]. This tool will be used also for purposes of this thesis.

- *Step 2b:* determination of the first-order bending resistance of the column M_{Rd0}
  In the *M-κ* curve, derived in step 2a, the maximum value of *M* is the bending resistance of the column determined for its deformed configuration (i.e. M_{Rd}). Thus, comparison of this value of *M* towards M_{Ed0} from step 1 of the procedure will not be possible in a direct manner. Recall that

M_{Ed0} was calculated according to the first-order theory meaning taking into account equilibrium of forces on undeformed column's configuration. Relationship (curve) M_0- κ should, thus, be derived as well, e.g., as suggested by [1]:

$$M_0 = M - M_2 \tag{25}$$

Here M is the second-order theory bending moment corresponding to a specified curvature κ, M_0 is the corresponding first-order theory moment, and M_2 is the nominal second-order moment. The latter can be determined by the equation:

$$M_2 = N_{Ed,0} e_0 \text{ , where} \tag{26}$$

$$e_2 = \frac{1}{r} l_0^2 \frac{1}{c} \tag{27}$$

In the last equation, $\frac{1}{r}$ is curvature of the column (=κ), l_0 is its buckling length (calculated according to EN 1992-1-1 [1], section 5.8.3.2), c is coefficient with value c ≈ 10.

Obviously, the ultimate first order moment capacity M_{Rd0} will be equal to the maximum value of moment M_0 found on the M_0- κ curve (i.e. the value of M_0 just before this curve takes a downward turn).
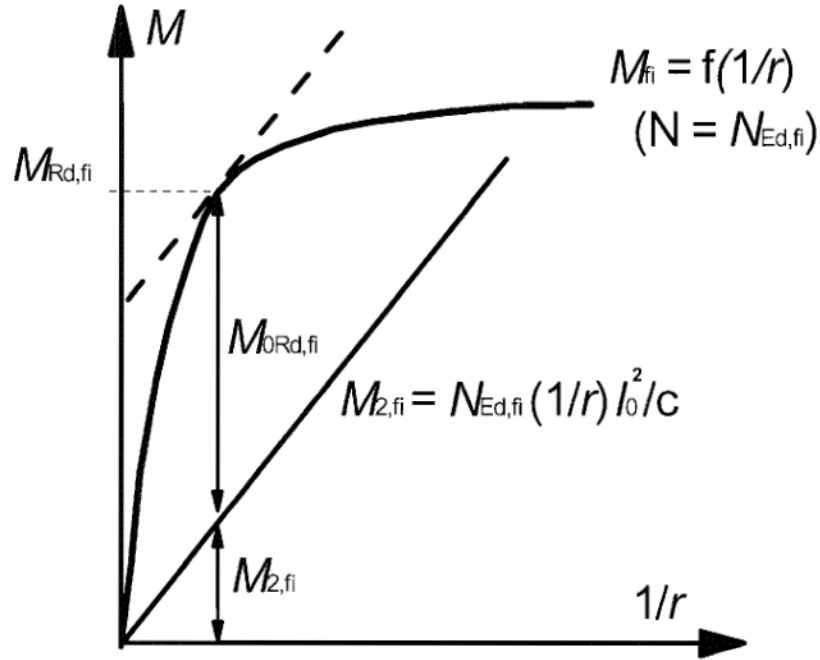
Figure 16: Schematic presentation of determination of the ultimate second-order and the ultimate first-order moment capacity of the column (M_{Rd} and M_{0Rd}) as suggested by EN 1992-1-2 (figure taken from EN 1992-1-2 [1]).[2]

- *Step 3:* comparison of M_{Rd0} and M_{Ed0}:
  - ➢ if $M_{Ed0} < M_{Rd0} \rightarrow$ the column cannot withstand combination of internal forces (N_{Ed0}, M_{Ed0}) in the assumed fire (it does not collapse at such a load)
  - ➢ if $M_{Ed0} > M_{Rd0} \rightarrow$ the column withstands combination of internal forces (N_{Ed0}, M_{Ed0}) in the assumed fire

Simplified procedure 2

This procedure is similar to simplified procedure 1 described above with only one significant difference. I.e. instead of accounting only for concrete inside the 500°C isotherm and assuming that this part of the cross-section preserves its initial material characteristics, we now account for the entire concrete region. For each of its rectangle portions, referred to when integrating stress across the cross-sectional area of the

---

[2] The reader should note that in EN 1992-1-2 the prefix 'fi' is also used as a part of subscripted text in connection to symbols M_{Rd}, M_{Rd0} and M_2 (i.e. $M_{Rd,fi}$, $M_{Rd0,fi}$, and $M_{2,fi}$). Symbol 'fi', which means 'fire' and indicates that the quantity refers to fire design situation, was omitted in this thesis for the sake of simplicity.

column, the actual temperature as calculated in the centroid of this part is accounted for in an exact manner (i.e. as calculated during the previous step of the fire analysis described in section 2.2.2 of the thesis). Correspondingly, suitable temperature-dependent material characteristics are also considered for each rectangle.

Advanced procedure

The exact method used for this Master's thesis is based on the equations of the geometrical and material nonlinear theory of solid body mechanics at high temperatures. As explained already in [5], "unfortunately, this complex theory exceeds the usual framework of the master's study program of civil engineering at the Faculty of Civil Engineering, Architecture and Geodesy in Split as well it goes beyond the framework of this master's thesis. Thus, we refrain from its detailed description here. Instead, we only mention that the governing equations of this theory are, in fact, a more complex version of equilibrium, kinematic, and constitutive equations of the corresponding first-order theory, which applies for the conditions of small displacements and rotations and is presented, e.g. in textbook [24]. Transformation of the basic equations of the problem (kinematic, constitutive and equilibrium) from the first- to the third-order theory of solid body mechanics as mentioned above generally leads to a system of nonlinear equations that can only be solved numerically, e.g. using FEM in appropriate softwares, such as ABAQUS [19], ANSYS [20], SAFIR [21] and others. While a detailed understanding of equilibrium and kinematic equations of the theory is usually not absolutely necessary for successful execution of structural fire analyses in these computer programs, a basic understanding of the constitutive equations is often a necessity (often suitability of our definition of the initial material input data will depend on it). Thus, these equations will be discussed in a more detail in what follows below.

Constitutive (i.e. 'material') equations define the relationship between stresses and strains of a material. Determination of this relationship usually begins in a laboratory with a uniaxial tension/compression test. Relationship between uniaxial stress and uniaxial strain is determined in this way, $\sigma = f(\varepsilon)$. For concrete and reinforcing steel at high temperatures, a proposal for such a relationship if provided in EN 1992-1-2 [1] (*Figure 2* and *Figure 3*). Furthermore, in order to be able to use the relationship between the uniaxial material stress and strain $\sigma = f(\varepsilon)$ also for cases of spatial stress-strain conditions, the term equivalent stress σ_e is often introduced in literature. For homogeneous[3] and isotropic[4] materials, that behave the same in compression and tension (in RC structures such a material, such a material, obviously, is steel reinforcement), the so-called Von Mises equivalent stress σ_e^M is often defined as follows:

---

[3] Homogeneous bodies are bodies that have the same density and mechanical properties inevery point of their volume.

[4] Isotropy is the property of a substance to behave the same in all directions.

$$\sigma_e^M = \sqrt{\frac{1}{2}\left[(\sigma_{11} - \sigma_{22})^2 + (\sigma_{22} - \sigma_{33})^2 + (\sigma_{33} - \sigma_{11})^2\right]} \qquad (28)$$

where σ_{11}, σ_{22} and σ_{33} are the components of the diagonalized stress tensor in the considered material point of the solid body. Obviously, the Von Mises equivalent stress defined in this way can also be used for modelling a material such as concrete, as long as the sign of material stress is the same throughout the entire structure, e.g., the material is loaded only in compression as typically in RC columns."

In addition to mechanical deformations, which is related to stresses through the uniaxial relationship $\sigma_e = f(\varepsilon_m)$, in any structural fire analysis temperature deformations should be discussed as well. In the case of spatial state of stresses and strains, the tensor of the latter can be defined by the equation:

$$\boldsymbol{\varepsilon_{th}} = \alpha_T \, \Delta T \, \boldsymbol{I} . \qquad (29)$$

Here, $\boldsymbol{I}$ is the unit tensor, and α_T is the temperature-dependent relative expansion coefficient, which EN 1992-1-2 [1] designates as $\Delta l / l$ (for details of definition of the latter, see section 2.1.2).

3. EFFECT OF DIFFERENT ANALYSIS PARAMETERS ON THE CALCULATED FIRE RESISTANCE OF THE COLUMN

3.1. Case study

The building that will be analysed in chapter 3 of this thesis follows the characteristics of the selected building for sales and services of cars in Jesenice (Slovenia), where a strong fire broke out at the end of 2016 described in [25]. The load-bearing structure of the buidling is a mixed system of RC walls, RC frames, and RC solid (floor and roof) slabs.

In 2016 a fire broke out in a part of the building's basement with floor area of roughly 600 m^2 as shown in below (*Figure 17*). At the time of the fire, a substantial share of this part of the basement was occupied with piles of waste tires stacked 2.2 m high (position of these piles is marked in the figure below). Several cars were also parked in the basement at the time of the fire.

The fire in the building, as assumed by the authors of [25], most likely occurred due to ignition of an overheated ceiling lamp wherefrom the flame was transferred further through falling of burning droplets to piles of tires below the ceiling.

The fire was extinguished by firefighters after 5 hours. It was estimated that approximately all tires (i.e. around 3000 pieces), which represented the main fire load of the basement, had burned completely during this time. The cars, however, were not affected substantially by the fire. The spread of fire to other areas of the building was sucessfully prevented.
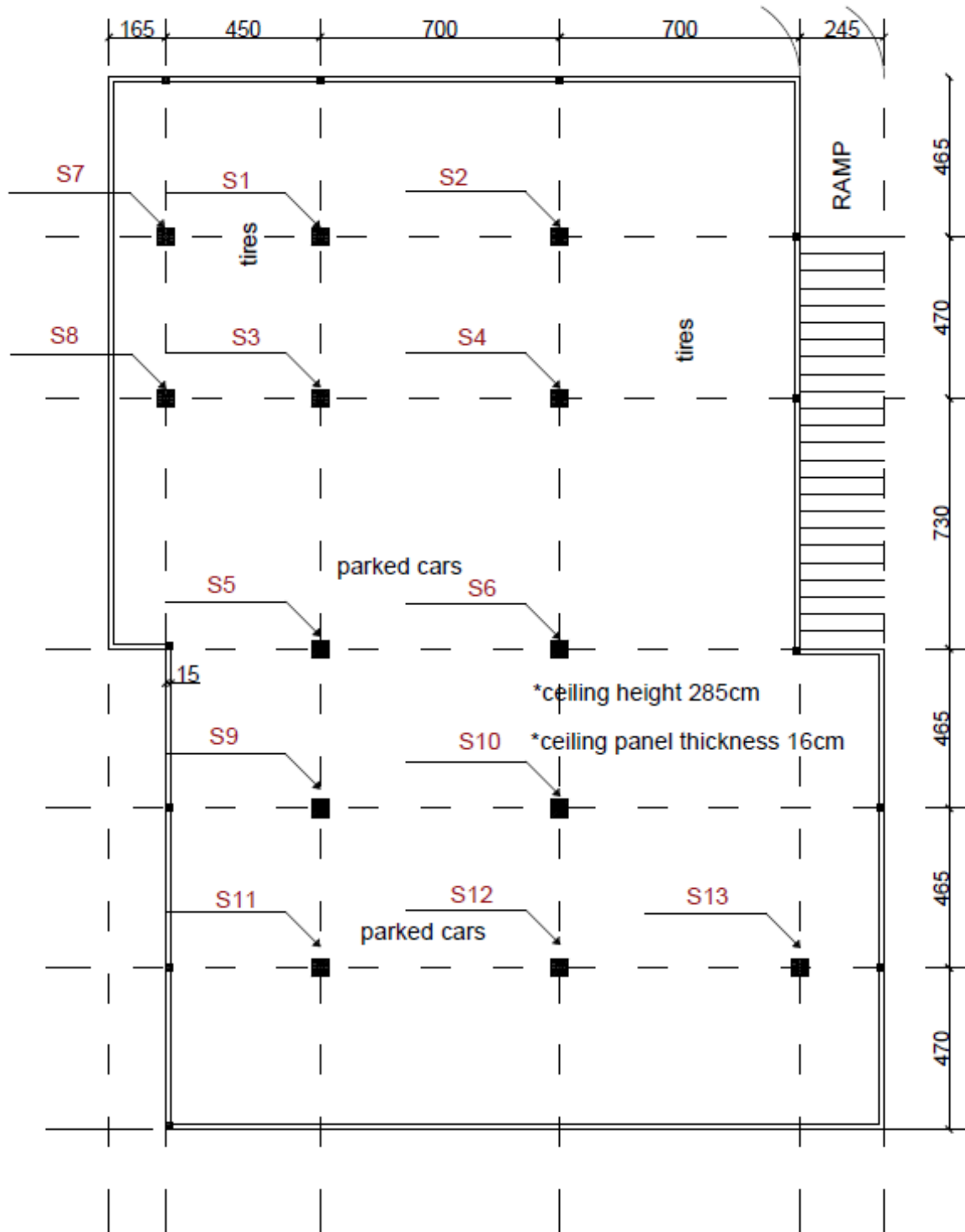
Figure 17: Floor plan of the part of the basement of the analysed building where fire occurred in 2016. Symbols S1-S6 label the RC columns that were exposed to highest temperatures in this fire. Figure is taken from [25].

In the actual case of the building in Jesenice, the vertical load-bearing structural system within the fire-affected part of the building was represented by RC walls and RC columns of 3 m height. The cross-section of the columns was round with 50 cm in diameter. As reported in [3], prior to the outbreak of the fire (i.e. at room temperature), the columns were loaded to only a small share (below 20 %) of their full axial cross-sectional load-bearing capacity $N_{Ed,fi}/(A_c \cdot f_{cd,fi})$. At such low level of the load, the columns could easily survive the 2016 fire as this was also confirmed by the after-fire field inspection of the columns described in [25] and lateron also by calculations of M. Maglica [3]. In order to enable a straight-forward (i.e. a time-of-collapse) comparison between results of our intended parametric study, however, in this thesis we will be interested more in slender and more loaded columns that would collapse in this fire. Thus, columns of square 20cm×20cm cross-section and with the initial 50% utilization of their load-bearing capacity will be analysed in this thesis instead of the actual ones. Figure below shows the selected reinforcement of these columns.
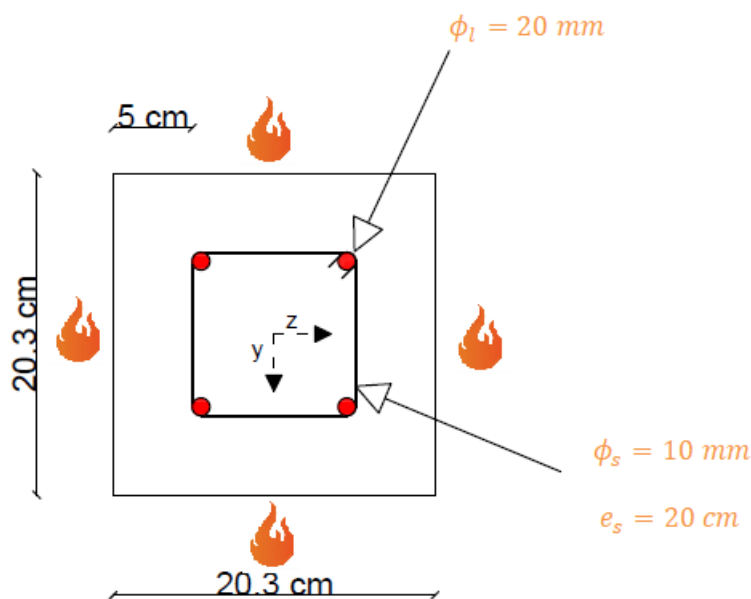
Figure 18: Cross-section of the RC columns selected for analyses of this thesis. Height of the columns is 3m.

3.2. Fire analysis of a selected RC column

3.2.1. Simulation 0

Step 1: Analysis of temperature of the column's surroundings

The fire in Jesenice was analyzed in a more detail also in the recent paper of Kolšek and Češarek [7]. For purposes of this paper, a computer reproduction of the 2016 fire in Jesenice was prepared in FDS (Fire Dynamics Simulator) Version 5.5.3 [12]. This simulation (called *Simulation 0* in this master's thesis) was recreated as a basis for the analyses of the thesis and is described in brief below (for more details see also [7]).

The computational domain is located in a 3D coordinate system with extension points in the x-axis direction from -22 m to 14 m, in the y-axis extension direction from -16 m to 20 m, and in the z-axis direction from 0 m to 20 m. Within this domain, the floor area of the analysed part of the basement (*Figure 17*) extends from -17 m to 14 m in the x-axis direction and in the y-axis direction from -7.7 m to 14.5 m.

The car tires representing the fire load of the basement are stacked in two piles, i.e the first one located from -16.5 m to -7.5 m along the x-axis and from 5.5 m to 11.5 m along the y-axis, and the second one being positioned between -16.5 m and -3.9 m along the x-axis and between -6 m to -1.8 m along the y-axis. Both piles are of a height of 2 m. The parameters for PMMA material as derived in the master's thesis of A. Matala [4] are applied for pyrolysis modelling of the material of the tires. Argumentation on why this material is suitable for modelling car tires is given in [7].

For inflow of fresh outside air and exhaust of smoke, an OPEN VENT feature is used in the model and its surface is placed over the entire top of the computaional domain.

The next modeling parameter concerns openings in the walls of the modelled basement, such as windows, doors, *etc.,* which are in FDS modeled via the HOLE feature. The openings are shown in *Figure 19* below. Starting with the doors, there are three of them in the model, all of them of 2 m height. The first door (i.e. marked *door to staircase* in the figure below) extends from -4.8 m to -3.8 m in the x-direction. The next one leads to a spiral staircase and extends from -2.8 m to -1.8 m in the x-direction. The third door (marked *door to hallway* in figure below) extends from 0.2 m to 1.2 m in the x-direction. Additionally, two openings are established at the top (x = -17 m) and the bottom (x = 0 m) of the drive-in ramp of the basement. Both of these extend from 12.1 m to 14.4 m in the y-direction and are of a height of roughly 3m. Finally, the window positions are defined. The first of them is located on the wall that separates the

entrance ramp from the rest of the basement and extends from -5 m to -2 m in the x-direction. Its height is 0.9 m (z-coordinates are 1.6m to 2.5m). The remaining 2 windows are the window in the north outer wall of the basement and the window in the outer wall of the drive-in ramp. The former is 1 meter high (z-axis from 1.8 m to 2.8 m) and its y-coordinates are from 0.5 m to 1.5 m. The latter is 2.2 m high and its x-coordinates are from -16.8 m to 11.6 m.

Parameters of kerosene burning are taken as parameters of the mixture fraction model describing chemical reaction in the gaseous phase. These are collected from [26].
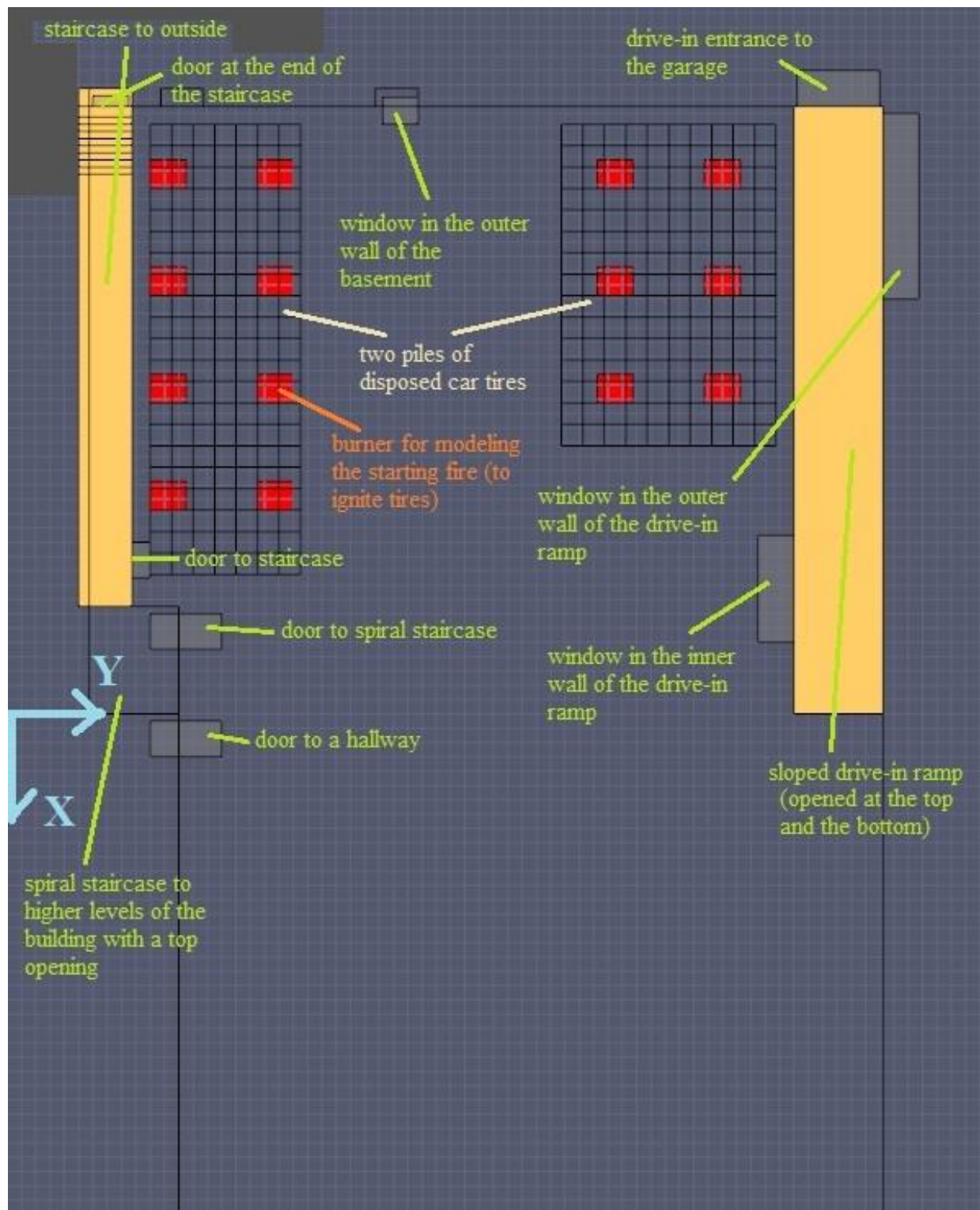
Figure 19: 2D view (from $Z = Z_{max}$) on the established computational domain with denotation of some of the most important parts of the model (figure is taken from [7]).

The material used for modelling the outer concrete walls and ceiling of the basement is concrete with thermal characteristics (density, thermal conductivity, and specific heat capacity) as suggested in Eurocode (see Section 2.2.2). Backing of the walls and the ceiling is taken as EXPOSED (see FDS5 Users' guide [12] for details of such definition). Thickness of the walls and the ceiling is taken as 20 cm.

RC columns, which represent the vertical load-bearing structure of the affected part of the basement, are not specifically modeled in FDS. Instead, GAS TEMPERTURE devices are installed in places representing the central point of these columns according to *Figure 19* above (figure showing the floor plan of the basement). These are positioned at a height of 2.5 m (30 cm below the basement ceiling).

The FDS simulation is performed using a single mesh only. The mesh is uniform with cell size 40 cm × 40 cm × 40 cm. Such a mesh is relatively coarse, however, refining it further was not feasible for purposes of this work according to the available computer equipment and the timeframes available for completion of the thesis. Effects of mesh refinement are, thus, remaining to be explored in the future.

Because of using just one mesh in the analysis, computations are done by only exploiting a single processor of the computer. Using computer of following characteristics CPU – Intel(R) Core(TM) i7 CPU 920 @ 2.67 GHz 2.79 GHz, RAM –24 GB, a single analysis does take about 90 hours to complete. More meshes, which would enable us a multi-processor analysis, were also tried out in the process of setting-up the FDS model following the rules of section 6.3 of the Users guide [12]. A substantial influence on computing time was noticed in such a case since a single analysis now needed only about 40 hours to complete. Nevertheless, a non-negligible influence was also observed for the analysis results. Thus, this way of modelling was not selected for further analyses.

Results of the above described step 1 of simulation 0 show that the fire in this simulation stops at around 15100 seconds (Figure *24*) with almost no parts of tires left unburnt. The fire compartment is full of black very dense smoke almost immediately (after around 500 seconds) (*Figure 21*) and this does not visibly improve almost until the end of the fire.
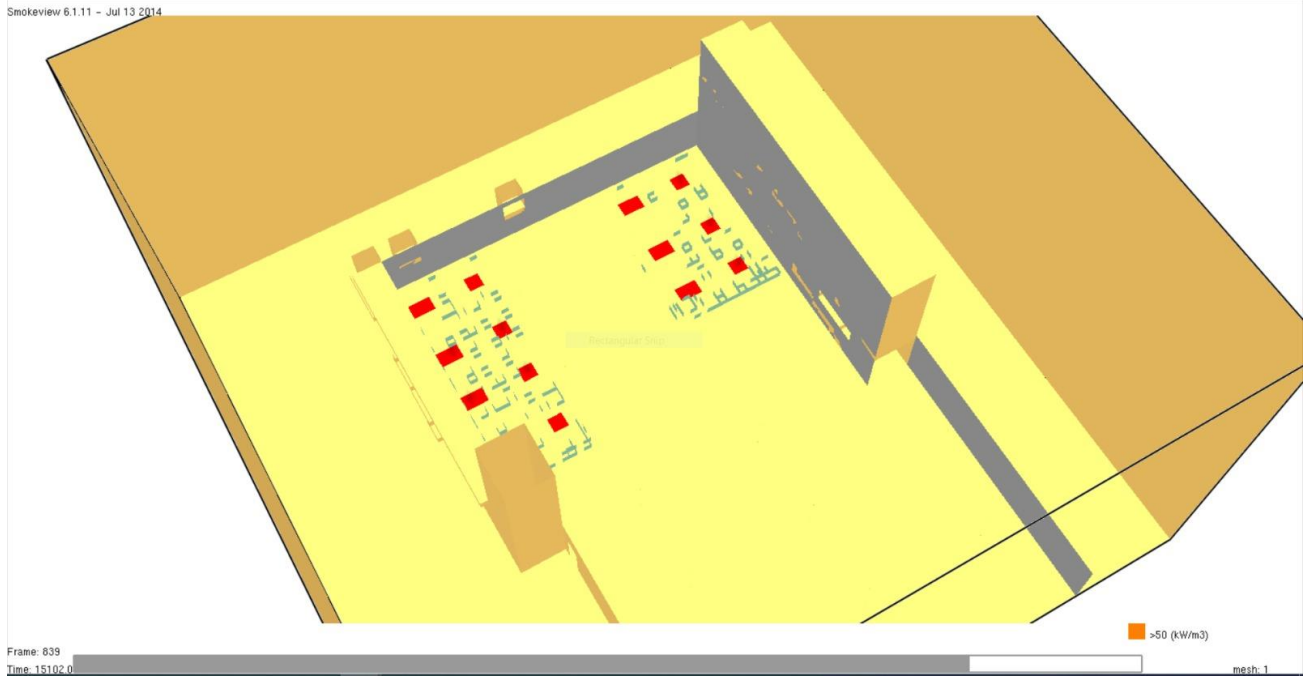
Figure 20: The moment when fire stops. There are just few parts of the tires left unburnt.
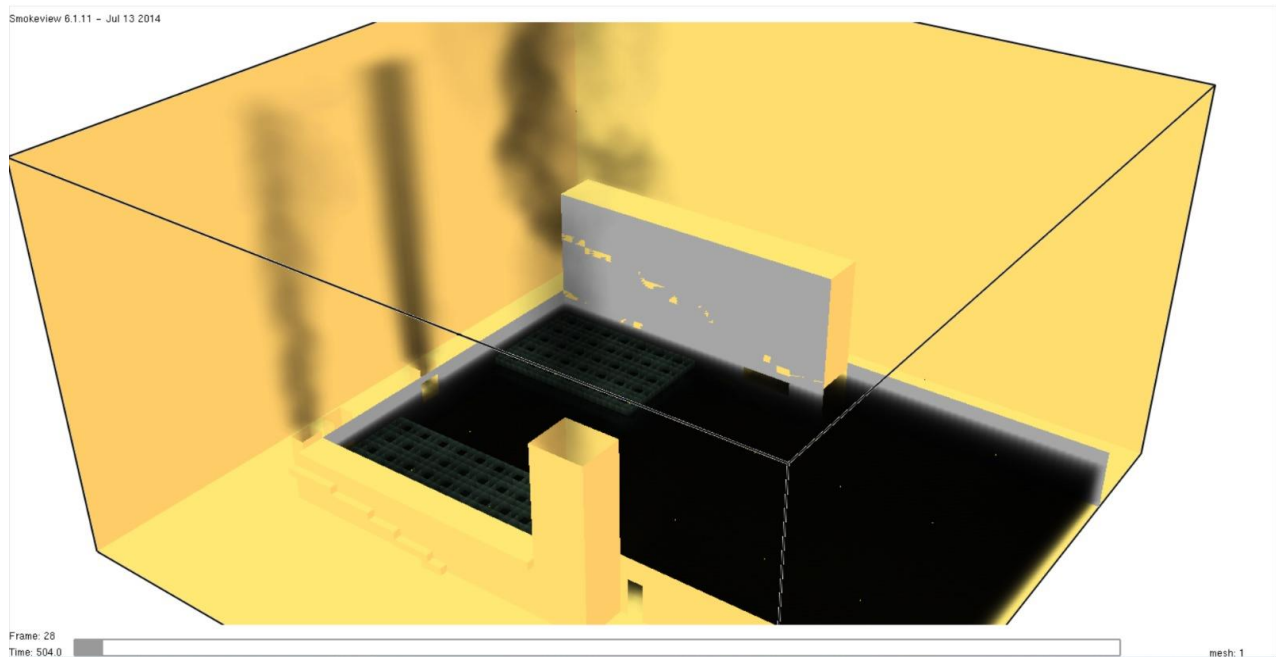
Figure 21: Smoke after 500 seconds.

The time evolution of the calculated fire-spread is shown in figures below.
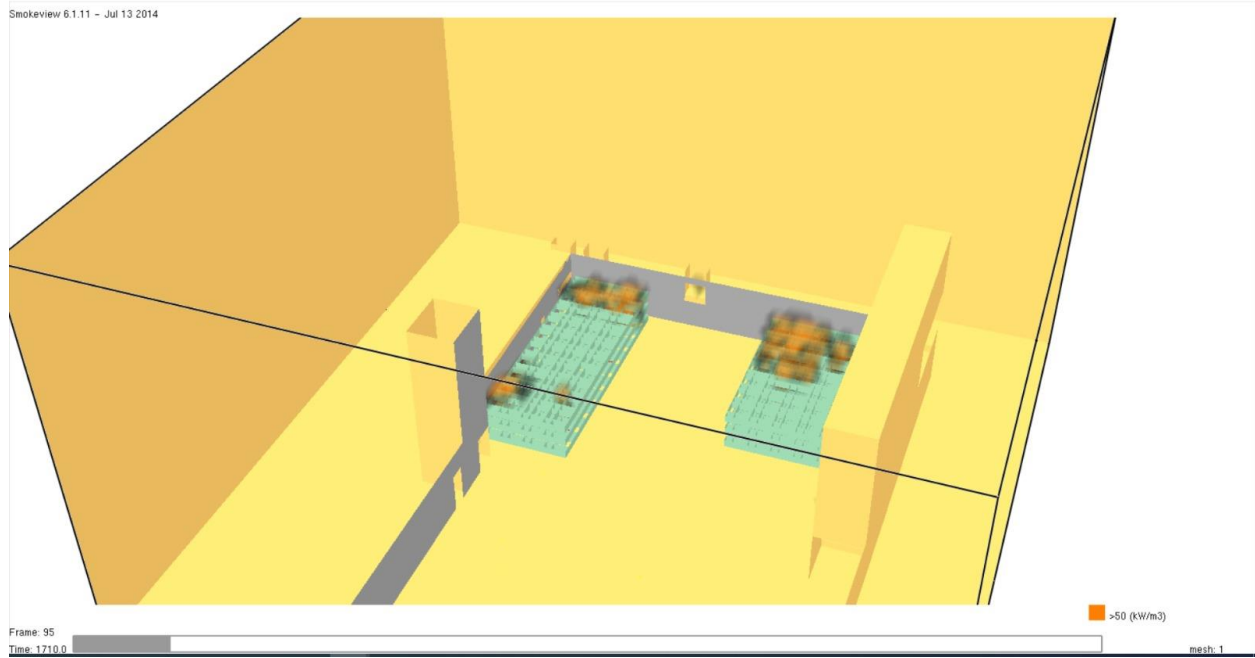
Figure 22: Fire-spread at 1700 seconds. A more violent burning is noticed on tires stacked next to the drive-in ramp (in the figure the right pile of tires).
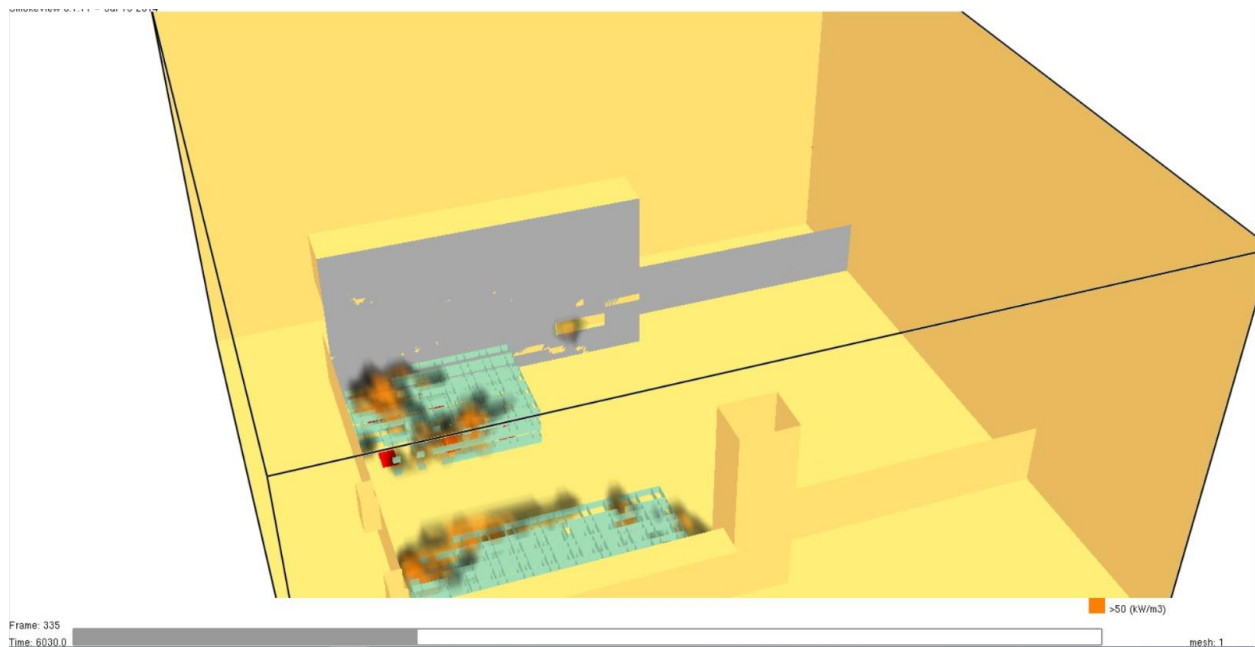
Figure 23: Fire-spread at 6000 seconds. A substantial part of tires stacked next to the drive-in ramp has already burnt out, more violent burning also begins on the other side (i.e. on tires stacked next to the staircase).
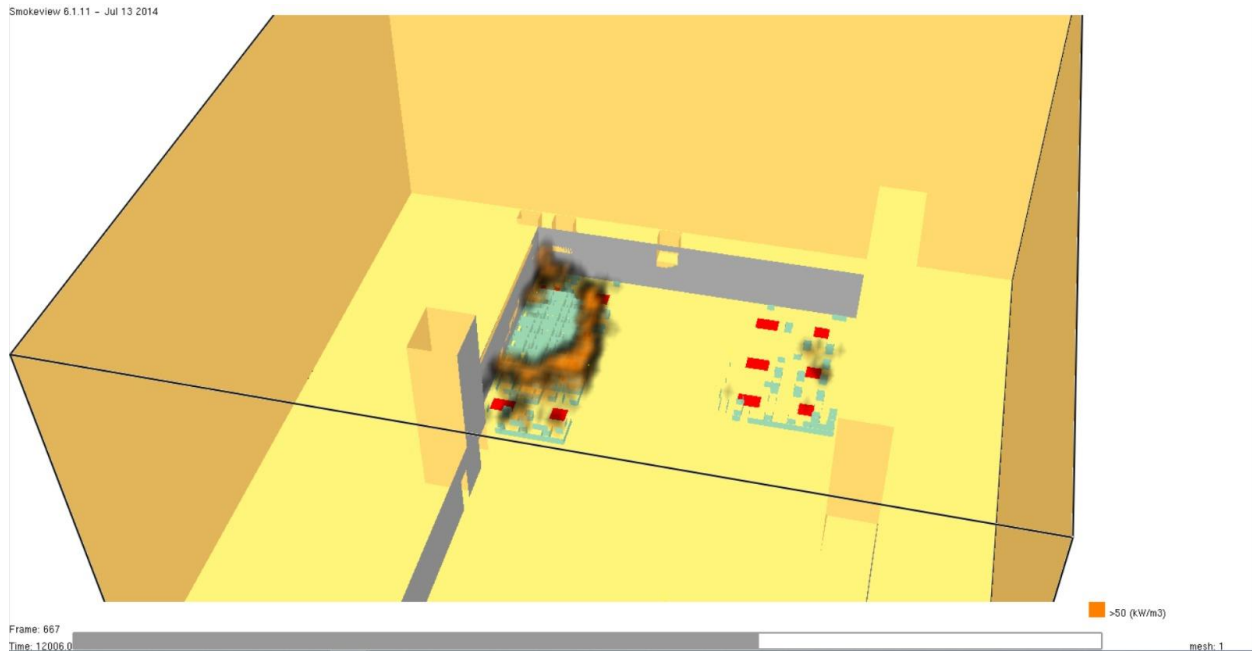
Figure 24: Fire-spread at 12000 seconds. Tires that were stacked next to the drive-in ramp has burnt out almost completely, burning continues on the other side.

In addition, the graphs below show the measurements of gas temperatures (symbol S1 here refers to the measurement taken at the position of the S1 column etc., see Figure *17* for position of the columns). As can be seen from the graphs, column S2 is expected to heat to highest temperatures in the shortest period of time and is, thus, expected to collapse first in the fire. Thus, temperatures of graph S2 will be taken as the fire curve in the following thermal and mechanical analysis of 20 cm × 20 cm column.

In addition, the graphs below show the measurements of gas temperatures (symbol S1 here refers to the measurement taken at the position of the S1 column etc., see Figure *17* for position of the columns). As can be seen from the graphs, column S2 is expected to heat to highest temperatures in the shortest period of time and is, thus, expected to collapse first in the fire. Thus, temperatures of graph S2 will be taken as the fire curve in the following thermal and mechanical analysis of 20 cm × 20 cm column.
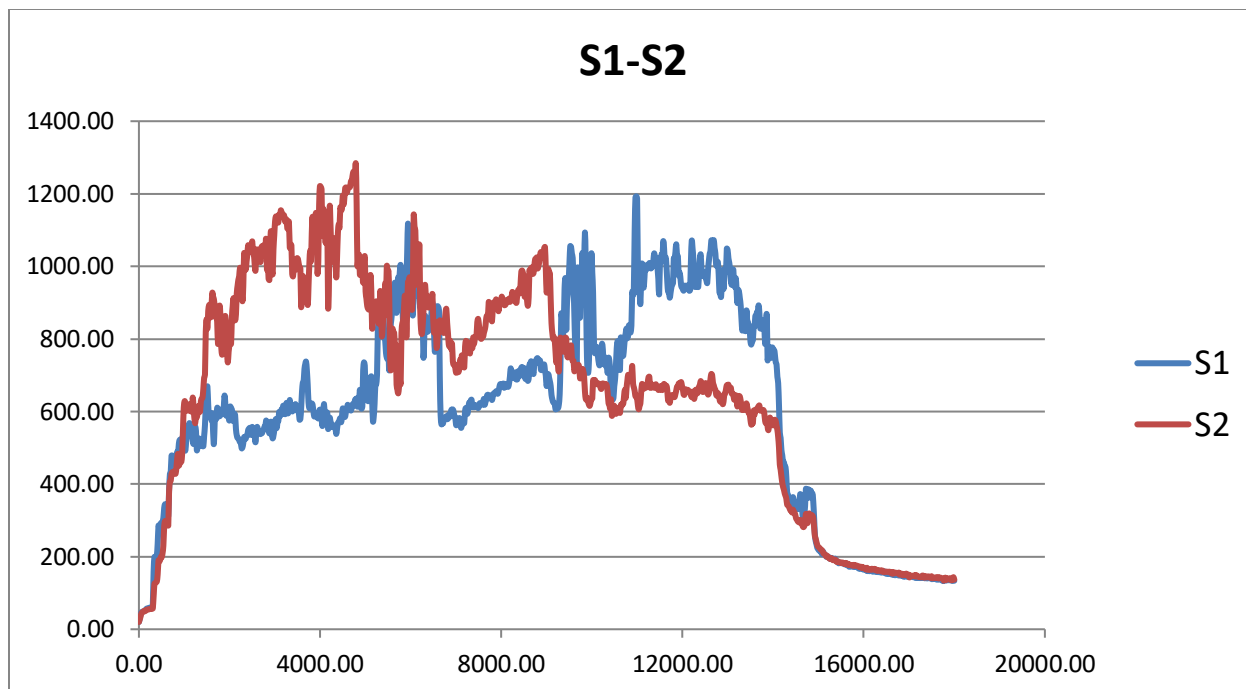
Figure 25: Gas temperatures at the positions of columns S1 and S2.
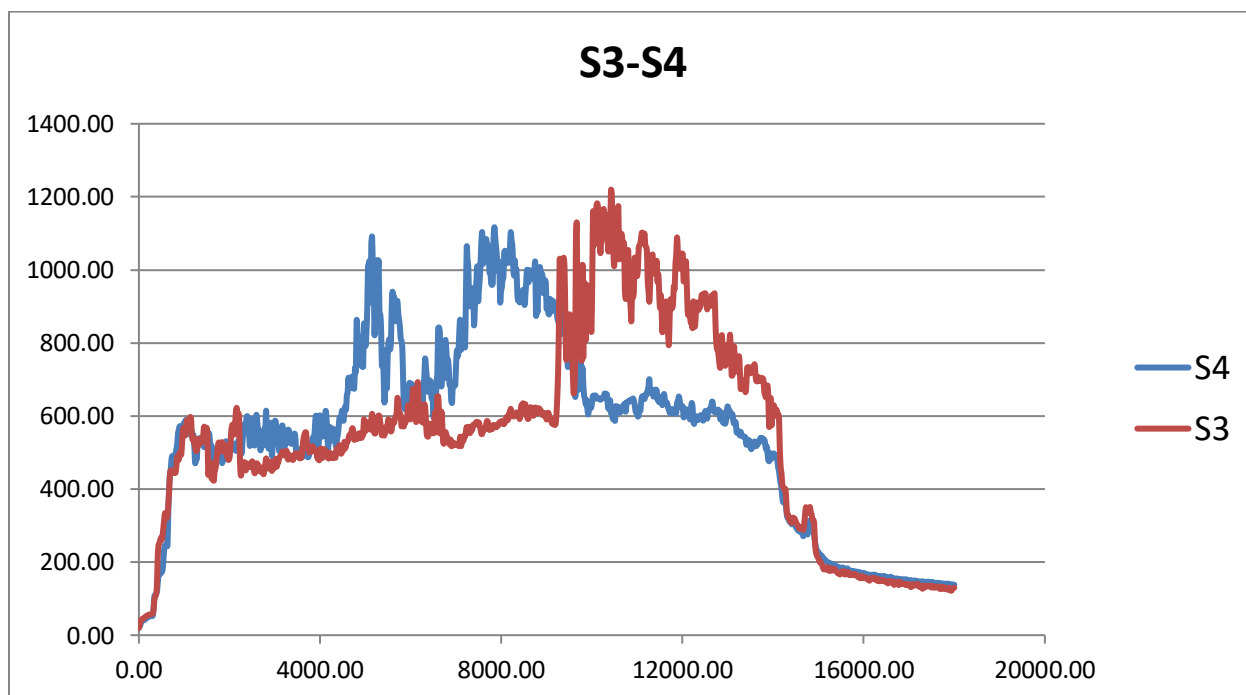
Figure 26: Gas temperatures at the positions of columns S3 and S4..
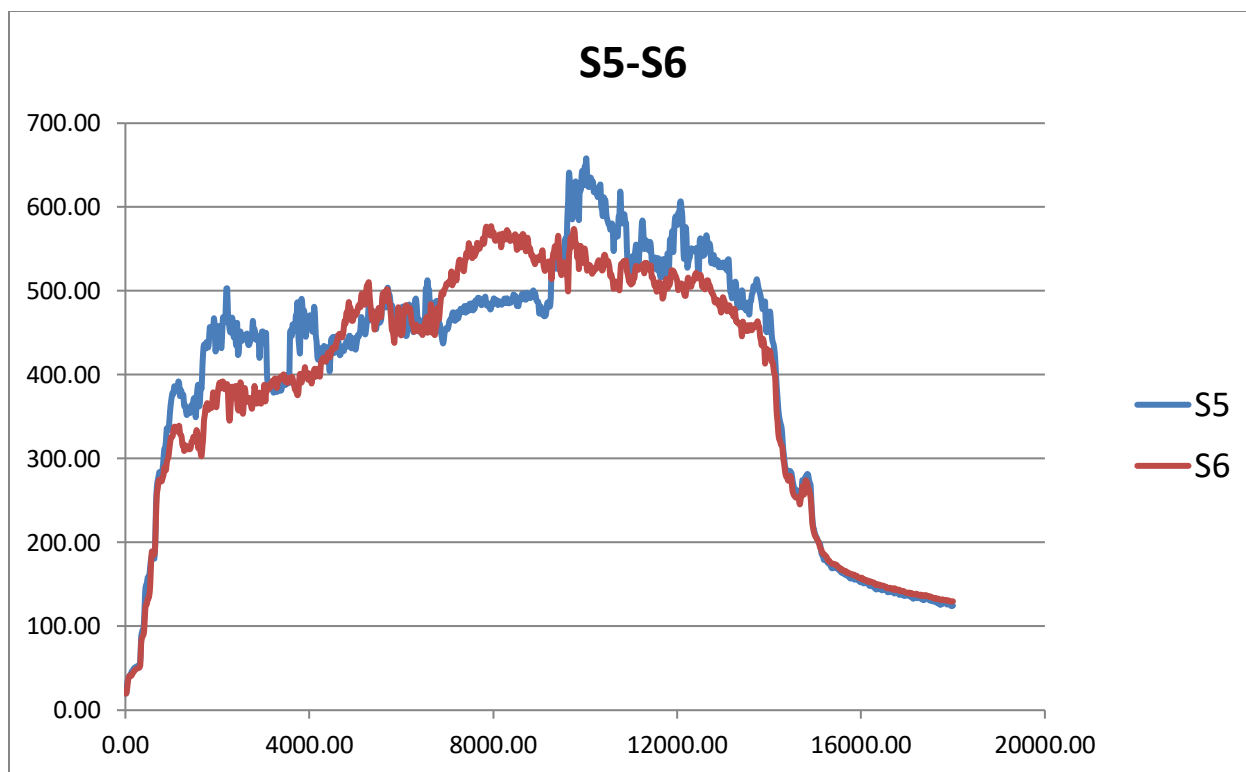
Figure 27: Gas temperatures at the positions of column S5 and S6.
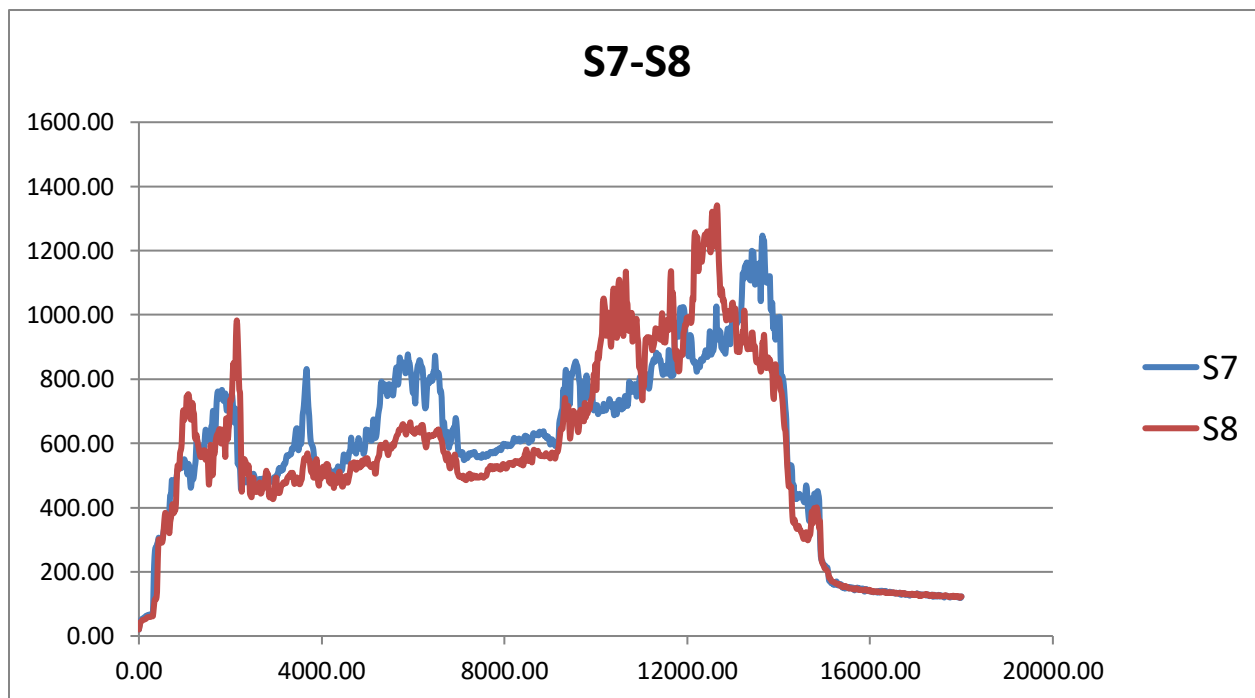
Figure 28: Gas temperatures of columns S7 and S8.
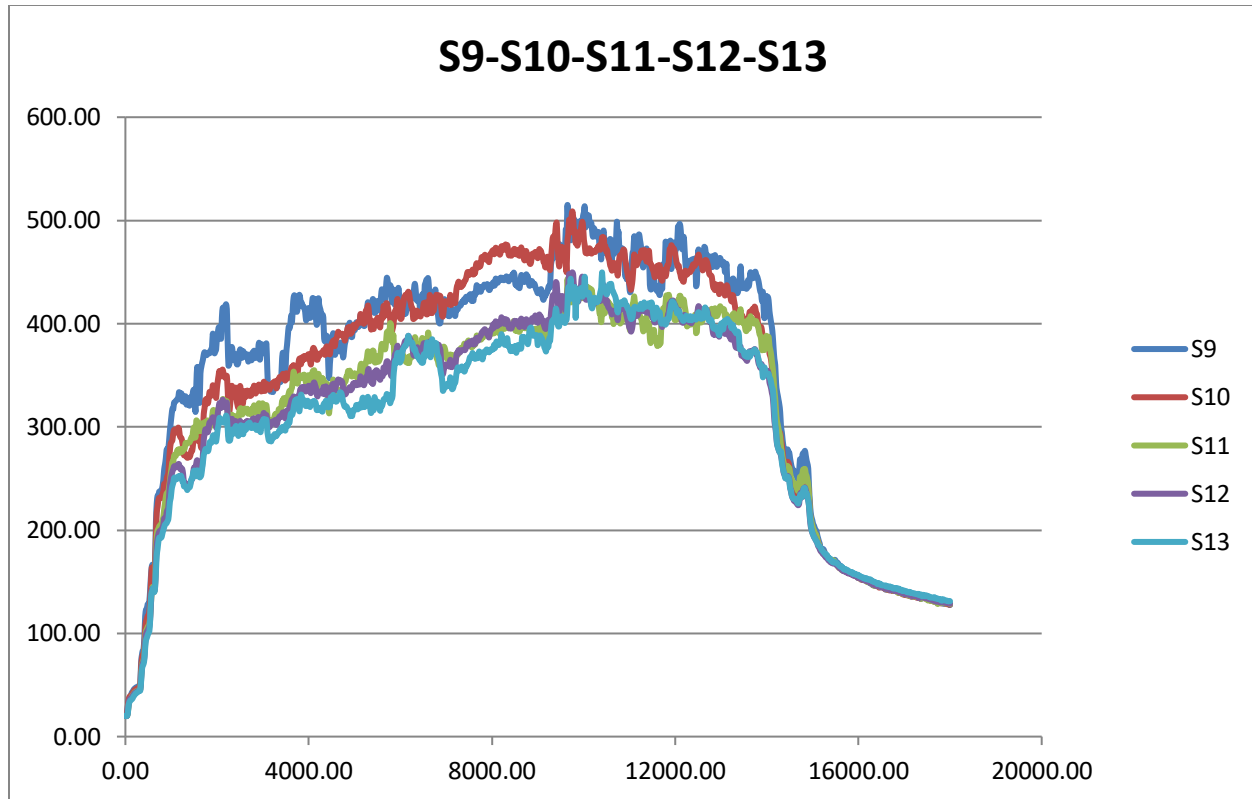
Figure 29: Gas temperatures at the positions of columns S9-S13.

Step 2: Thermal analysis of the column

The model for thermal analysis of the selected column was set up in ABAQUS [19] following the corresponding instructions of paper [7].

This analysis calculates the column temperature change when exposed to a selected fire curve. We have to take into account the geometric properties of the column and the thermal properties of the concrete material (thermal conductivity, density, specific heat of concrete). The dimensions of the model of the RC column are 0,2 x 0,2 x 3,0 [m], with the mesh density of 0,02 x 0,02 x 0,02 [m]. Quadratic type finite elements are applied. Fire curve is selected from the first step of a simulation (*Figure 25*) and it is prescribed for the whole height of the column . Type of the fire in this dissertation is considered to be of a natural fire type, thus, and according to EN 1991-1-2 [2] coefficient of convective heat transfer is taken as 35 W/m2K in the analysis. Radiation coefficient is taken as 0,7 [1]. Defined properties of concrete are density, conductivity, expansion and specific heat. Density is defined as 2500kg/m^3 and the rest of properties are defined with different values for temperatures from 0 °C up to 1200 °C as described in section 2.2.2.

The results of thermal analysis are presented in following Figures:

Note : Time shown in Figures is in seconds. Temperatures are given in °C (for example $8,281x10^2$ is 828 °C).
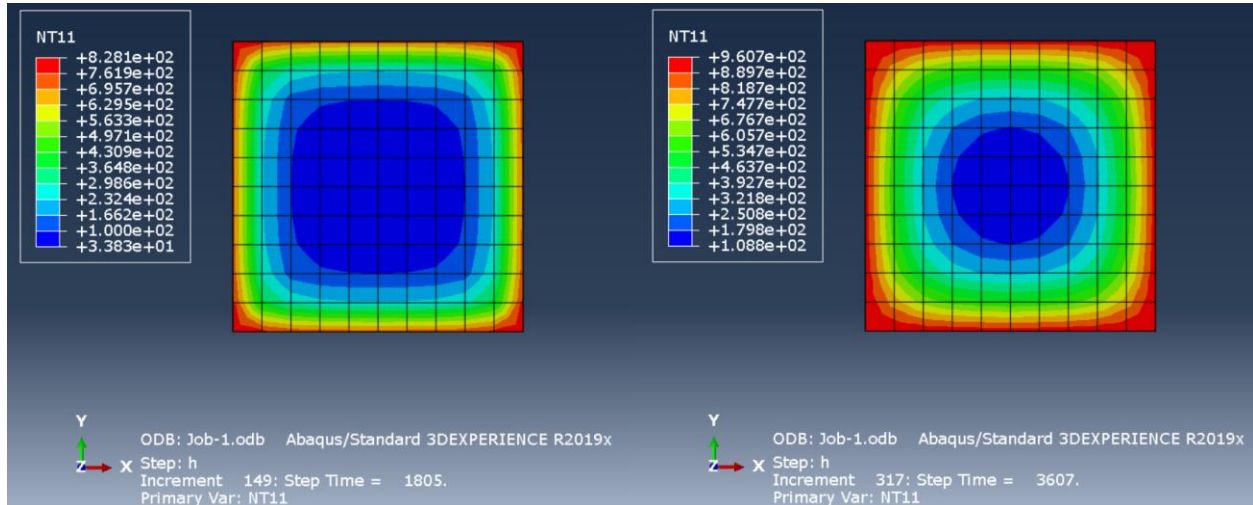
Figure 30: Column temperatures after 30 minutes of fire (left) and 60 minutes (right) of the fire
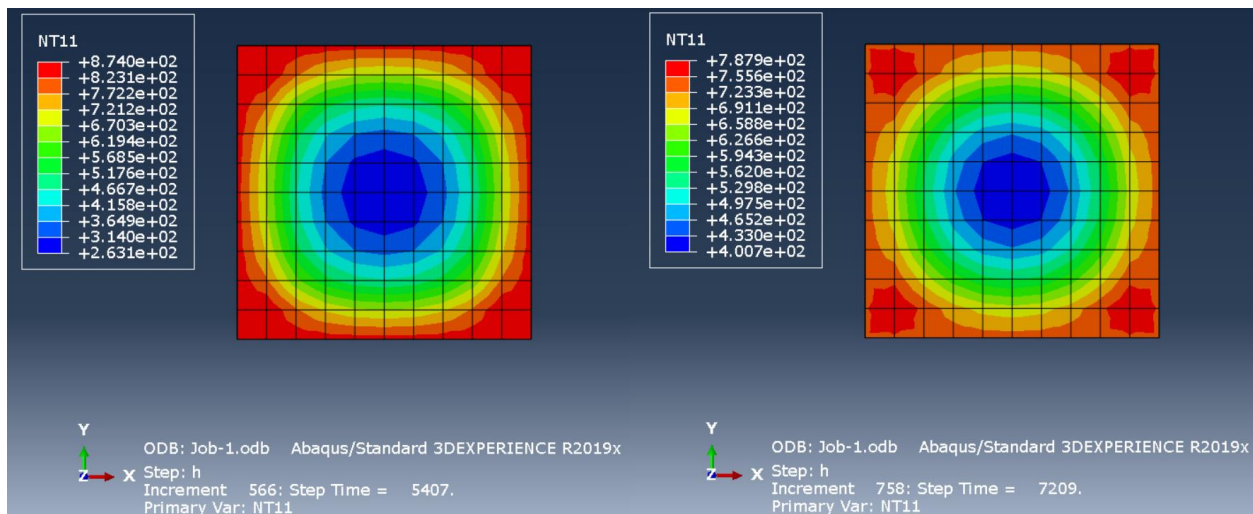
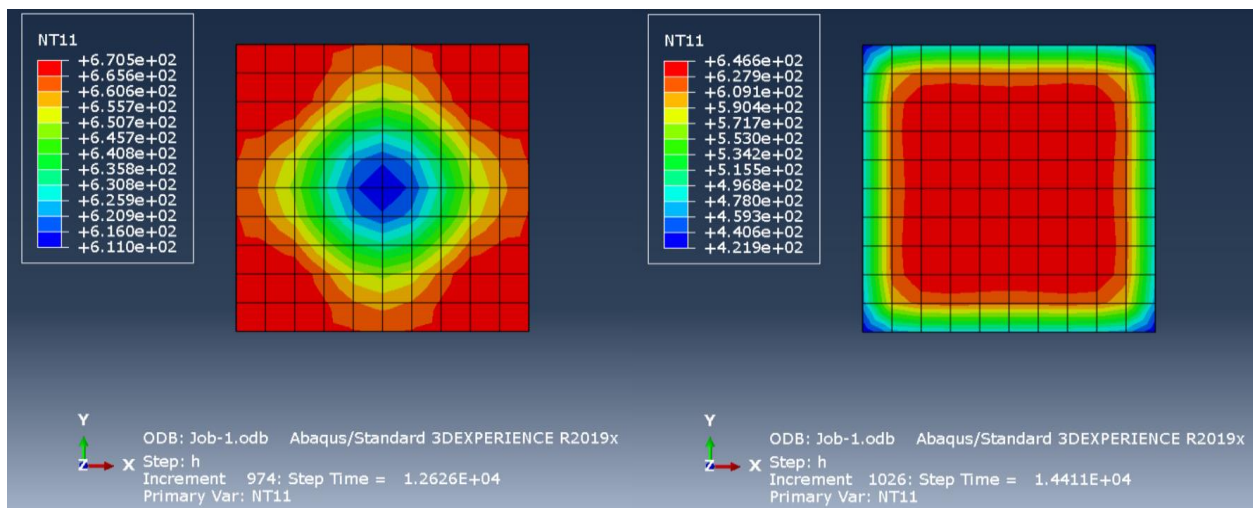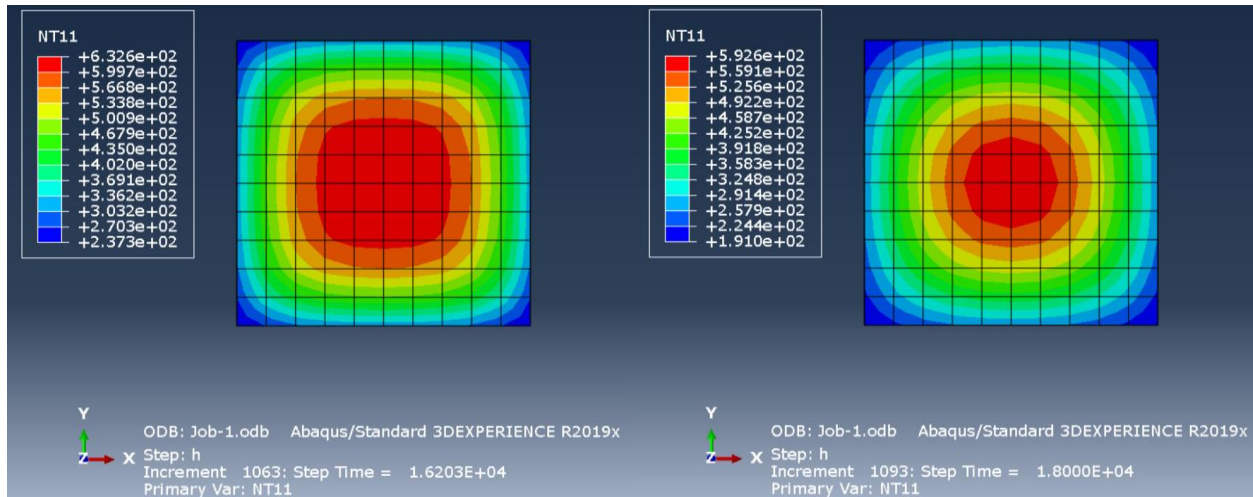Figure 31: Column temperatures after 90 minutes of fire (left) and 120 minutes (right) of the fire

48
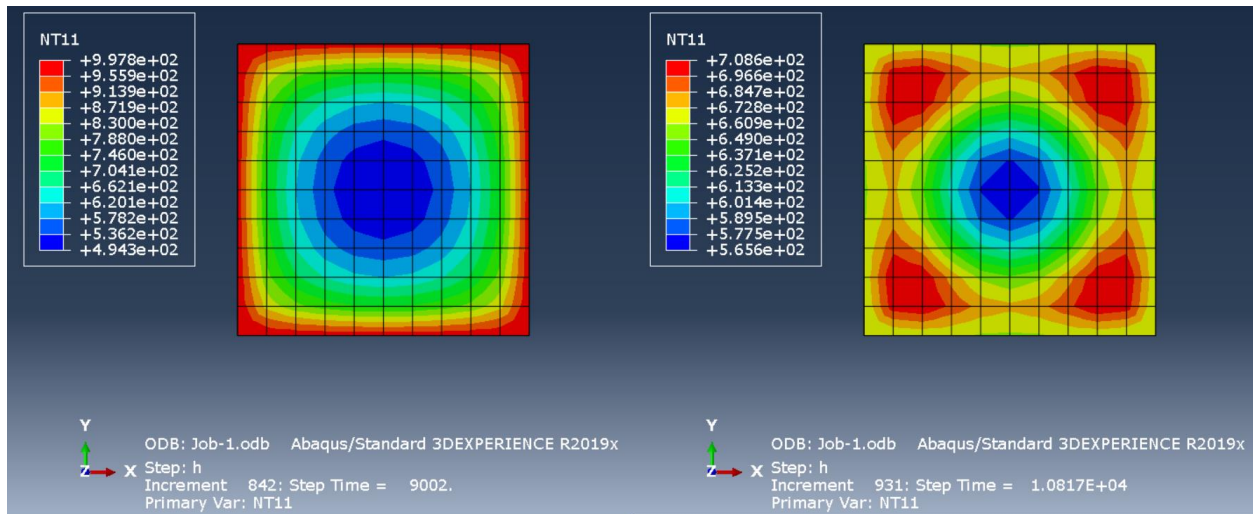
Figure 32: Column temperatures after 150 minutes of fire (left) and 180 minutes (right) of the fire

Figure 33: Column temperatures after 210 minutes of fire (left) and 240 minutes (right) of the fire

Figure 34: Column temperatures after 270 minutes of fire (left) and 300 minutes (right) of the fire

Step 3: Structural analysis of the column

The results of the previous thermal analysis of the column were then imported as temperature fields in the corresponding structural model. The model for structural analysis was set up in ABAQUS [19].

The structural model is based on the thermal one, but with all changes necessary for a structural type of an analysis. The mesh density has the same density as in the thermal model, which is 0,02 x 0,02 x 0,02 [m]. Suitable kinematic boundary conditions are applied at the bottom and at the top end of the column. At the bottom end, rotations and displacements of all nodes are fixed. At the top end, horizontal displacements of all nodes are prevented using a restriction of horizontal displacements of one node (so called *reference point* which in this model coincides with the center of the column) and additional application of a rigid body constraint to the rest of the nodes of the cross-section. The axial force of 600 kN is applied as a concentrated load in the center of the upper end of the column. 600kN represents the value which is 50% of the ultimate load-bearing resistance of the column at room temperature. The eccentricity of the load is given as 2 cm. In order to induce buckling of the column as simply as possible, another force of 10 kN is added to the model in the middle of the column in the transverse direction. Furthermore, in this analysis, it was also necessary to define density, expansion, elastic and plastic material properties. Density of concrete is defined as 2500kg/m^3. Its expansion coefficient is defined according to temperature and is taken as explained in Section 2.1.2 (Fig. 2). While for elastic properties, Young`s modulus is defined according to temperature but Poisson`s ratio is defined as a constant value (0.15) independent of temperature. For plastic properties, both Yield stress and Plastic strain are defined according to temperature up to 1200 °C following Table 1 of Section 2.1.2. Reinforcement is not modeled explicitly

since it does not contribute noticeably to the load-bearing capacity of the column (note that prior to its buckling, the column is remaining in compression only at all times).

The time of collapse of the column was also defined according to the proposition of [7], where limiting vertical contractions or limiting rates of vertical contraction of the column were followed according to proposition of standard EN 1363-1: Fire resistance tests - Part 1: General requirements. In our case, the limiting rate of the column's vertical contraction was exceeded at the moment of 4613 seconds. Therefore, we considered that the column collapsed just after 76 minutes of the fire.

Figures below show the most important results of the structural analysis, i.e. deformed shape of the column at the time of the column collapse (scale factor is 1), the time development of the column's axial displacement at the top of the column, the time development of the column's transverse displacement at mid-span.
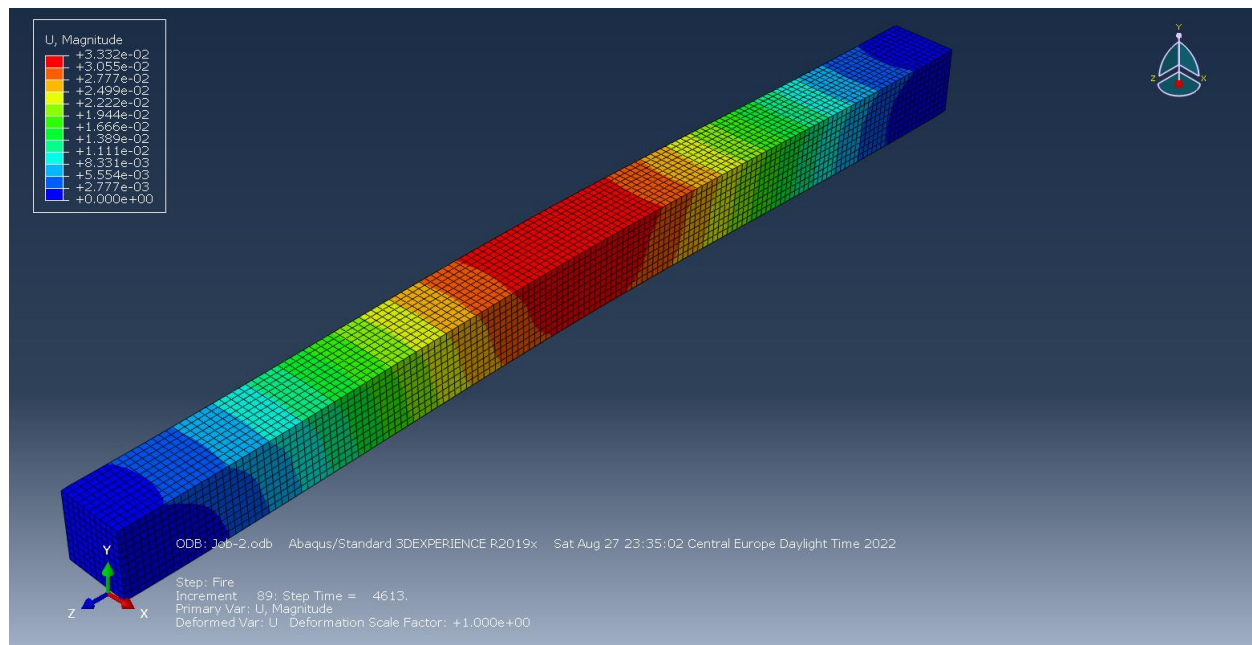
Figure 35: Deformed shape of the column at the time of the column collapse.
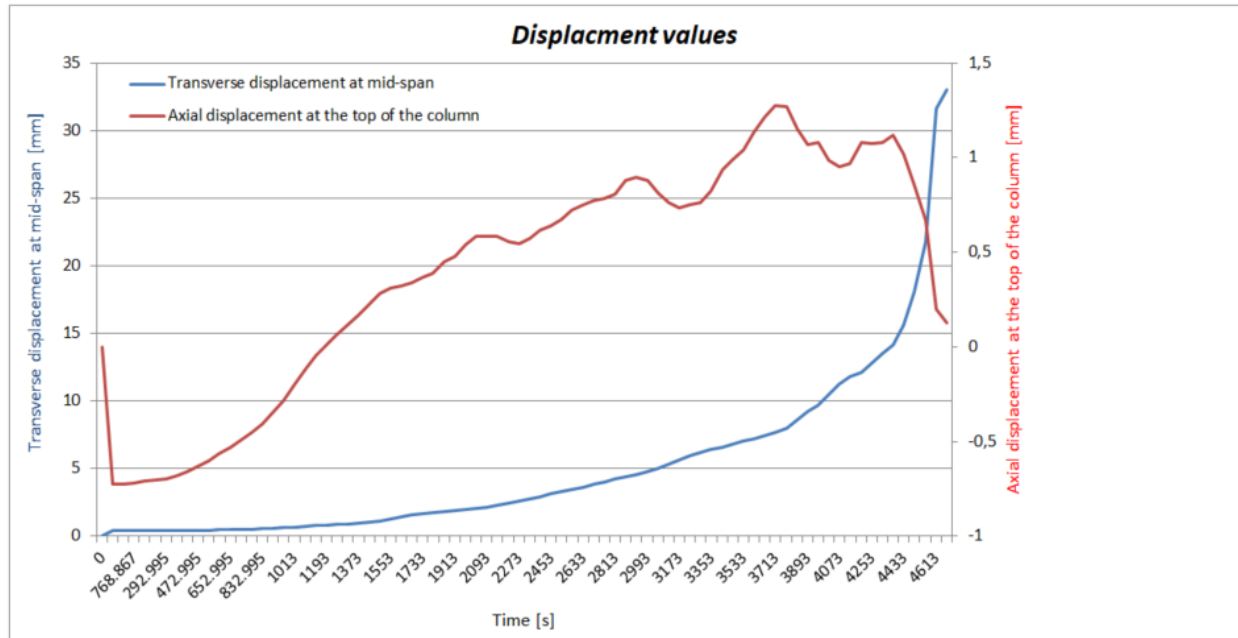
Figure 36: The time development of the column's axial displacement at the top of the column, the time development of the column's transverse displacement at mid-span.

3.2.2. Simulation 1: Effect of mathematical description of structural response

Step 1: Analysis of temperature of the column's surroundings

No changes were applied here compared to Simulation 0 procedure.

Step 2: Thermal analysis of the column

No changes were applied here compared to Simulation 0 procedure.

Step 3: Structural analysis of the column

Instead of the materially and kinematically exact non-linear theory that was used for description of structural response in case of Simulation 0, a simplified second-order theory was used here as described in Section 2.2.3. Firstly (Simulation 1a), only the ambient-temperature material properties were used for concrete inside the 500°C isotherm and concrete outside this isotherm was left out from (not accounted for in) the analysis. Secondly (Simulation 1b), the actual temperature-dependent material properties were applied for concrete and the entire concrete cross-section was accounted for in this manner in the analysis. In both cases (Simulation 1a and 1b) the structural analysis of the column was then repeated at different times of the fire until the time of collapse was found at the time when MEd0 was equal to MRd0.

All calculations of structural response were performed using the tool FindMKappa [23] mentioned previously in Section 2.2.3.

Results and observations

Compared to the results of simulation 0, the time of the column's collapse has reduced to 71 minutes in the Simulation 1a analysis (a 8 % reduction) and to 71 minutes in the Simulation 1b analysis (a 8 % reduction).

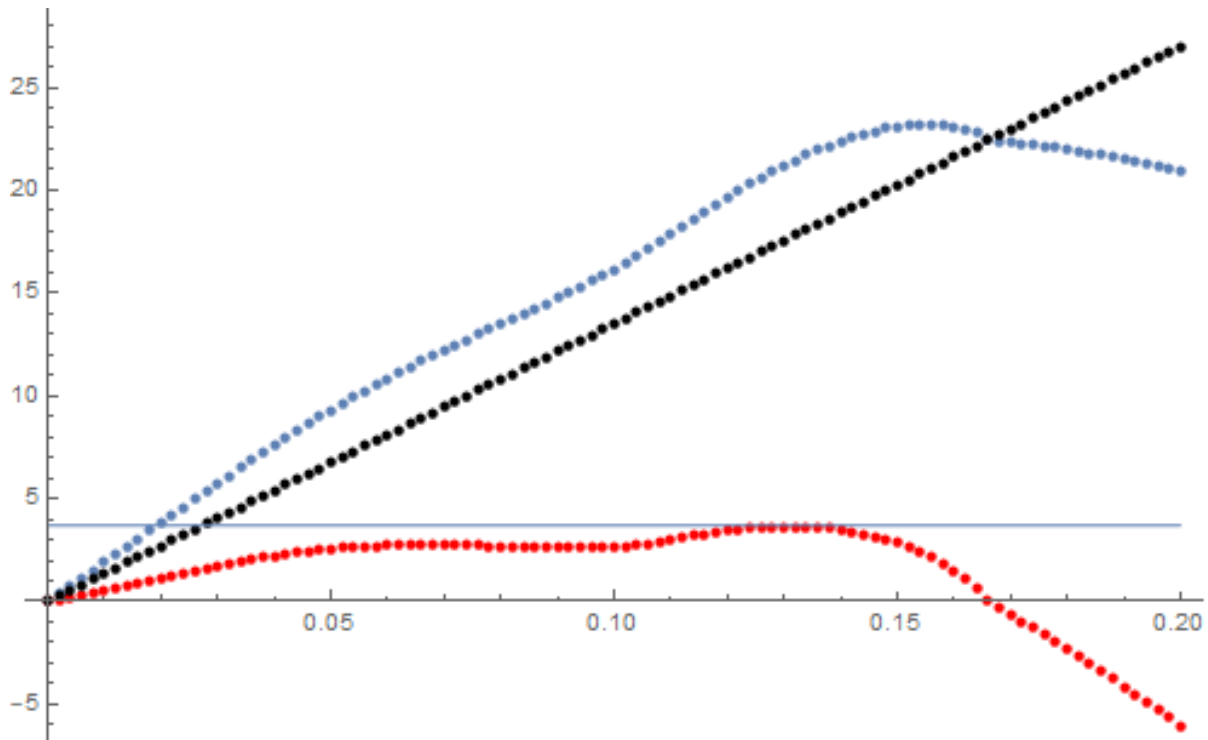Figures below show results for curves M-kappa for the two analyses for the time of detected collapse of the column .

Figure 37: M-kappa curve for situation after 71 minutes of the fire. MRd0 is equal to MEd0. Simulation 1a.

From Figure *37* for this analysis, we consider that the collapse happened right after 71 minutes of fire.
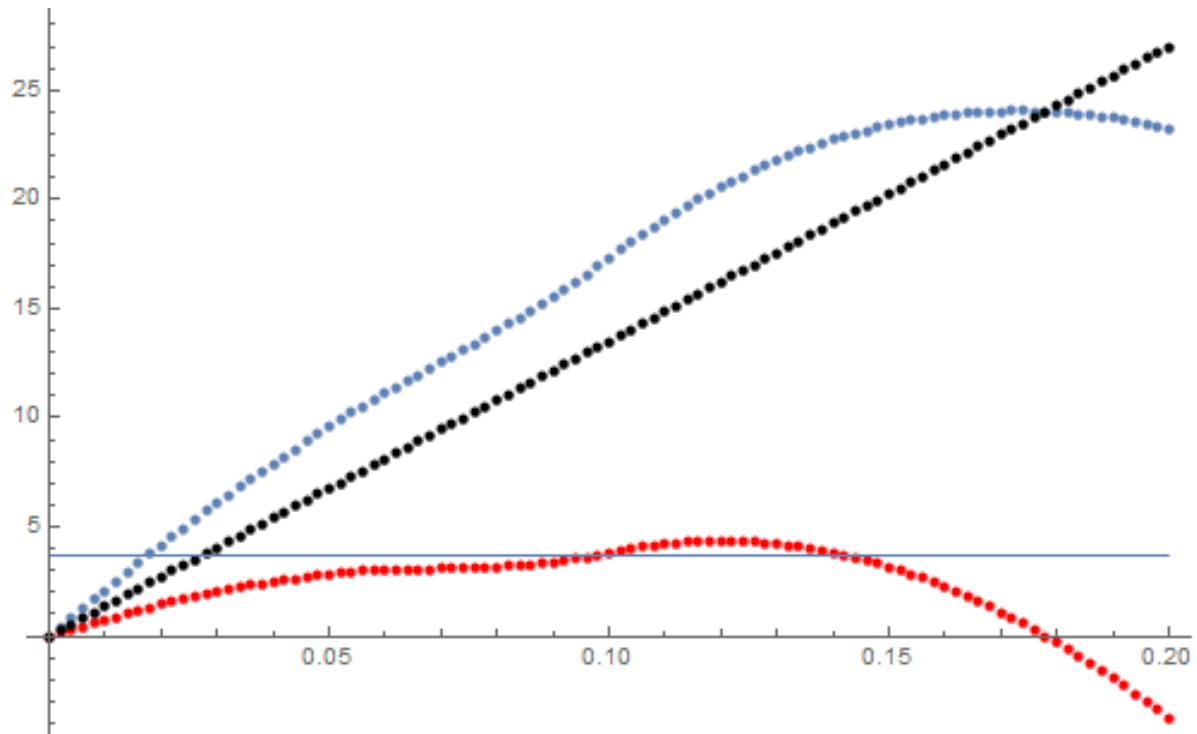
Figure 38: M-kappa curve for situation after 70 minutes of fire. Med0 is still not equal to MRd0. Simulation 1b.
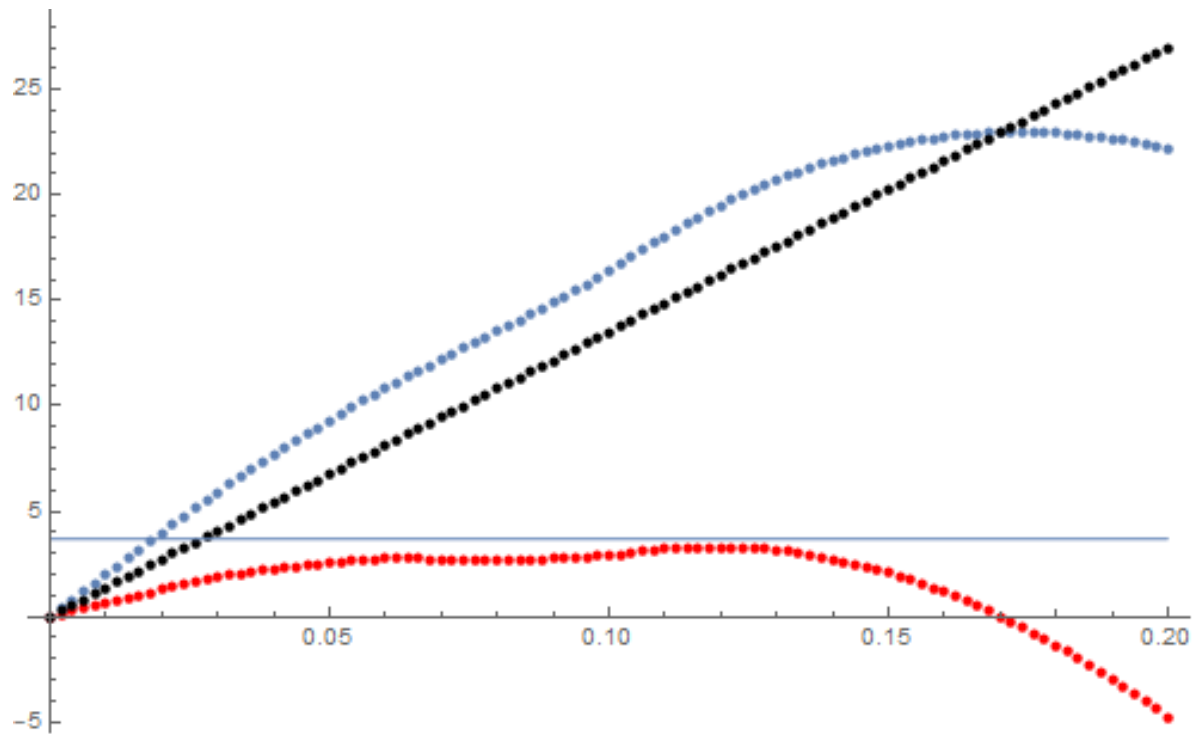
Figure 39: M-kappa curve for situation after 71 minutes of fire. MRd0 is a bit bellow MEd0. Simulation 1b.

From Figure *38* and Figure *39* it is visible that a collapse happened in betwen 70 and 71 minutes of fire. For this analysis, we consider that the collapse happened right after 71 minutes of fire. Mathematical structural response is more conservative than a response of structure from Abaqus. In both simulations column behavior is the same.

3.2.3. Simulation 2: Effect of selection of output for temperature Tg (the fire curve temperature) and selection of convection coefficient

As explained in section 2.2.1., in the thermal analysis of the structure (step 2 of the fire analysis), the temperatures across the volume of the RC column are calculated using the classic Fourier equation (8). Here convective and radiative heat transfer at the solid boundary depend on T_g. T_g is normally the temperature represented by the fire curve from the 1st step of the analysis and is defined as temperature of the surroundings of the structure that the latter is exposed to during the fire. The term 'surroundings' here refer to, firstly, surrounding gas being important for convective transfer of heat to and from the analysed structure and, secondly, temperature of the surrounding flame, walls and other obstructions exchanging heat with the structure through radiation. Obviously, with equation (8) we assume that the temperature of all of these components (gas, flame, walls and other obstructions within fire compartment) is essentially the same or very similar. The latter does not hold true excatly in each case, so temperature Tg really needs to be considered more as a fictitious rather than a real temperature. In FDS, a special quantity called ADIABATIC SURFACE TEMPERATURE (AST) is available as an output representing excatly this fictitious temperature Tg. AST is calculated in the way that the net convective and the radiative heat flux at the solid boundary $\dot{q}''_r + \dot{q}''_c$ as calculated from CFD and radiation models in FDS (1st step of the fire analysis) is equal to the equation used for definition of boundary condition later in the 2nd (thermal) step of the analysis:

$$q_r^n + \dot{q}_c^h = \varepsilon\,\sigma\,(\,T_{AST}^4 - T_w^4\,) + h\,(T_{AST} - T_w) \tag{30}$$

Not all of the softwares for calculation of fire growth (alternatives for FDS), however, have this option. In such cases, instead of outputting an AST-like quantity, engineers normally go for outputting the temperature of gas near the analysed structure – similar to what has been done in Simulation 0 of this thesis. To see, what difference could this make for our analysed case, in this section of the thesis instead of outputting GAS TEMPERATURE in Step 1 of the fire analysis we will output ADIABATIC SURFACE TEMPERATURE.

Step 1: Analysis of temperature of the column's surroundings

AST device in FDS [11] can only be connected to a solid surface, because its value will not only depend on the temperature of gas surrounding the column but also on the velocity of gas flow and the manner of gas flow movement (laminar or turbulent flow). In addition, it will also depend on the emissivity of the column's surface. Thus, special obstructions representing RC columns will now be added to the original FDS model. Each side of each column will be modelled using a surface of 10 cm thickness with an INSULATED backing and with suitable material thermal characteristics for concrete (see chapter 2.2.3 for details). On the surface of each column four AST measuring devices will be put at height 2.5 m. The value of AST for each column for this height will then be calculated as the average of the four measurements. For completness of the simulation, in addition HEAT TRANSFER COEFFICIENT will be also outputted at the same positions and averaged in the same manner. In the above equation, this coefficient will represent the value of coefficient 'h'. Recall that in Simulation 0 for this particular coefficient an approximation of 35 W/m2K was adopted from EN 1991-1-2 [2]. In Eurocode such value is suggested for cases where a natural fire curve is used in the analysis but there is no possibility for calculation of the corresponding actual convective coefficients.

Figure *40* below shows graphs of measured average air temperature and mean AST temperature for column S2 at a height of 2.5 m. For comparison, the measured air temperature at the position of this column at the same height is also added from Simulation 0 to the same graph. We can see that the temperatures are similar to each other, so the decision whether to set the temperature of the fire curve in the further process of fire analysis as the gas temperature from Simulation 0, gas temperature from Simulation 2 or as the AST temperature from Simulation 2 analysis will most likely not have a major impact on the results of the analysis (i.e. the time of collapse of the S2 column). In contrast, however, we expect a greater influence in terms of the selection of the convection coefficient. As can be seen in Figure *41*, this is significantly different in Simulation 2 from the value of 35 W/m^{2}K , which was used for this coefficient in Simulation 0.
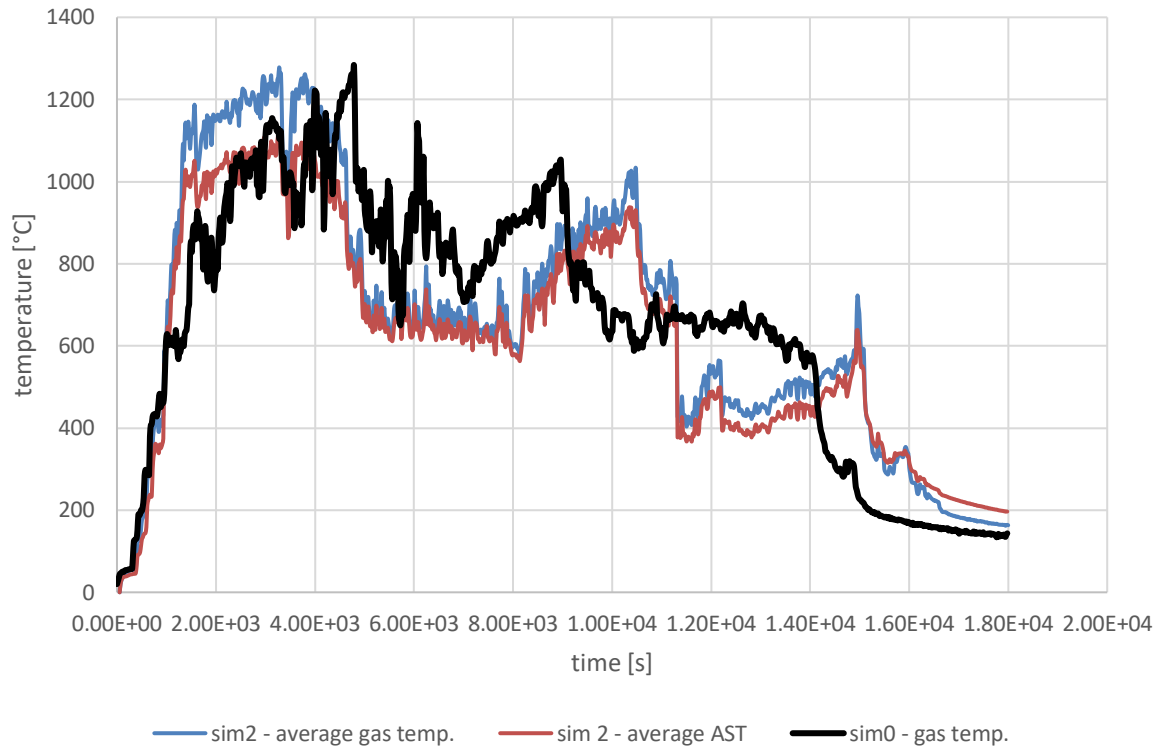
Figure 40: Average gas temperature (blue curve) and average adiabatic surface temperature (AST; orange curve) for column S2 at height 2.5m in Simulation 2. For comparison, gas temperature at the same position is also shown as measured in Simulation 0 (thick black line).
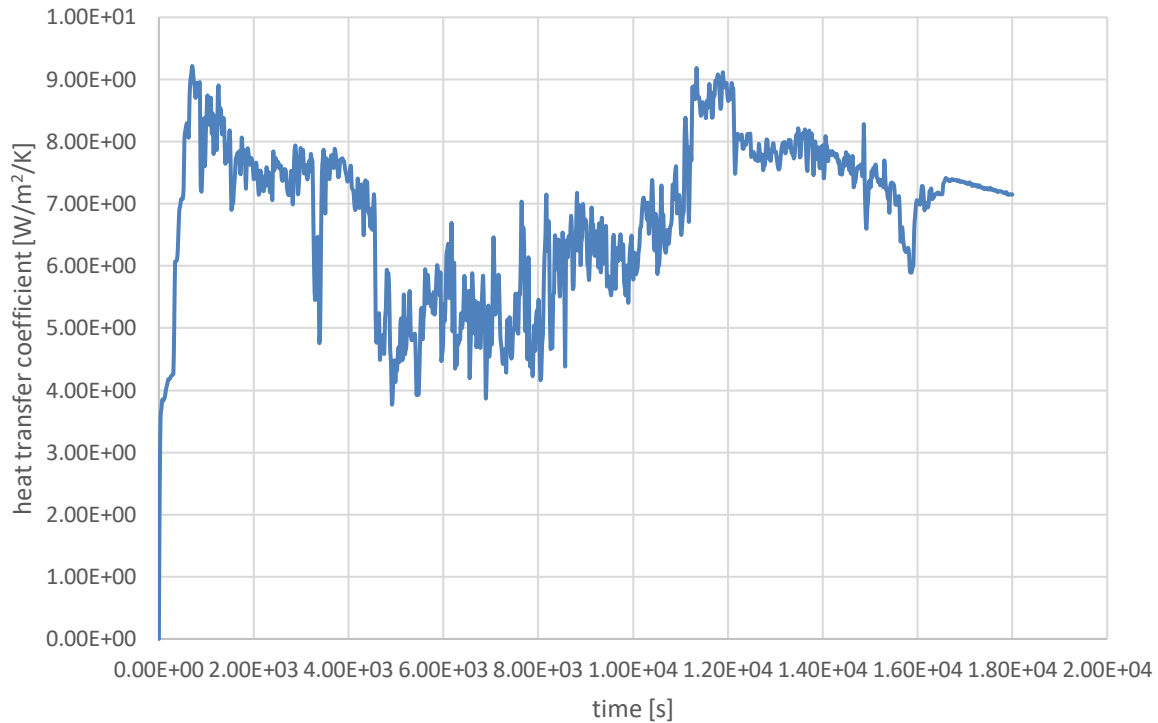
Figure 41: Average heat transfer coefficient for column S2 at height 2.5m as measured in Simulation 2.

Step 2: Thermal analysis of the column

No changes were applied here compared to Simulation 0 procedure with the exception of somewhat different selection of the fire curve and the convective heat transfer coefficient. The former was selected according to the average AST temperature from Figure *40* and the latter was applied according to Figure *41*.

Step 3: Structural analysis of the column

No changes were applied here compared to Simulation 0 procedure.

Results and observations

Compared to the results of simulation 0, the time of the column's collapse has increased to 160 minutes (9593 seconds) in Simulation 2. This means a 84 minute (i.e. a 110 % increase) compared to results of Simulation 0.

Figures below show other results of the analysis, i.e. deformed shape of the column at the time of the column collapse (scale factor is 1), the time development of the column's axial displacement at the top of the column, the time development of the column's transverse displacement at mid-span.
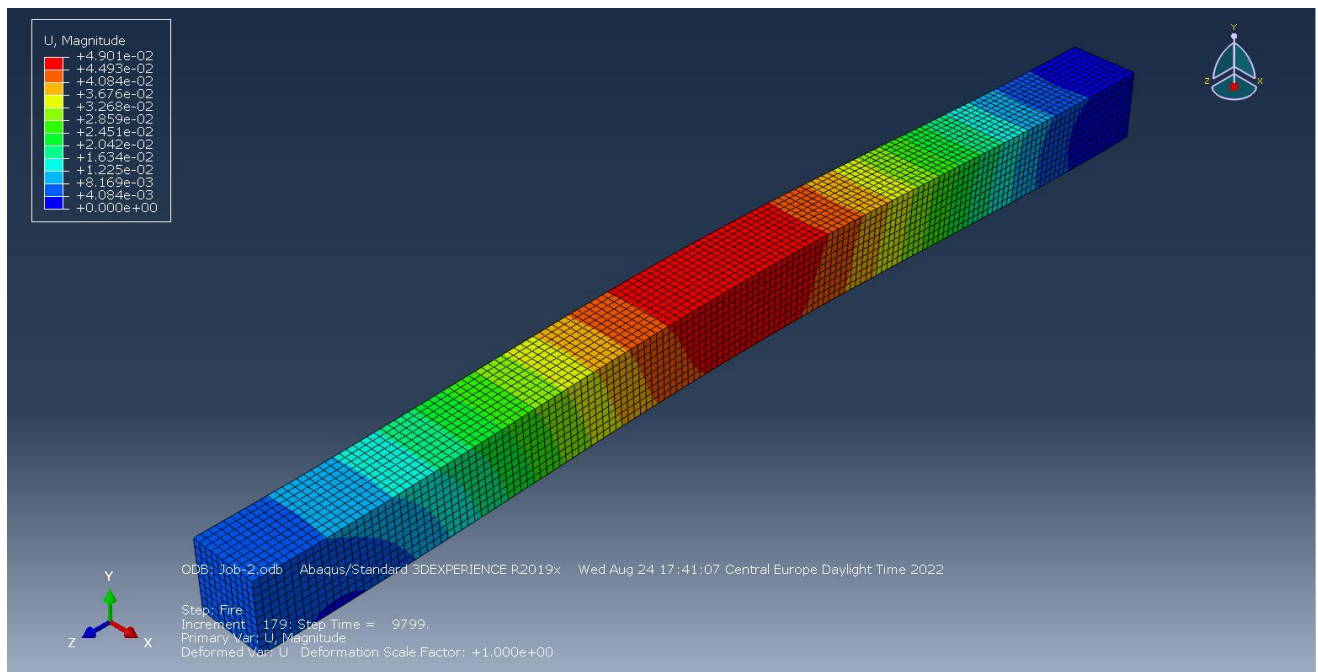
Figure 42: Deformed shape of the column at the time of the column collapse.
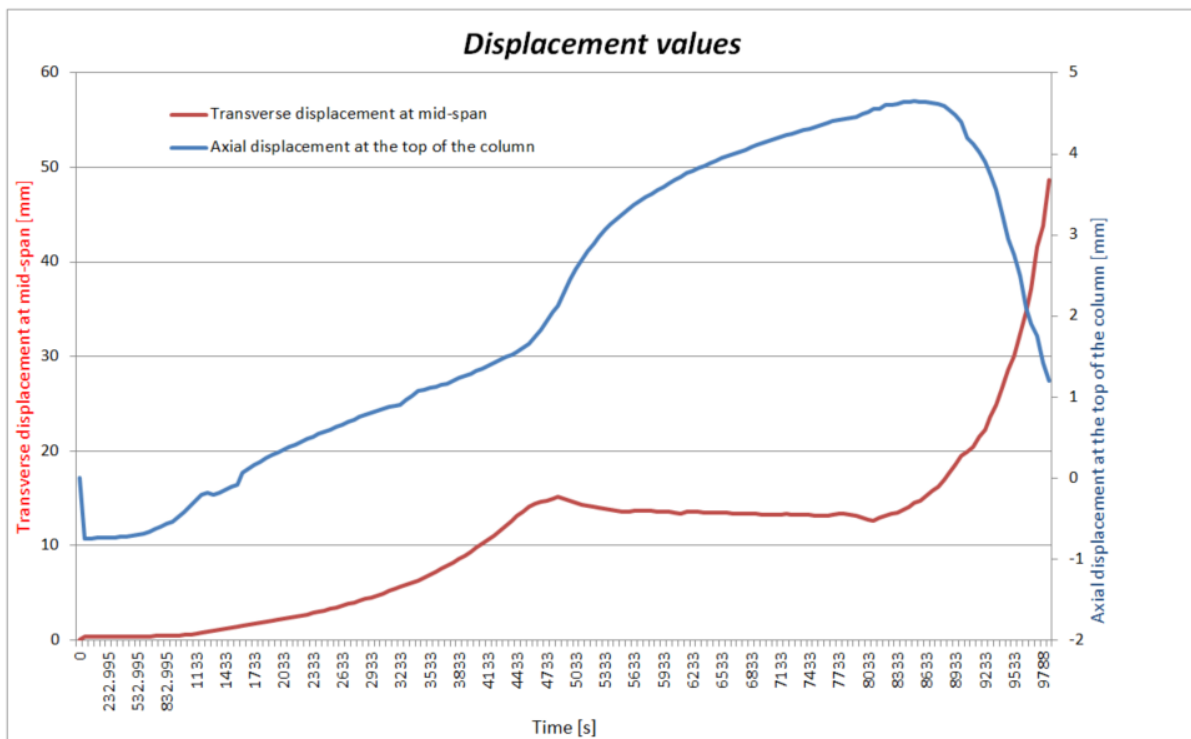
Figure 43: The time development of the column's axial displacement at the top of the column, the time development of the column's transverse displacement at mid-span.

3.2.4. Simulation 3: Effect of number of heat zones selected along the column's height in the column's thermal analysis

Step 1: Analysis of temperature of the column's surroundings

This simulation is an upgrade of simulation 2 presented in the previous chapter (Section 3.3.3.) of this dissertation. In simulaton 2 only 1 temperature curve was applied along the entire height of the column. We now apply 2 (Simulation 3a), 3 (Sim. 3b) or 6 (Sim 3c) different curves, numbers 2, 3 and 6 here represent the number of heat zones across the column's height (heights of individual zones are equal to each other in a specific simulation). In the same way, convective heat transfer coefficient varies from zone to zone as well. Figures below show how AST and HFT are calculated and applied to each zone according to each simulation. Values that we used to calculate AST and HFT are taken from FDS [11] analyses.

Calculation of average AST and average HFT	
Z	average AST
2,7 m`	$(S2\_1\_ AST_d + S2\_2\_ AST_a + S2\_3\_ AST_a)/3$
2,5 m`	$(S2\_1\_AST + S2\_2\_AST + S2\_3\_AST)/3$
2,0 m`	$(S2\_1\_ AST_b + S2\_2\_ AST_b + S2\_3\_ AST_b)/3$
1,5 m`	$(S2\_1\_ AST_c + S2\_2\_ AST_c + S2\_3\_ AST_c)/3$
1,0 m`	$(S2\_01\_AST + S2\_02\_AST + S2\_03\_AST)/3$
0.5 m`	$(S2\_1\_ AST_d + S2\_2\_ AST_d + S2\_3\_ AST_d)/3$
* HFT is calculated in the same way	

Table 3: Calculation of average AST and average HFT
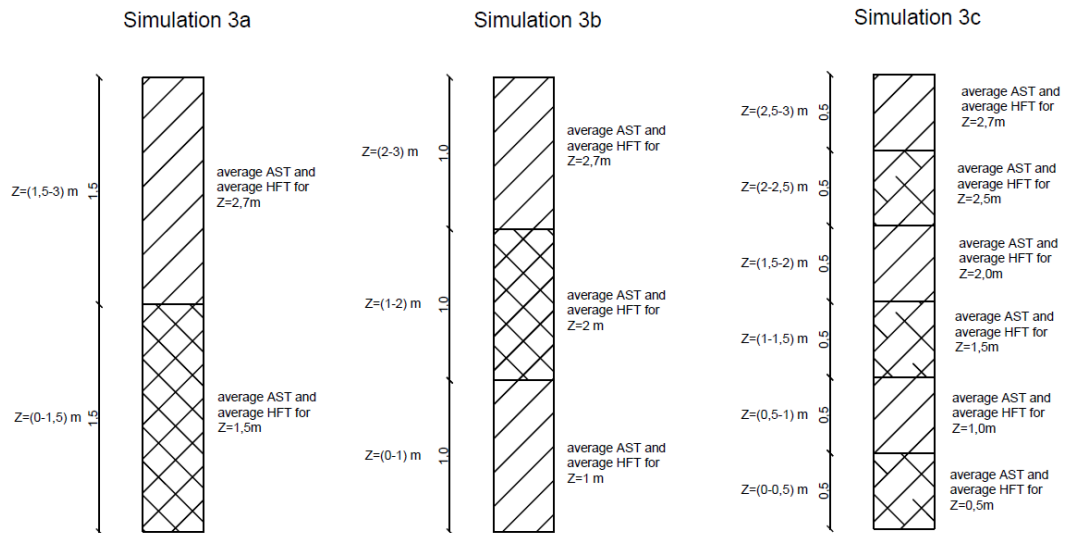
Figure 44: Heat zones in simulation 3a (left), heat zones in simulation 3b (middle) and heat zones in simulation 3c (right)
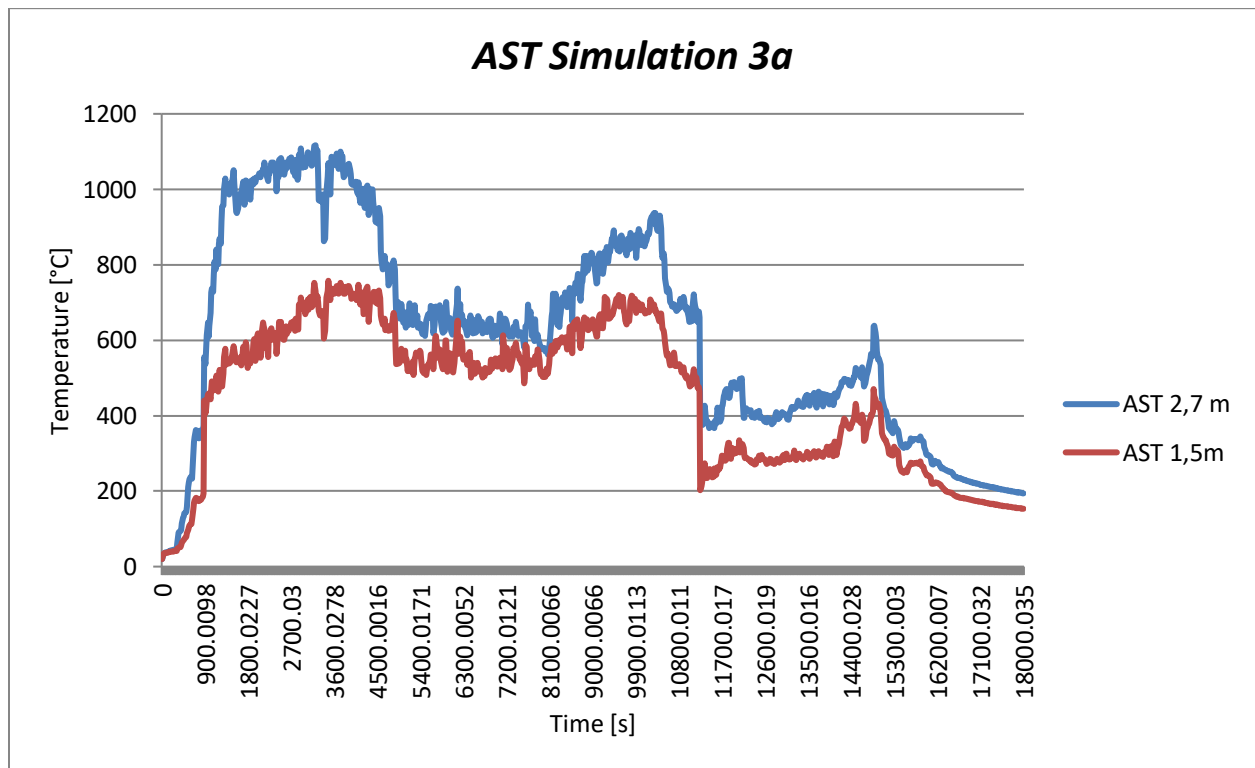
Figure 45: Average AST curves for column S2 in simulation 3a. For this simulation average AST curves are measured at heights 2,7m and 1,5m.
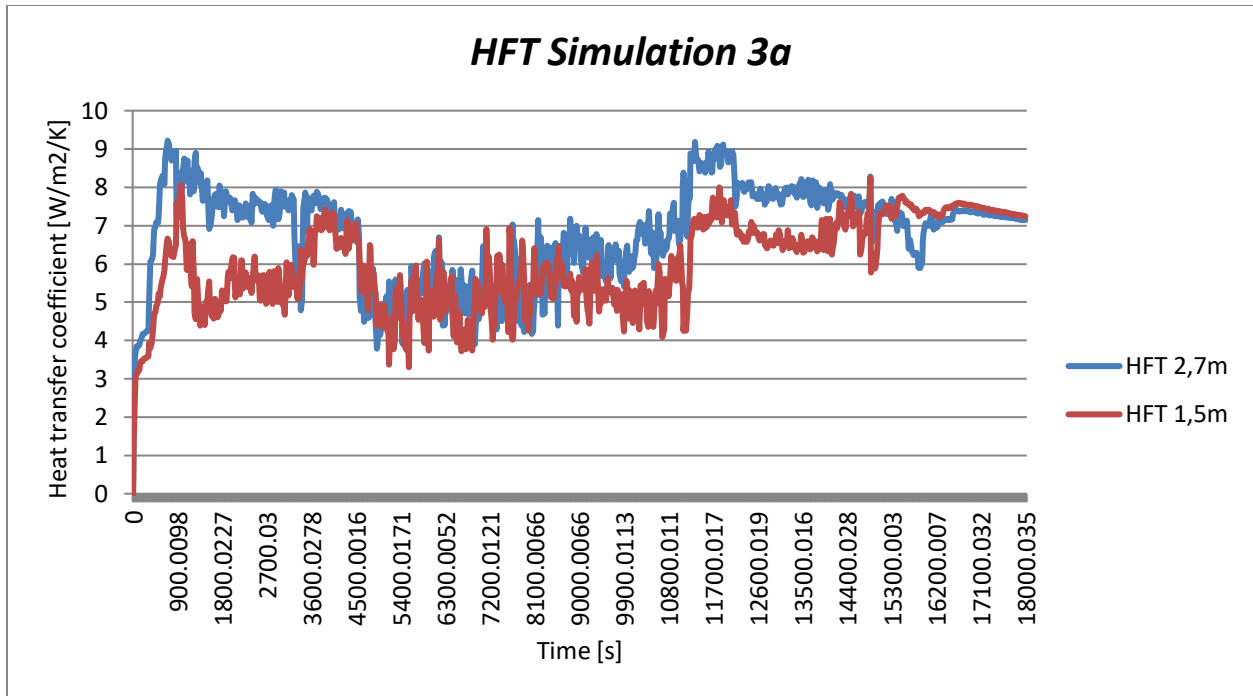
Figure 46: Average heat transfer coefficient for column S2 in simulation 3a. Values are measured at heights 2,7m and 1,5m.
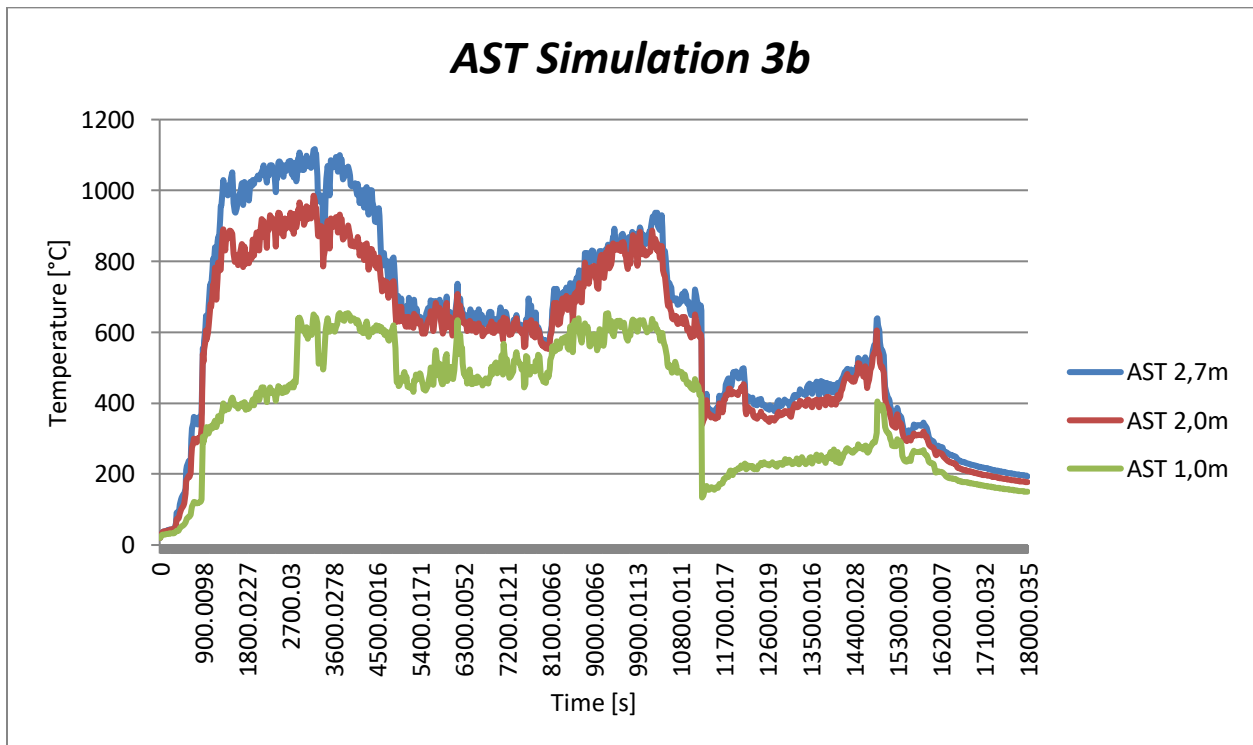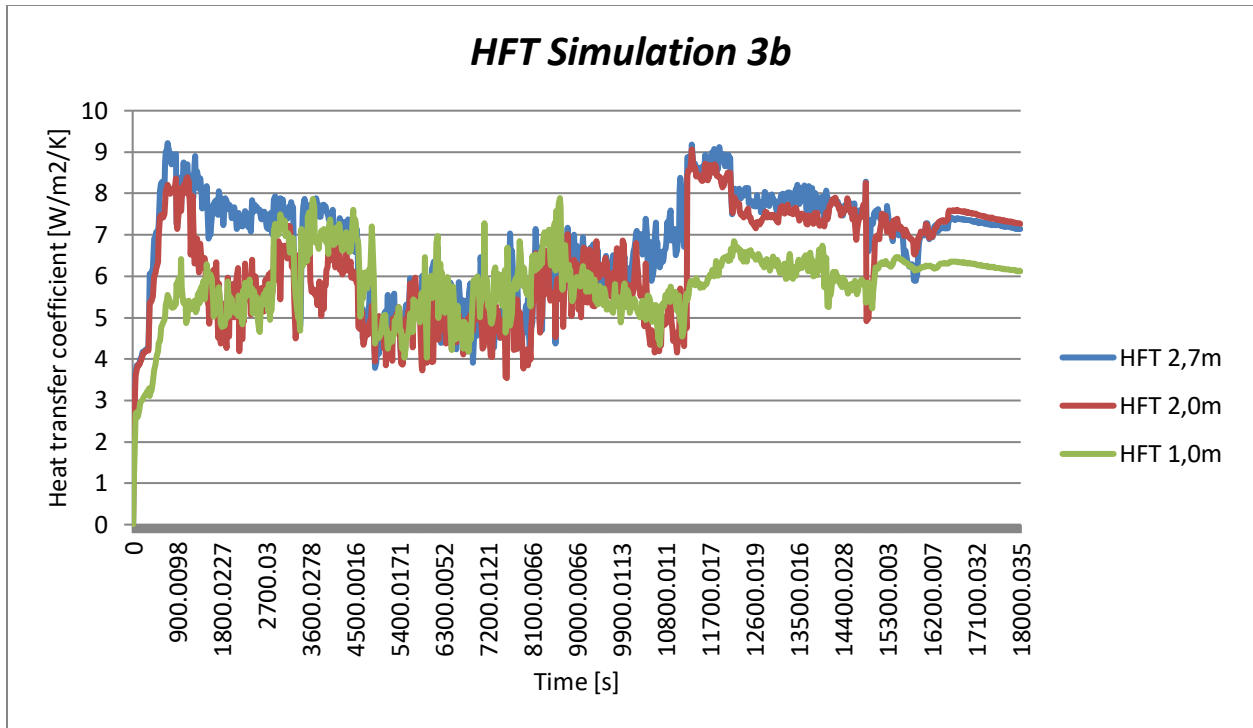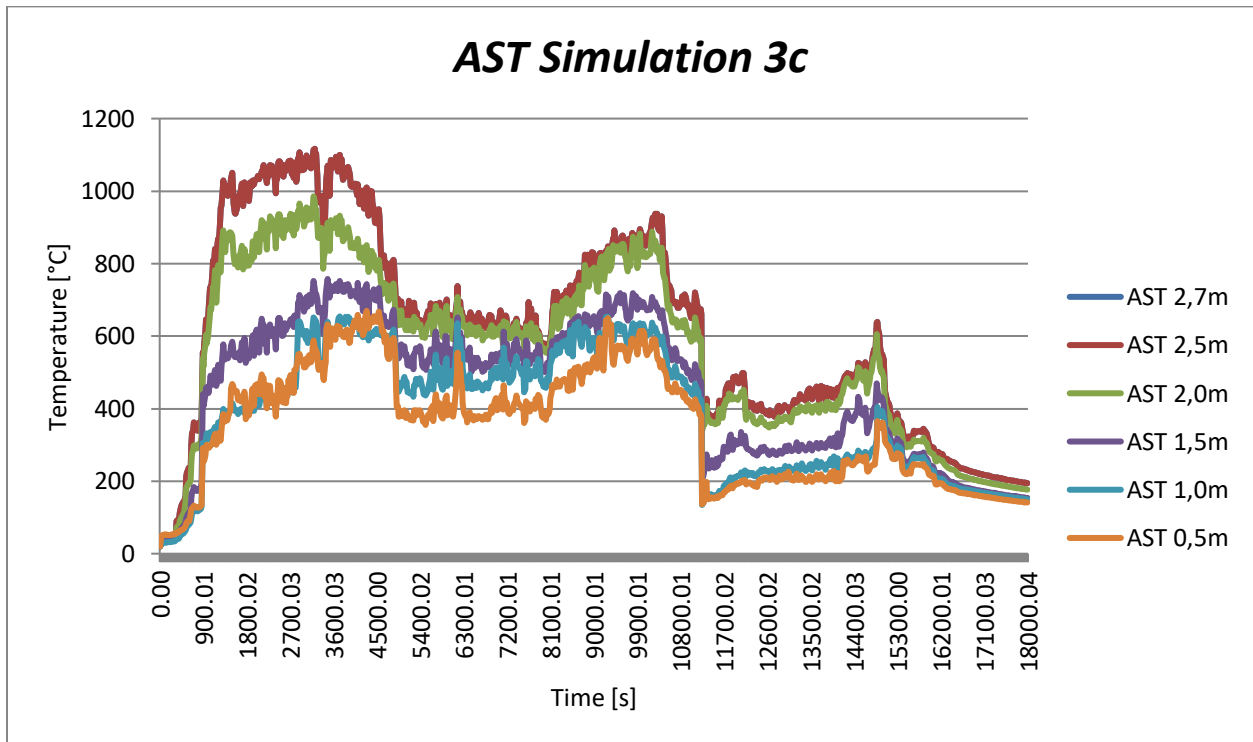

Figure 47: Average AST curves for column S2 in simulation 3b. For this simulation average AST curves are measured at heights 2,7m , 2,0m and 1,5m.

Figure 48: Average heat transfer coefficient for column S2 in simulation 3b. Values are measured at heights 2,7m, 2,0m and 1,5m.

Figure 49: Average AST curves for column S2 in simulation 3c. For this simulation average AST curves are measured at heights 2,7m , 2,5m, 2,0m, 1,5m1 1,0m and 0,5m.
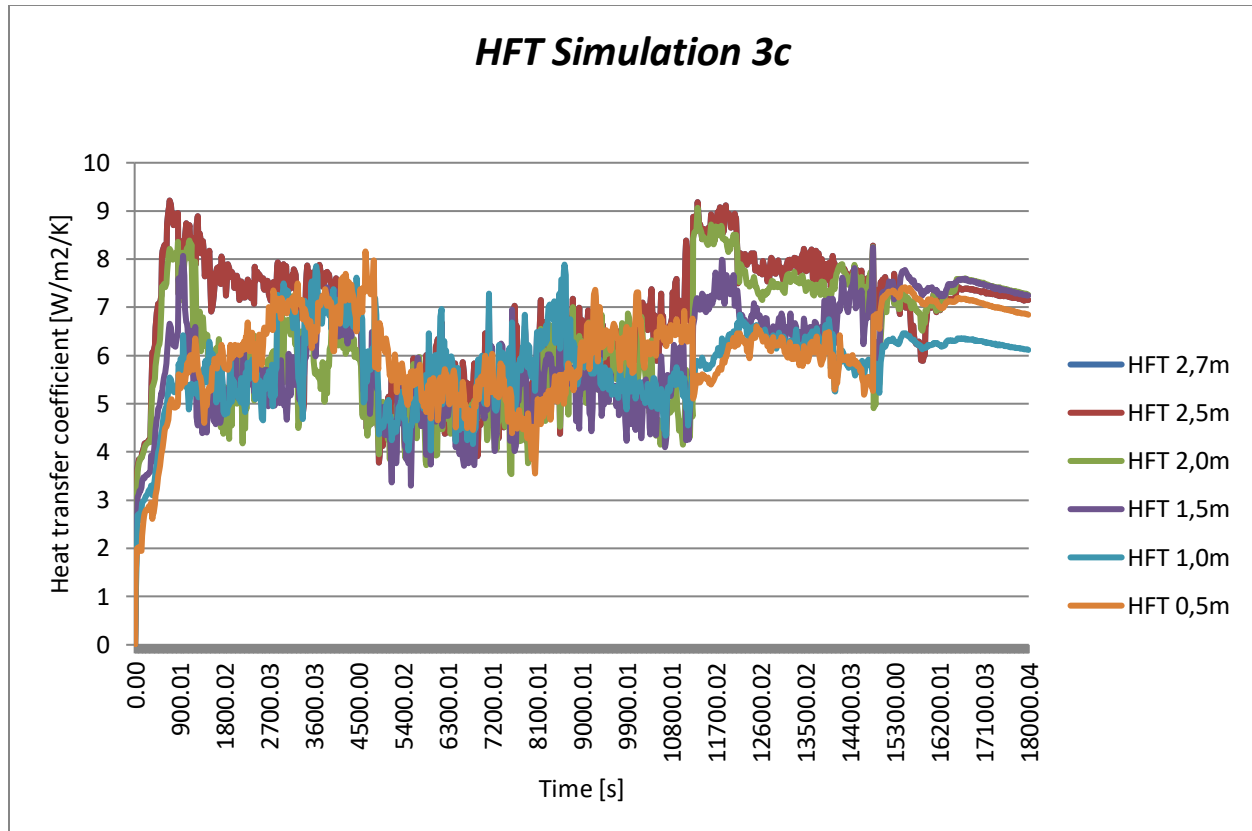
Figure 50: Average heat transfer coefficient for column S2 in simulation 3c. Values are measured at heights 2,7m, 2,5m, 2,0m, 1,5m, 1,0m and 1,5m.

Simulation 3a

Step 2: Thermal analysis of the column

No changes were applied here compared to the Simulation 2 procedure except for adding two fire curves and two the convective heat transfer coefficients. The former was selected according to the average AST temperature from Figure *45* and the latter was applied according to Figure *46*.
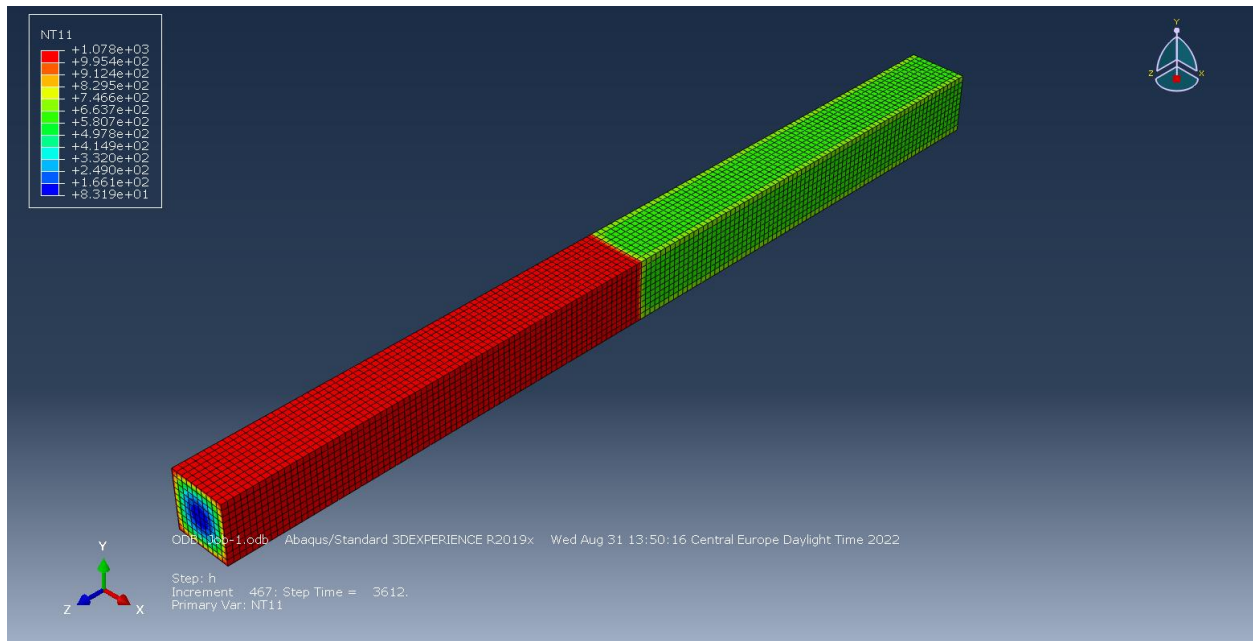
Figure 51: Column surface temperature after 60 minutes of fire.
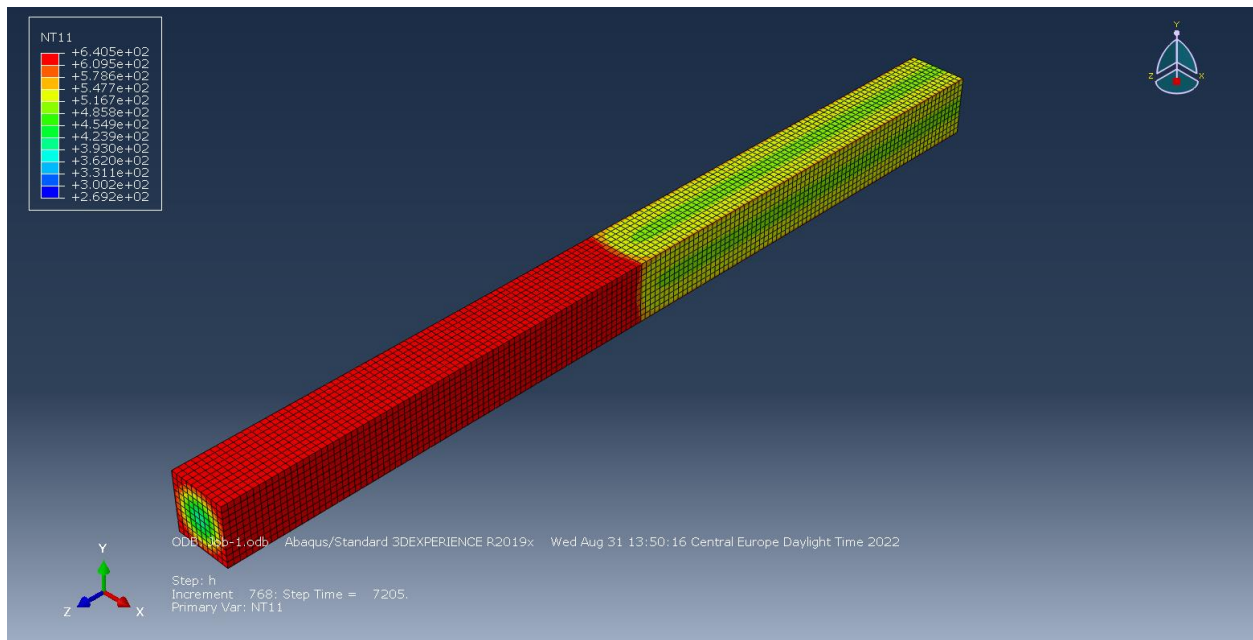
Figure 52: Column surface temperature after 120 minutes of fire.
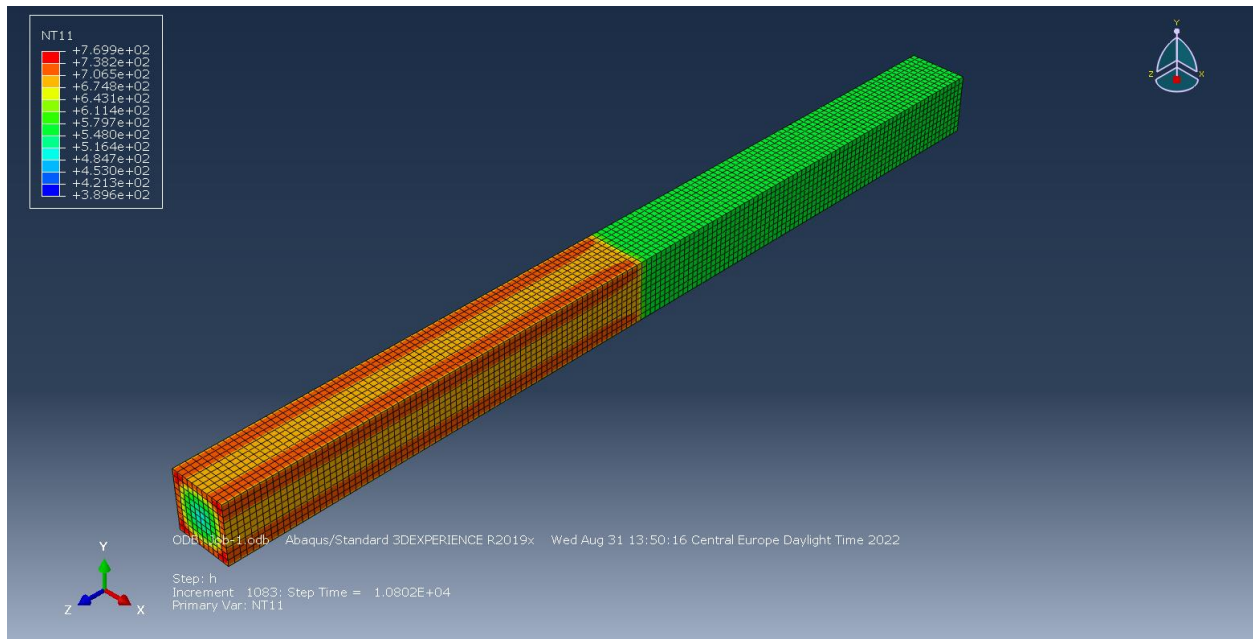
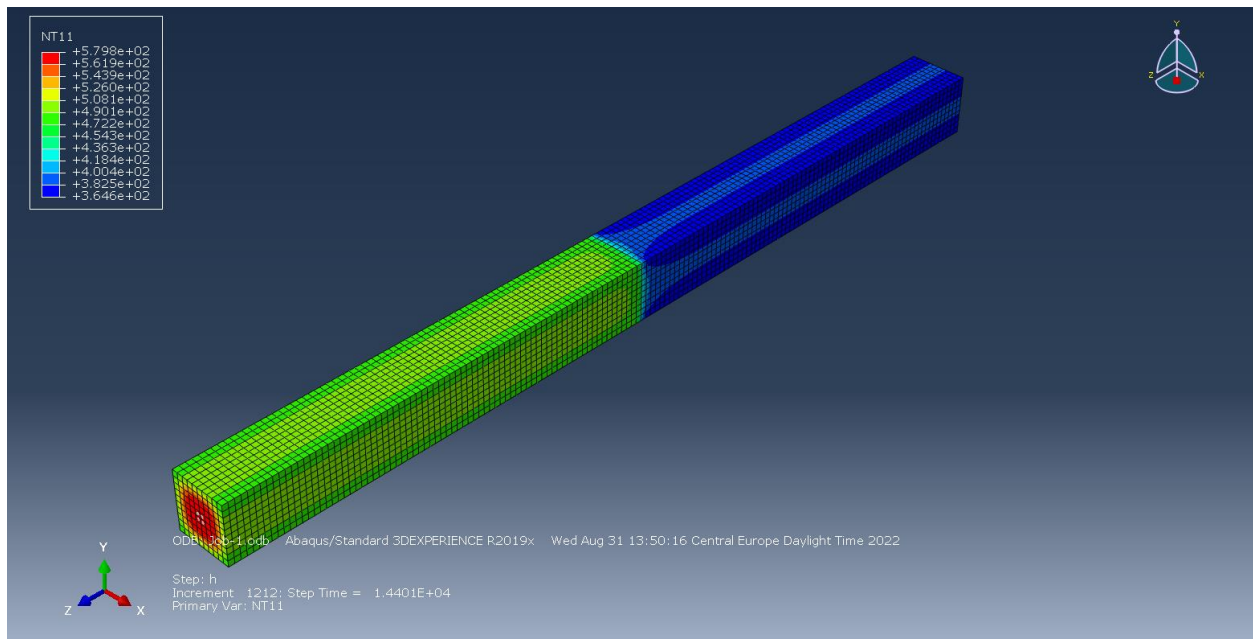Figure 53: Column surface temperature after 180 minutes of fire.

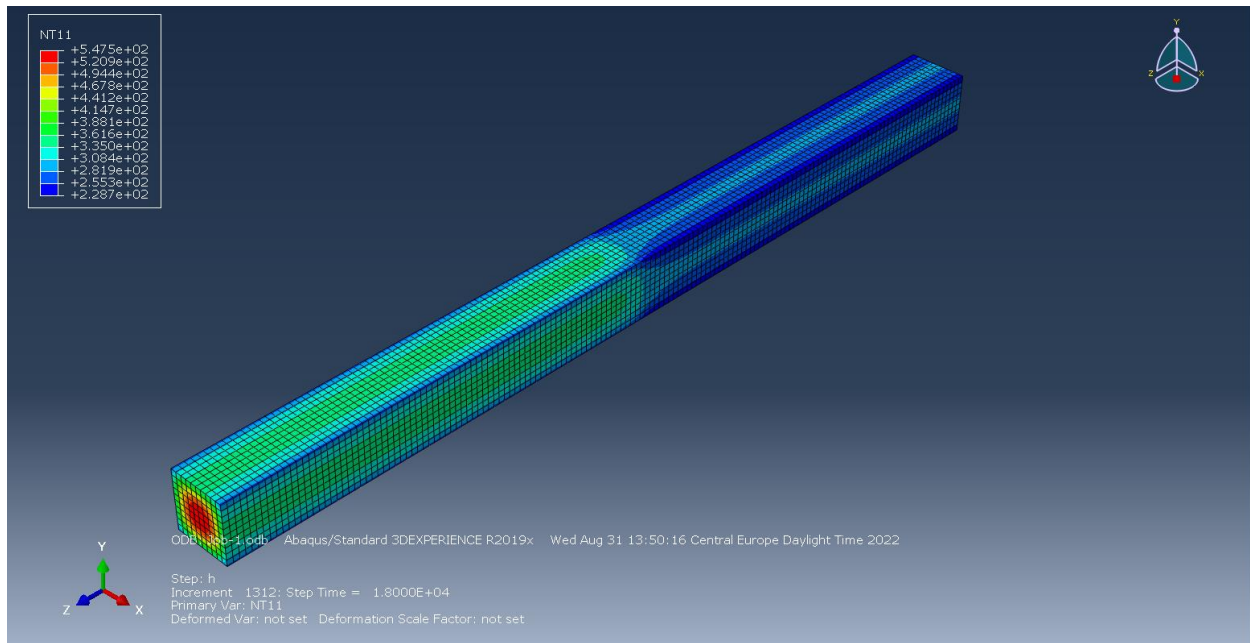Figure 54: Column surface temperature after 240 minutes of fire.

Figure 55: Column surface temperature after 300 minutes of fire

Step 3: Structural analysis of the column

No changes were applied here compared to Simulation 0 procedure.

Results and observations

Compared to the results of simulation 0, the time of the column's collapse has increased to 165 minutes (9953 seconds) in Simulation 3a . This represents a 117 % increase compared to results of Simulation 0 and 3% increase compared to results of Simulation 2.

Figures below show other results of the analysis, i.e. deformed shape of the column at the time of the column collapse (scale factor is 1), the time development of the column's axial displacement at the top of the column, the time development of the column's transverse displacement at mid-span.
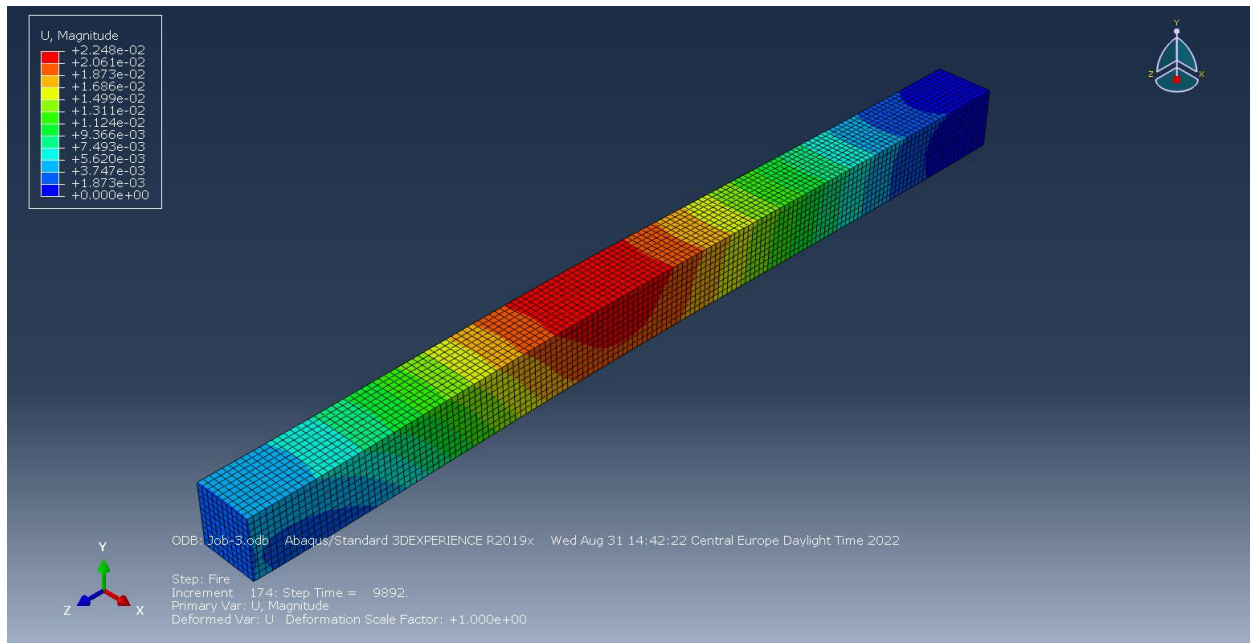
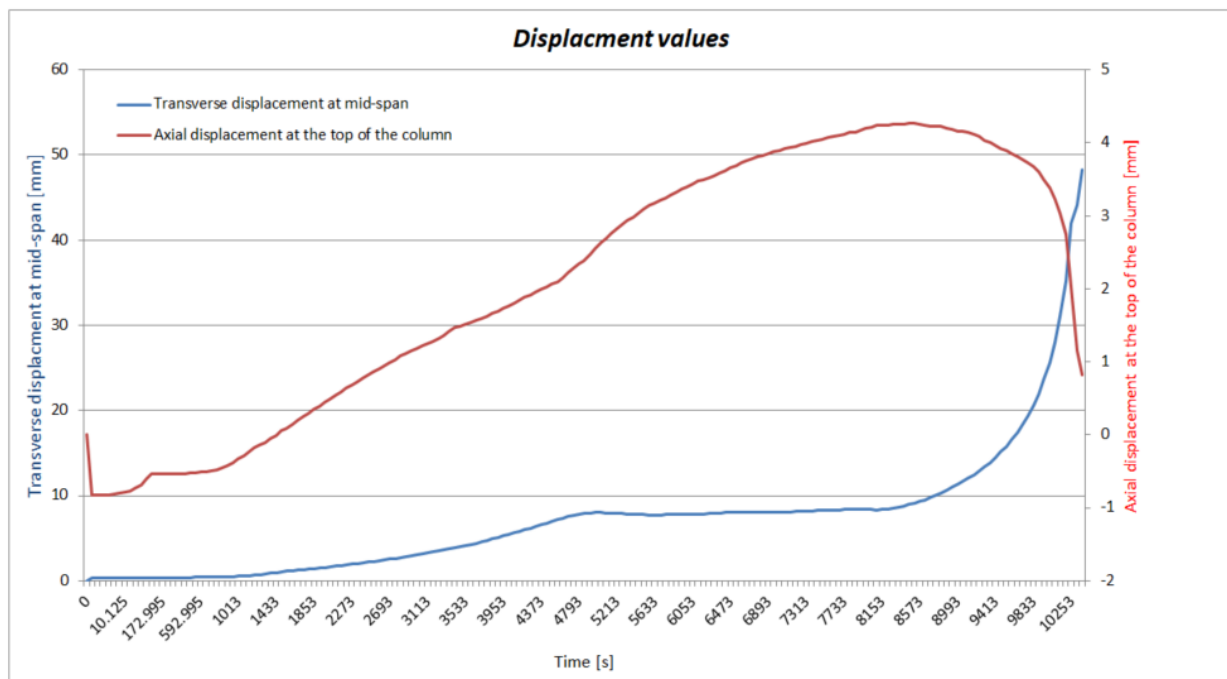Figure 56: Deformed shape of the column at the time of the column collapse.

Figure 57: The time development of the column's axial displacement at the top of the column, the time development of the column's transverse displacement at mid-span.

Simulation 3b

Step 2: Thermal analysis of the column

No changes were applied here compared to the Simulation 2 procedure except for adding three fire curves and three the convective heat transfer coefficients. The former was selected according to the average AST temperature from *Figure 47* and the latter was applied according to *Figure* 48.
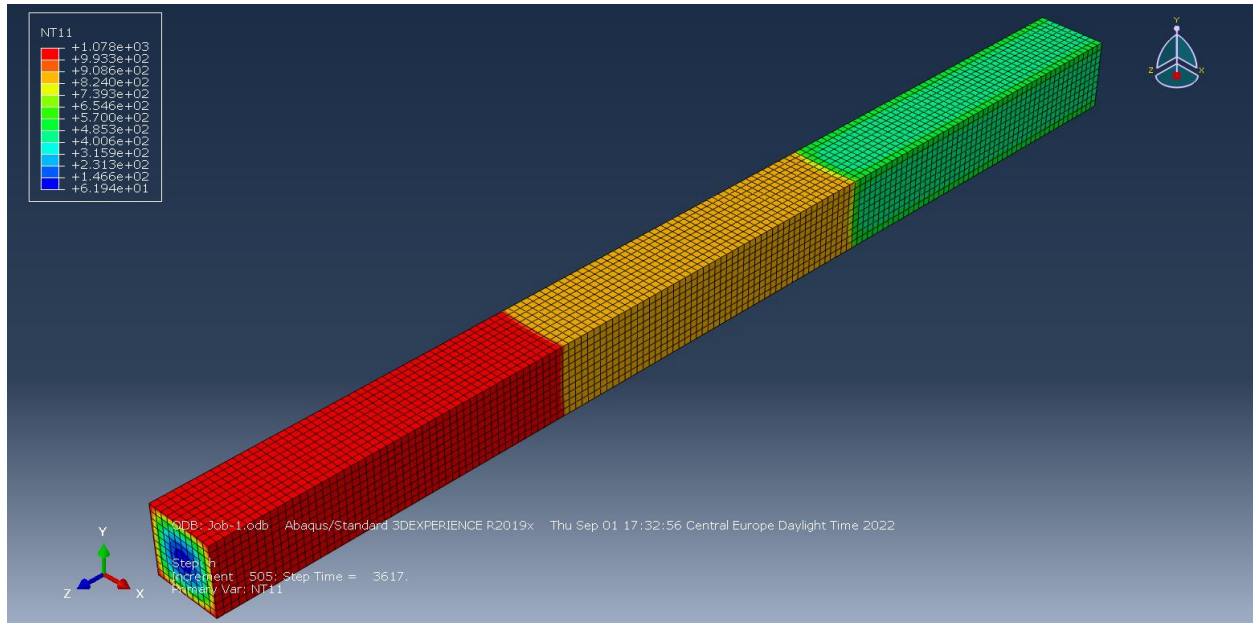

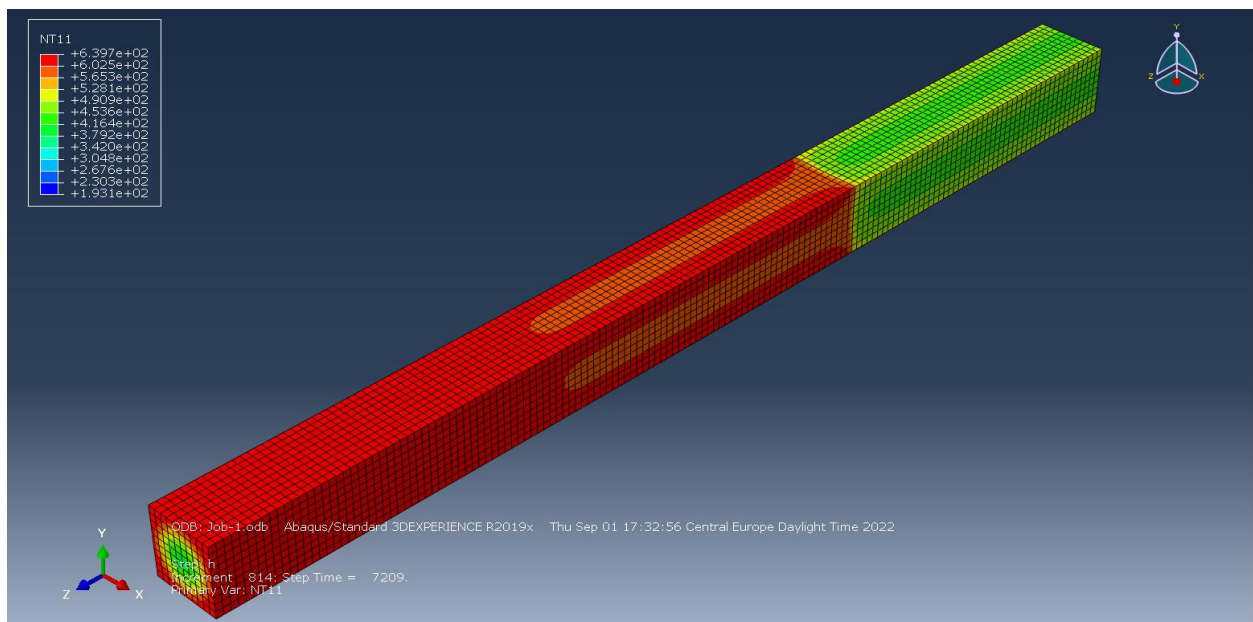Figure 58: Column surface temperature after 60 minutes of fire.

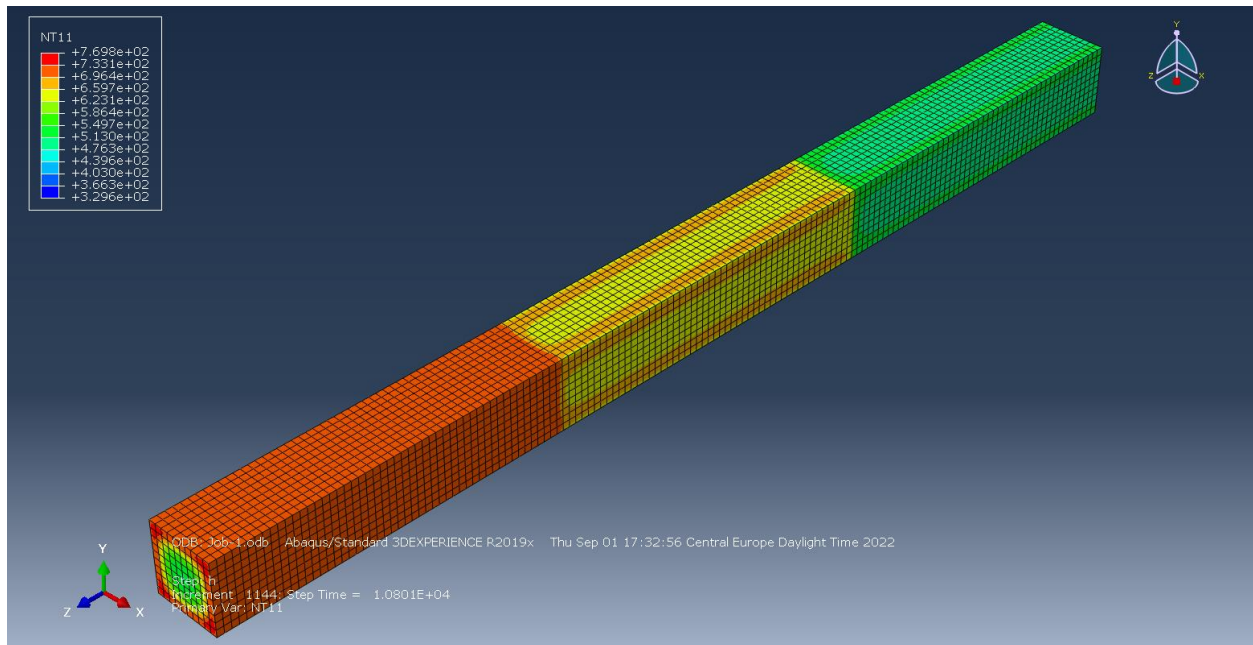Figure 59: Column surface temperature after 120 minutes of fire.

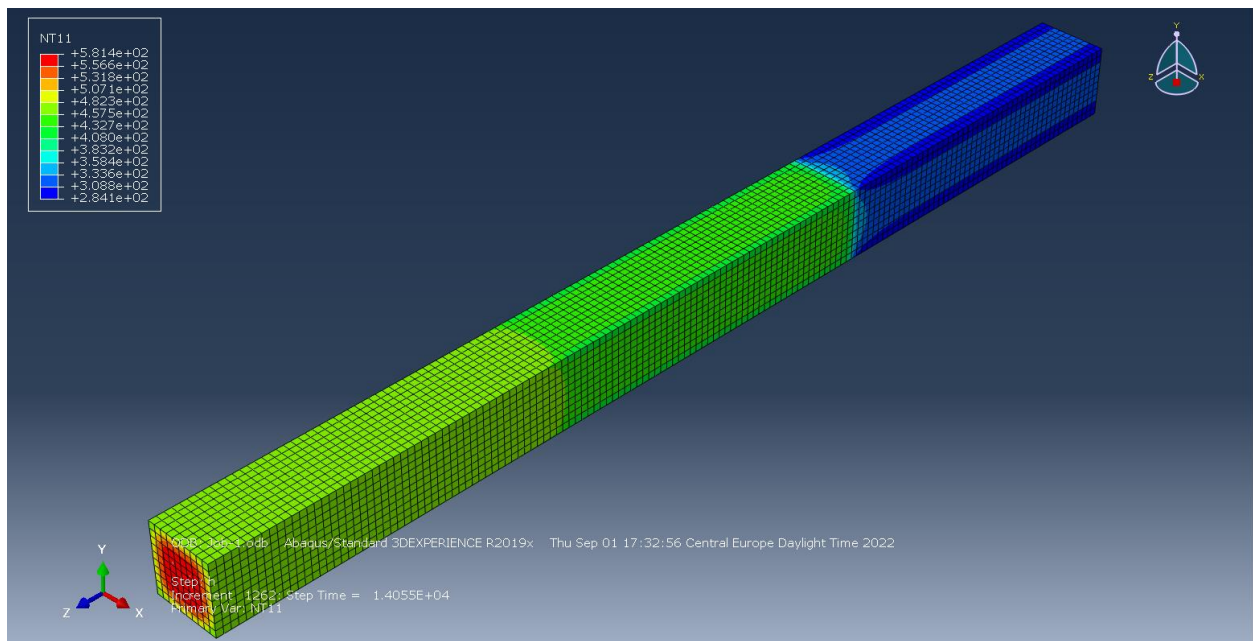Figure 60: Column surface temperature after 180 minutes of fire.

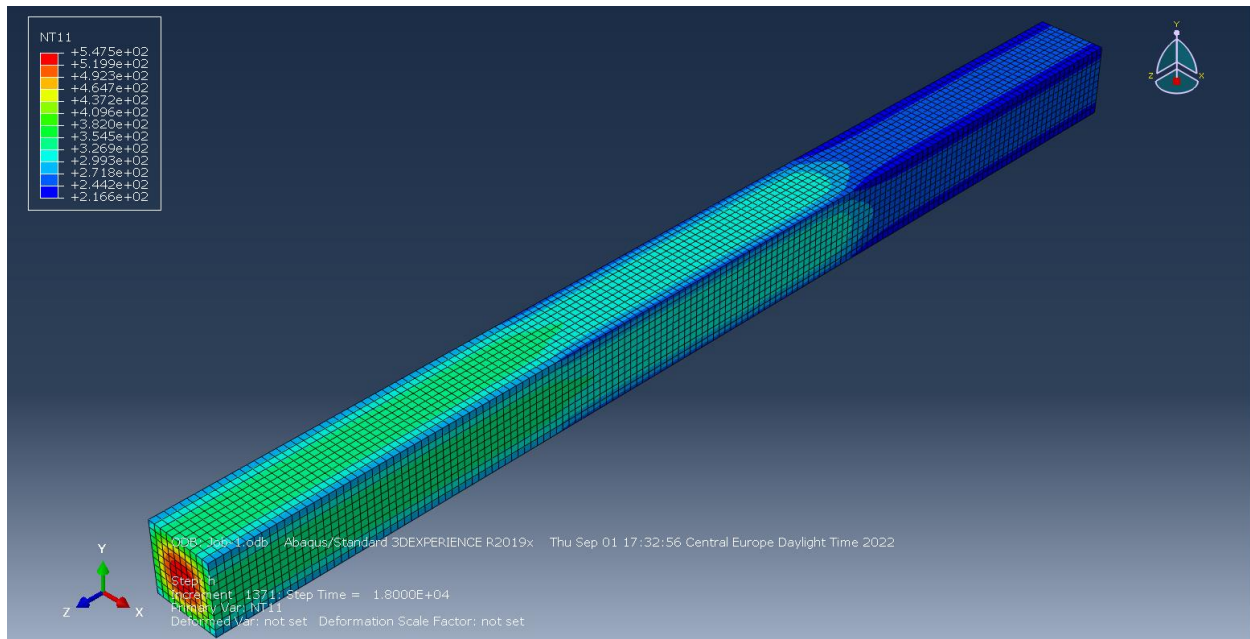Figure 61: Column surface temperature after 240 minutes of fire.

Figure 62: Column surface temperature after 300 minutes of fire.

Step 3: Structural analysis of the column

No changes were applied here compared to Simulation 0 procedure.

Results and observations

Compared to the results of simulation 0, the time of the column's collapse has increased to 171 minutes (10253 seconds) in Simulation 3b . This represents a 125 % increase compared to results of Simulation 0 and 7 % increase compared to results of Simulation 2.

Figures below show other results of the analysis, i.e. deformed shape of the column at the time of the column collapse (scale factor is 3), the time development of the column's axial displacement at the top of the column, the time development of the column's transverse displacement at mid-span.
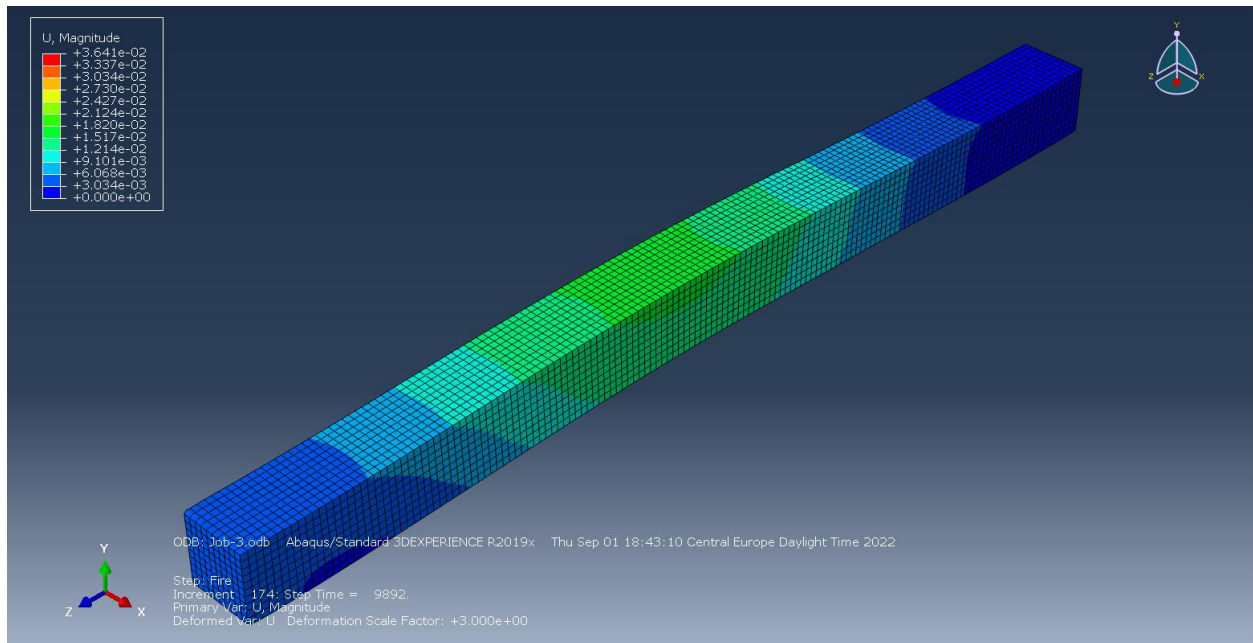
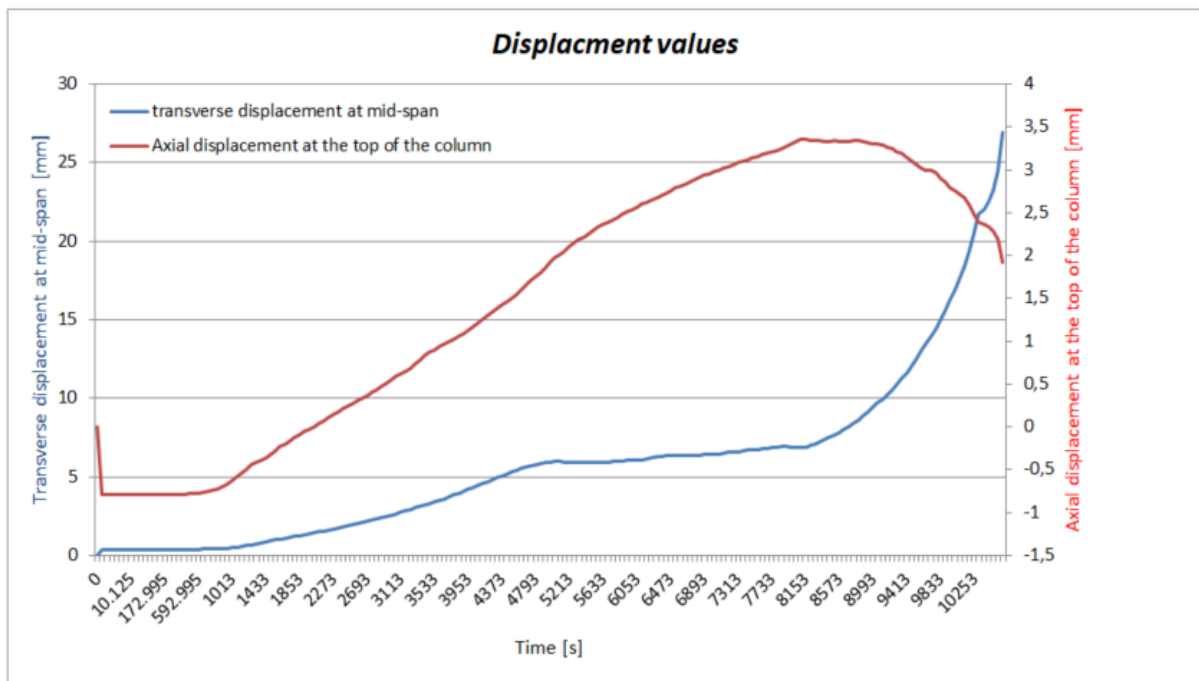Figure 63: Deformed shape of the column at the time of the column collapse.

Figure 64: The time development of the column's axial displacement at the top of the column, the time development of the column's transverse displacement at mid-span.

Simulation 3c

Step 2: Thermal analysis of the column

No changes were applied here compared to the Simulation 2 procedure except for adding three fire curves and three the convective heat transfer coefficients. The former was selected according to the average AST temperature from *Figure 49* and the latter was applied according to *Figure 50*.
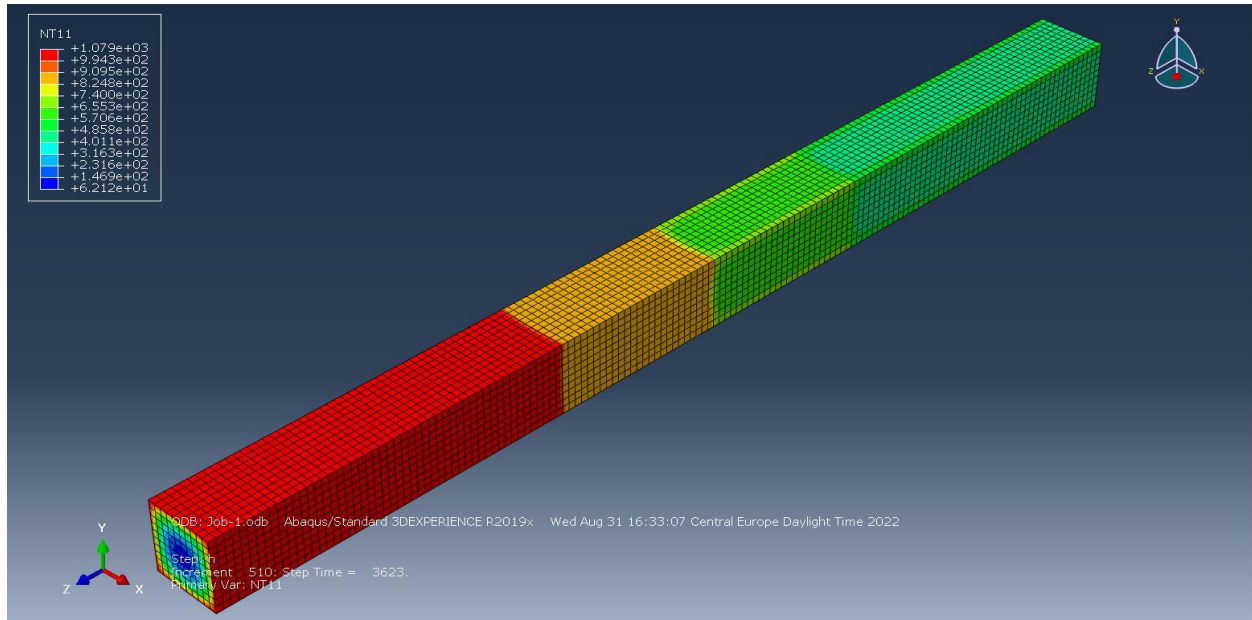

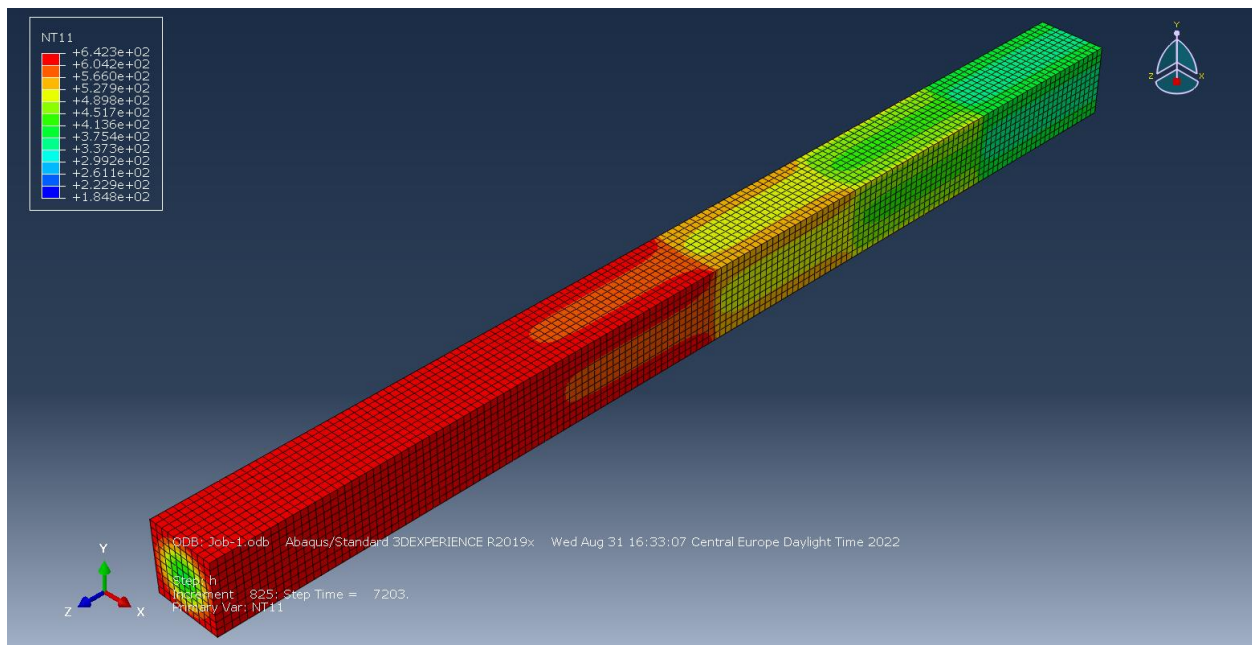Figure 65: Column surface temperature after 60 minutes of fire.

Figure 66: Column surface temperature after 120 minutes of fire.
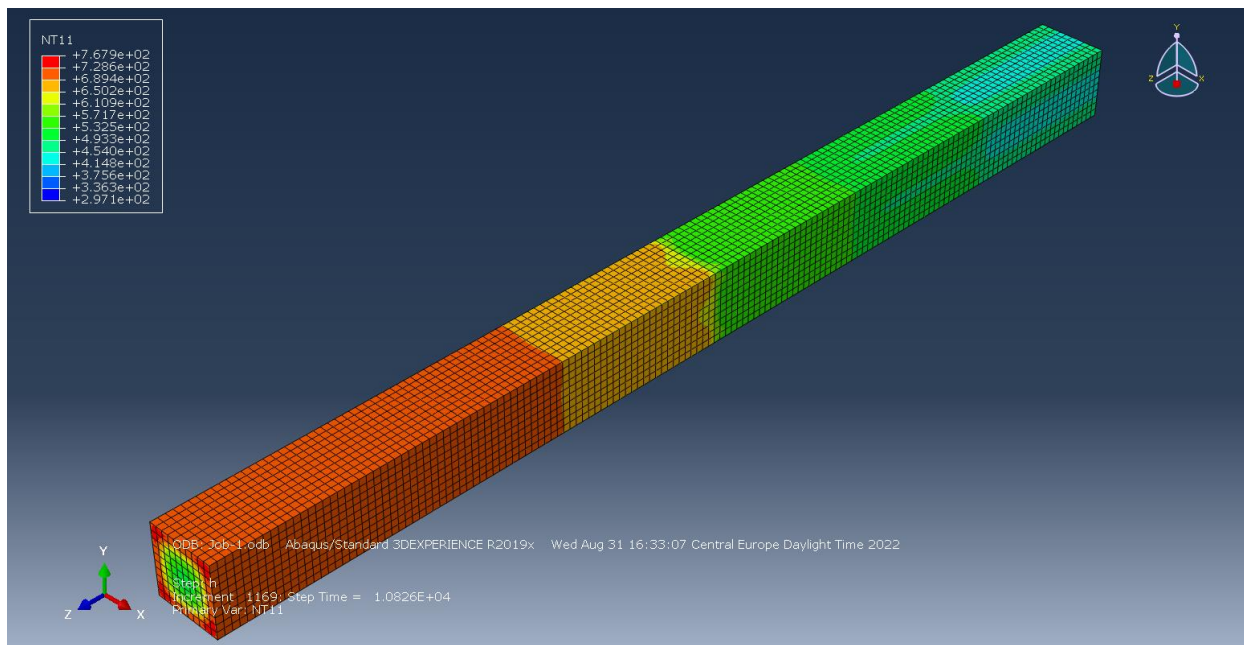
Figure 67: Column surface temperature after 180 minutes of fire.
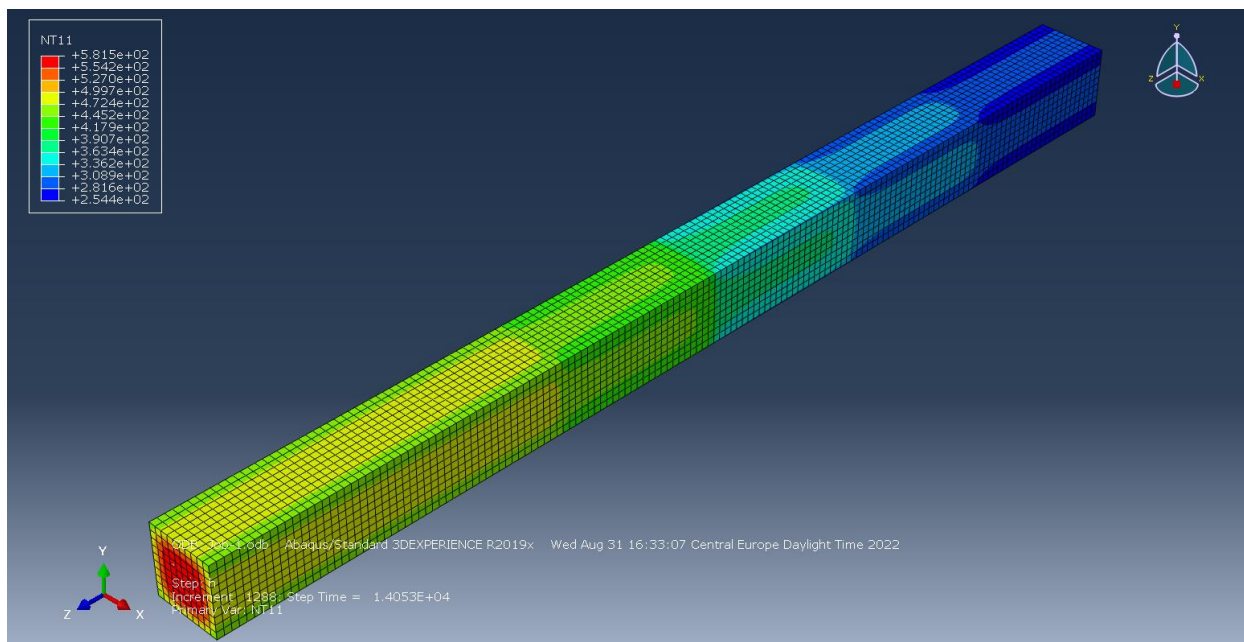
Figure 68: Column surface temperature after 240 minutes of fire.
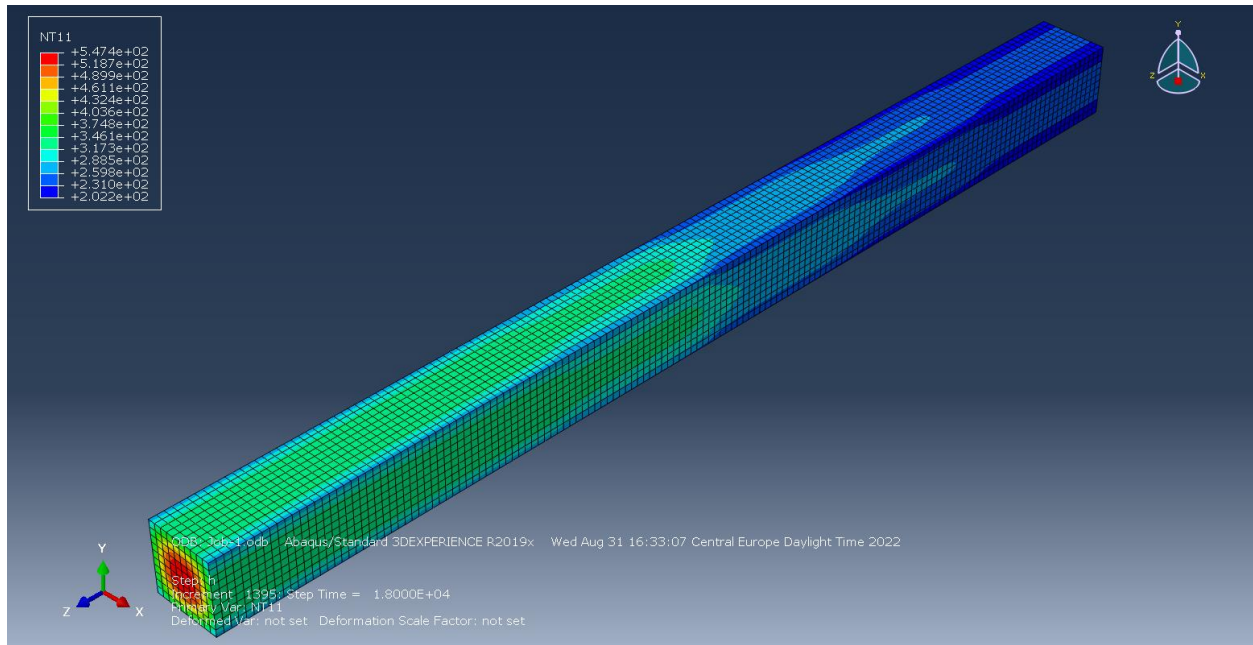
Figure 69: Column surface temperature after 300 minutes of fire.

Step 3: Structural analysis of the column

No changes were applied here compared to Simulation 0 procedure.

Results and observations

Compared to the results of simulation 0, the time of the column's collapse has increased to 172 minutes (10 313 seconds) in Simulation 3c. This represents a 126 % increase compared to results of Simulation 0 and 7,5 % increase compared to results of Simulation 2.

Figures below show other results of the analysis, i.e. deformed shape of the column at the time of the column collapse (scale factor is 5), the time development of the column's axial displacement at the top of the column, the time development of the column's transverse displacement at mid-span.

Figure 70: Deformed shape of the column at the time of the column collapse.

Figure 71: The time development of the column's axial displacement at the top of the column, the time development of the column's transverse displacement at mid-span.

3.2.5. Concluding remarks on gathered results

When comparing the results of simulation 0 and simulation 1, we can conclude that the degree of conservatism introduced into the analysis when the response of the structure was mathematically described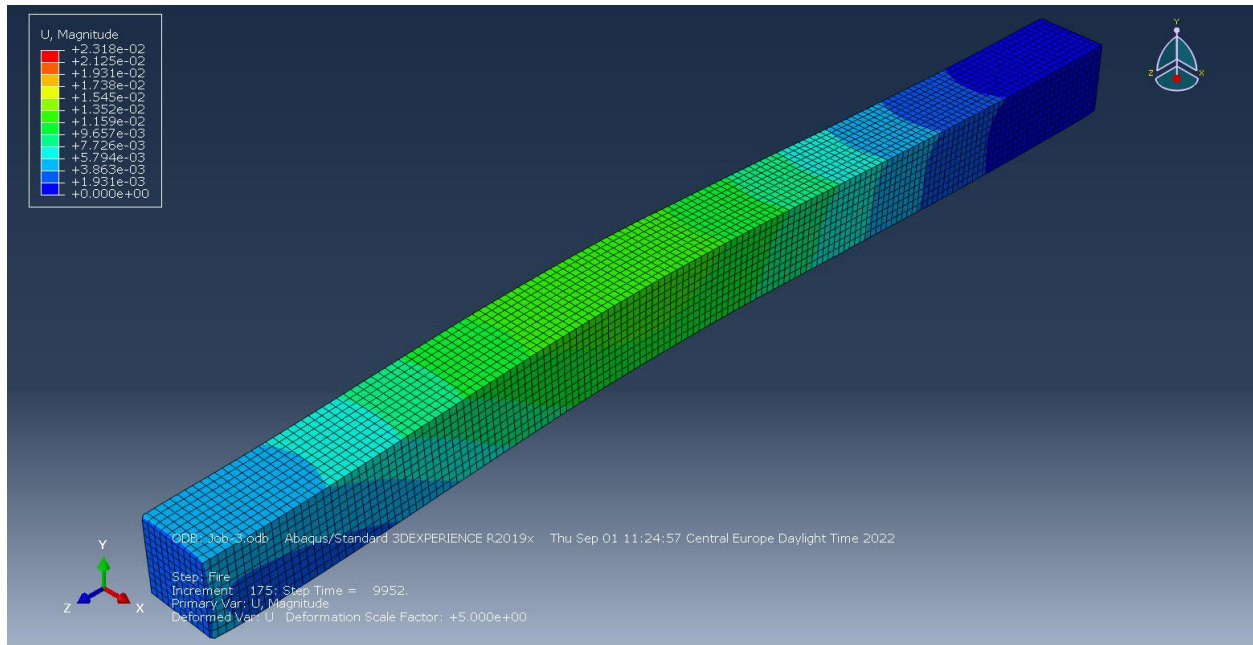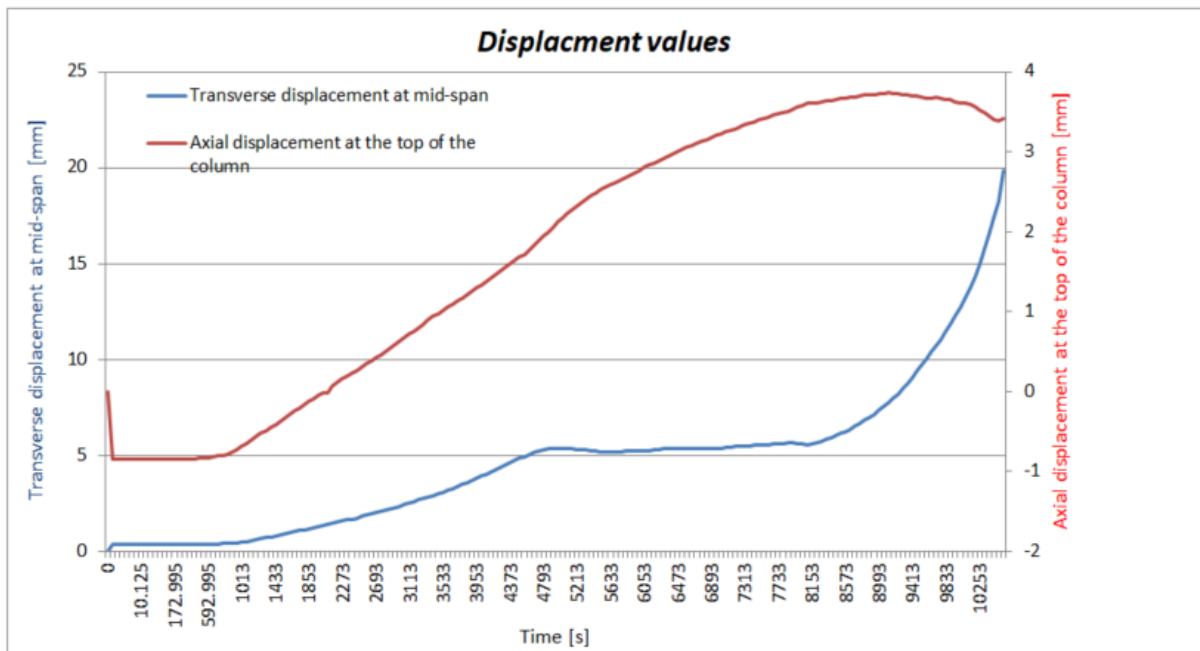 according to the second-order theory instead of the most precise third-order theory, was small for the analyzed building and fire case (8% difference). In the future, this effect should be studied on examples of other RC columns with different geometries, levels of utilization of initial load-bearing capacity and at different fire conditions.

By comparing the results of simulation 0 and simulation 2, we can further conclude that the influence of the parameters that were observed in these cases (i.e. using the AST temperature instead of gas temperature when exporting a fire curve from an FDS simulation and using real values of convection coefficient instead of the fixed value suggested by EN 1991-1-2 [2]), was very large for the observed building and fire case. This finding seems unexpected at first glance – especially considering the fact that the difference in fire curves between simulations 0 and 2 was in fact small (*Figure 40*). And it also seems unexpected considering the fact that large changes in convection coefficients would normally not also mean larger differences in the calculated cross-sectional temperatures of the structure (note that influence of radiation would be much more important in this respect because temperatures of the surroundings of the structure are raised to the fourth power in this case; see Eq. 18). The latter holds true also for our analyzed case as further examination of the collected data would show where noticeable differences between cross-sectional temperatures between the two analyses would only be noticed after the elapsed 73rd minute. And where even after that the discovered differences would be relatively small (max 100°C in a specific cross-sectional point or less). However, since the time of collapse of the observed column at its 50% initial load-bearing utilization would occur at the 76th minute in simulation 0, even the observed small difference in cross-sectional temperatures (100°C or less) would be apparently sufficient that in Simulation 2 the collapse of the column was however avoided at this time. In addition to surviving the 76th minute, as a consequence of the decrease of fire curve temperature that follows this minute (*Figure 40*), the column in Simulation 2 would even survive a considerable time of the continuation of the fire.

Considering the above it is, thus, clear that if the degree of initial utilization of the column's bearing capacity was selected differently, the differences between the results of simulations 0 and 2 could be significantly lower.

By comparing the results of simulation 0 and simulation 3a, we further conclude that for vertical structural elements, such as RC columns, division of the element into two zones (upper warmer and lower colder zone) and consideration of a different fire curve for each of these two zones could substantially improve reliability of fire analysis. A question remains for our observed building and fire case, however, to what extent this effect would really be a result of the considered parameter (i.e. the chosen number of zones) and to what extent would it be merely the result of an 'unfortunately' chosen level of initial utilization of the column (see the discussion regarding comparison of simulations 0 and simulation 2 above).

By comparing the results of simulation 3a to results of simulations 3b and 3c, we finally discover that increasing the number of zones along the height of the column from two to three or even more does not make much sense for our analyzed building and fire case since this would not significantly reduce the conservativeness of the analysis.

4. CONCLUSIONS

According to requirements of EN 1992-1-2 [1], fire analyses of reinforced concrete (RC) columns today can be performed in several different ways, which can have different levels of accuracy depending on which and how many assumptions (simplifications) they entail. Some of the most often applied simplifications are: (i) internal forces in the element will not change during fire and there will be no changes in kinematic boundary conditions at the ends of the element (the column can thus be treated as a structural member isolated from the rest of the structure), (ii) temperature of the column's surroundings at a specific time of the fire will be the same along the column's entire height and perimeter, (iii) convection coefficients dictating convective heat fluxes at the contact of the column and its surroundings during a fire will be such as suggested in EN 1991-1-2 [2] (e.g. 35 W/m^2K for natural fires), (iv) mathematical description of the mechanical response of the column can be simplified, for example, described by equations according to the *second-order theory* instead of according to the most accurate *third-order* theory, (v) concrete strength can be considered as being preserved in full up to the temperature of 500°C and as being equal to zero at temperatures higher as 500°C *etc*.

In general, fire analysis of a RC column can be upgraded from a more simple form to a more advanced one by omitting one or more of the above assumptions. It is already well known today that engineers in their daily engineering practice should strive for such an upgrade as much as possible. Namely, because of their conservatism, the more simple methods are often more on the so-called "safe side" and thus can lead toward more expensive engineering solutions (e.g. prescribing excessive structural fire protection).

Unfortunately, however, to date it is not yet clarified sufficiently which of the above assumptions would make the most sense to be eliminated first (i.e. which are the ones that most influence conservatism of the results of the simpler methods). Thus, this master's thesis tried to contribute to answering this question. This was done by analysing a selected case of a RC building, i.e the building for sales and services of cars in Jesenice (Slovenia) where a strong fire of roughly 3000 disposed car tyres broke out in a part of the building's basement at the end of 2016. Reports about this building and the fire were found in available professional literature.

To provide answers to main questions of this thesis highlighted in the two paragraphs above, several fire analyses of the selected Jesenice building were performed throughout the thesis in different ways, i.e. by applying one or more of the above mentioned simplifications of simpler calculation methods and than comparing the gathered results. In this way, degree of conservatism of each of the applied simplification could be assessed for the analysed building case.

The first part of each of the perfomed fire analyses was modeling of fire development based on previously known knowledge about the real fire. This was done in software FDS (Fire Dynamics Simulator). Here burning of the tyres was described by a complex pyrolysis submodel which showed a good prediction of heat release rate and temperature development around the observed RC structure.

The second part of each fire analyses was dedicated to calculation of in this dissertation 3D heat transfer trought the column using the classic non-stationary Fourier heat transfer analysis. This was performed in software ABAQUS.

Based on temperatures obtained from thermal analysis, structural analysis was performed in the third part of each fire analyses. In addition to thermal load, in each of these the column was loaded with constant axial compression force and a small constant transverse force. The latter was applied to induce buckling. The time elapsed from the beginning of the fire until the column collapses was obtained.

To conclude, notwithstanding the more precise fire analyses are often complex and time consuming, benefits of it could be noticed in terms of increasing safety and reliability. Further research steps should be done to make these analyses familiar enough for every engineer to use.

REFERENCES

[1]   EN 1992-1-2: Eurocode 2: Design of concrete structures

[2]   EN 1991-1-2: Eurocode 1: Actions on structures - Part 1-2: General actions - Actions on structures exposed to fire

[3]   Martin Maglica, Fire analysis of reinforced concrete strucutre, Master`s thesis, University of Ljubljana, Faculty of Civil and Geodetic engineering, 2021. (in Slovene)

[4]   Anna Matala, Estimation of solid phase reaction parameters for fire simulation, Master`s thesis, Helsinki University of Technology, Faculty of Information and Natural Sciences, 2008.

[5]   Ivan Tadić, Požarna analiza AB stupova: Proračun realnog (varijabilnog) aksijalnog opterećenja modeliranjem većeg dijela konstrukcijskog sustava , Master`s thesis, University of Split , Faculty of Civil Engineering, Architecture and, 2022.

[6]   H. Mostafei, Hybrid fire testing for assessing performance of structures in fire—Application, Fire Safety Journal 56 (2013)

[7]   J.Č.Kolšek and P. Češarek, ALI AB KONSTRUKCIJE, PROJEKTIRANE PO UVELJAVLJENIH POENOSTAVLJENIH POSTOPKIH EVROKODA IN TEHNIČNIH SMERNIC ZA ZAGOTAVLJANJE POŽARNE VARNOSTI V STAVBAH, LAHKO PREŽIVIJO TUDI REALNE POŽARE?,Požar, December 2022 (submitted, in Slovene)

[8]   Barbara Kralj, Vpliv požara v načrtovanem jeklenem prizidiku na nosilnost obostoječega armiranobetenskega objekta (The impact of fire in the planned steel extension on the load capacity of the existing reinforced concrete building), Master`s thesis, University of Ljubljana, Faculty of Civil and Geodetic engineering, 2019. (in Slovene)

[9]   EN 1990: Eurocode - Basis of structural design

[10]   Cadorin, J-F. Franssen, J-M. 2003. A tool to design steel elements submitted to compartment fires - OZone V2. Part 1: pre- and post-flashover compartment fire model. Fire Safety Journal, Vol. 38, iss. 5, pp: 395-427

[11]   Kevin McGrattan, Simo Hostikka, Randall McDermott, Jason Floyd, Craig Weinschenk, Kristopher Overholt, Fire Dynamics Simulator User's Guide, NIST Special Publication 1019 Sixth Edition, FDS Version 6.0.0 , November 2013

[12] Kevin McGrattan, Bryan Klein, Simo Hostikka, Jason Floyd, Fire Dynamics Simulator (Version 5) User's Guide, October 2007

[13] Jerneja Kolšek, univ. dipl. inž. grad., Fire analysis of two-layered composite planar structures, Doctoral thesis, University of Ljubljana, Faculty of Civil and Geodetic engineering, 2013

[14] Khoury, G.A. 2000. Effect of fire on concrete and concrete structures. Progress in Structural Engineering and Materials, 2, 4: 429-447. Khoury, G.A. 2000. Effect of fire on concrete and concrete structures. Progress in Structural Engineering and Materials, 2, 4: 429-447.

[15] Yaqub, M., Bailey, C.G., Nedwell, P., Khan, Q.U.Z., Javed, I. 2013. Strength and stiffness of post-heated columns repaired with ferrocement and fibre reinforced polymer jackets. Composites Part B: Engineering, 44, 1: 200–211.

[16] Fire-spalling of self-compacting concrete - TunnelTalk.com, https://www.tunneltalk.com/TunnelTech-May12-Concrete-fire-spalling.php

[17] Kolšek Češarek, Jerneja, Češarek, Peter. Primer performančnega načina izračuna požarne obtežbe konstrukcije pri požaru v tovarni XPS (An example of performance-based calculation of the fire load of a structure in a XPS factory fire). V: Lopatič, Jože (ur.), Može, Primož (ur.), Maarkelj, Viktor (ur.). 40. zborovanje gradbenih konstruktorjev Slovenije, Bled, 19.-20. 11. 2018.

[18] Kolšek Češarek, Jerneja. Comparison of Simplified and Advanced Simulation of a Fire in a Factory of XPS Panels. V: Kaloop, Mosbeh (ur.). Advanced materials and application. International Symposium on Advanced Materials and Application ISAMA 2018, Seoul, South Korea, January 19-21, 2018. Stäfa: Trans Tech Publications, 2018. Vol. 1147, str. 30-35. Advanced materials research, vol. *1147.*

[19] Abaqus. Dassault Systèmes Simulia Corp., Johnston, RI, USA.

[20] ANSYS, Inc. Workbench User's Guide. Canonsburg. Pennsylvania.

[21] Franssen, J-M. Gernay, T. 2017. Modeling structures in fire with SAFIR®: theoretical background and capabilities. Journal of Structural Fire Engineering, Vol. 8 No. 3, pp: 300-323.

[22] Srpčič, S. 2003. Mehanika trdnih teles.(Mechanics of solid bodies), , University of Ljubljana, Faculty of Civil and Geodetic engineering: 651 page, (in Slovene)

[23] Češarek Kolšek J. Fire design of RC structures: Summary of theoretical background and guided examples. E-study material for Erasmus students participating in course Selected chapters from RC structures at University of Ljubljana, Faculty of Civil and Geodetic Engineering (personal files of the author).

[24] Srpčič, S. 2015. Trdnost I. Ljubljana, University of Ljubljana, Faculty of Civil and Geodetic engineering: 420 page, (in Slovene)

[25] J.Kolšek and A. Rebec, Analiza nosilne konstrukcije po požaru objekta ASP na Jesenicah(Analysis of the load-bearing structure after the fire at the ASP building in Jesenice) , Fire, december 2017., (in Slovene)

[26] P.J.DiNenno. SFPE Handbook of Fire Protection Engineering.

[27] Ozawa, M., Uchida, S., Kamada, T., Morimoto, H. 2012. Study of mechanisms of explosive spalling in high-strength concrete at high temperatures using acoustic emission. Construction and Building Materials, 37, 621–628